発表論文リスト

1. "**Substituent Effects on Intermolecular Electron Transfer: Coumarins in Electron Donating Solvents**", Y. Nagasawa, A. P. Yartsev, K. Tominaga, A. E. Johnson, and K. Yoshihara, *J. Am. Chem. Soc.*, 115, 7922-7923 (1993).

2. "**Solvent and Nuclear Dynamics in Ultrafast Intermolecular Electron Transfer in Diffusionless, Weakly Polar Systems**", A. P. Yartsev, Y. Nagasawa, and K. Yoshihara, *Chem. Phys. Lett.*, 102(4,5,6), 546-550 (1993).

3. "**Femtosecond Intermolecular Electron Transfer: Dye in Weakly Polar Electron Donating Solvents**", K. Yoshihara, A. P. Yartsev, Y. Nagasawa, H. Kandori, A. Douhal, and K. Kemnitz, in "*Ultrafast Phenomena VIII*", Springer Berlin, 571-575 (1993).

4. "**Femtosecond Intermolecular Electron Transfer between Dyes and Electron-Donating Solvents**", K. Yoshihara, A. P. Yartsev, Y. Nagasawa, H. Kandori, A. Douhal, and K. Kemnitz, *Pure Appl. Chem.* 65(8), 1671-1675, (1993).

5. "**Femtosecond Intermolecular Electron Transfer in Condensed Systems**", K. Yoshihara, Y. Nagasawa, A. P. Yartsev, S. Kumazaki, H. Kandori, A. E. Johnson, and K. Tominaga, *J. Photochem. Photobiol. A*, in press.

その他の論文リスト

1. "**Structure of Spiropyranic Photomerocyanines Investigated by Time-Resolved Resonance Raman Spectroscopy** ", Y. Nagasawa, S. Hashimoto, and H. Takahashi, *"Time Resolved Vibrational Spectroscopy V"*, Ed.: H. Takahashi, Springer-Verlag, Berlin, 171-173 (1992).

2. "**Molecular Orbital and Resonance Raman Studies of the Structures of N,N'-Disubstituted Indigo Dyes** ", J. Abe, Y. Nagasawa, and H. Takahashi, *J. Chem. Phys*, 91(6), 3431-3434 (1989).

STUDIES ON A NEW TYPE OF ELECTRON TRANSFER FASTER THAN SOLVATION PROCESS

Yutaka Nagasawa

DOCTOR OF PHILOSOPHY

Department of Structural Molecular Science
School of Mathematical and Physical Science
The Graduate University for Advanced Studies

1993

Contents

CHAPTER I
INTRODUCTION

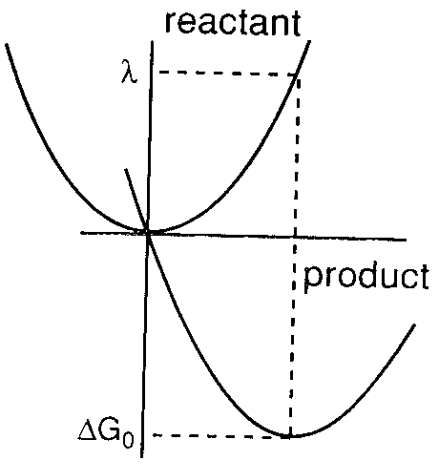

I-1. Transition state theory

Since electron transfer (ET) governs chemical processes of oxidation and reduction and thus is very important in chemistry, biology, and physics, it has been studied extensively for many years. For ET in solution, many theories have been developed on the basis of transition state theory (TST).[1] Therefore, as an introduction, I would like to mention the basis of TST of ET. For many cases, TST was applied successfully, however, with the recent development of ultrashort pulse lasers, cases are found, in which TST failed.

TST can be applied when the distribution of reactant is kept under equilibrium during the reaction. For simple linear reaction (A → B), reaction rate k_{TST} can be determined from three terms; (1) the population at the transition state $z_0^{-1}exp(\Delta G^*/k_BT)$, (2) the velocity of the reactant to cross the transition state v, and (3) the probability to become a product p. Therefore, simplest formula for k_{TST} can be written as;

$$k_{TST} = \frac{pv}{2z_0} \exp(-\frac{\Delta G^*}{k_BT}) \qquad \text{(I. 1)}$$

where z_0 is a partition function, ΔG^* an activation energy, k_B Boltzmann's constant, and T temperature. The factor 1/2 comes from an estimation that half of the reactant is moving toward product and half are not, at the transition state. For the exponential term, Marcus and many other researchers have studied the energy gap (free energy difference) dependence of ET. For the pre-exponential term, discussions on adiabaticity and non-adiabaticity of the reaction have been carried out. At the adiabatic limit, reaction rate should depend on solvent dynamics. Therefore, studies comparing reaction rate constants and the solvent relaxation times have been carried out.

I-2. Energy gap dependence

When it is assumed that the free energy surfaces of the reactant and product are quadratic function with a same curvature, the activation energy can be expressed as;[2]

$$\Delta G^* = \frac{(\lambda + \Delta G)^2}{4\lambda} \qquad \text{(I. 2)}$$

with reorganization energy λ, and the free energy gap ΔG of the reaction. The famous Marcus "inverted region" can be introduced by this simple expression. As is shown in Figure I-1, λ is the value of a free energy on the reactant surface at the position of the bottom of the product well. It is used to represent the deviation between the bottom of the reactant and product well. The energy gap dependence of ET rate can be separated in three regions, (a) $-\Delta G < \lambda$, the region where the reaction becomes faster as $-\Delta G$ increases. (b) $-\Delta G = \lambda$, the reaction occurs the fastest because the activation barrier vanishes. The free energy surface of the product crosses the bottom of the reactant surface. (c) $-\Delta G > \lambda$, the reaction become slower again as $-\Delta G$ increases. Therefore, the rate of ET shows a bell-shape energy gap dependence. Case (a) is called the "normal region", and (c) is called the "inverted region". Usually, the bell-shape is not symmetric, as is shown in Figure I-1, because of the effect of high frequency quantum mechanical mode.[3] In the inverted region, reaction also occurs to the vibrationally excited states of the product. Many experimentalists have tried to confirm the prediction of Marcus. Some of them observed Marcus inverted region but some did not.[4~8] The charge shift and charge recombination reaction showed a quite good bell-shape dependence while charge separation did not.

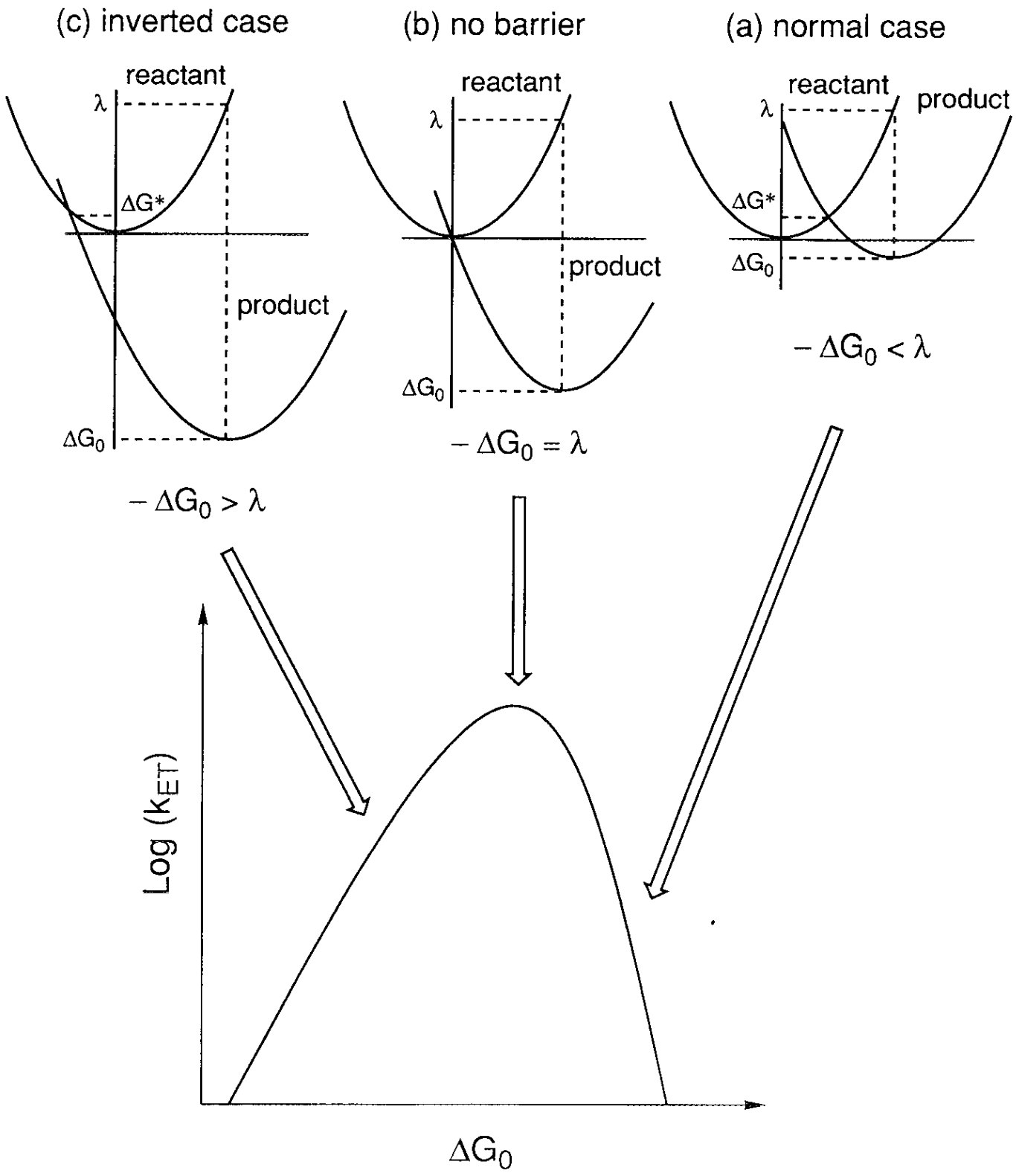

Figure I-1. Energy gap dependence of ET rate k_{ET} and its relation to the configuration of the free energy surfaces of reactant and product. The bell-shape is not symmetric because of the effect of high frequency quantum mechanical mode.

I-3. Adiabatic and non-adiabatic reaction in solution

The most of the theories treat the energy relaxation caused by solvent polarization as a driving force for the ET in solution. The importance of solvent polarization can be seen in many systems, which show no ET in the gas phase but in a polar solvent. Therefore, a solvent coordinate, which describes the solvent polarization, is used to express the free energy surface for ET. Polar solvent molecules organize around the solute molecule to minimize the dielectric interaction energy. Therefore, ET is treated as a process for the reactant to cross the transition state to the product by the fluctuation of surrounding solvent molecules. Before the reaction, the solvent and reactant molecules are in an equilibrium. Then a large fluctuation of the solvent brings the reactant to the transition state. After reaching the transition state, reaction takes place by probability p. Then the excess energy will be disposed into the solvent heat bath and the system relaxes to a new equilibrium for the product. The reorganization of the solvent molecules are often treated as infinitely fast.

For simplicity, normalized solvent coordinate x_S is often used to describe ET. The coordinate is normalized for the bottom of the reactant energy surface to be at 0, and that of the product at 1. Therefore, when linear response of the solvent polarization against instantaneous change in solute dipole is assumed, the free energy surface for the reactant $G_r(x_S)$ and product $G_p(x_S)$ can be written as;[9,10]

$$G_r = \lambda_S x_S^2 \qquad \text{(I. 3)}$$

$$G_p = \lambda_S(x_S - 1)^2 + \Delta G \qquad \text{(I. 4)}$$

where λ_S is a reorganization energy on the solvent coordinate.

The probability p can be determined by the electronic matrix element V_{el} in the case of ET. V_{el} is an overlap integral between the wave function of the reactant and product. When V_{el} is small, the free energy surface becomes non-adiabatic, and when it is large, the surface becomes adiabatic. To make this distinction clearer, a region called Landau-Zener (LZ) region is defined. The length of LZ region l_{LZ}, shown in Figure I-2 (a), is defined by;[11]

$$l_{LZ} = \frac{2V_{el}}{G_r' - G_p'} = \frac{V_{el}}{\lambda_s} \qquad \text{(I. 5)}$$

where G_r' and G_p' are the differential of the both surface. When l_{LZ} is much smaller than the mean-free-path l_{mfp} of a imaginary particle fluctuating on the energy surface, the reaction becomes non-adiabatic, and when $l_{LZ} >> l_{mfp}$, the reaction becomes adiabatic. The mean-free-path l_{mfp} is the length of the path before the fluctuating particle changes its direction.

When reaction is non-adiabatic ($l_{LZ} << l_{mfp}$), as is shown in Figure I-2 (b), the particle crosses the LZ region ballistically. Therefore, the velocity v can be determined from the temperature and the effective mass of the imaginary particle m;

$$v = \sqrt{\frac{k_B T}{\pi m}} \qquad \text{(I. 6)}$$

The probability p will be proportional to the ratio between the time for the reactant to stay in the LZ region t_{LZ}, and the time needed for the transition from the reactant to the product state t_{hop};

$$p = 2\pi \frac{t_{LZ}}{t_{hop}} = 2\pi \left(\frac{l_{LZ}}{v}\right) / \left(\frac{\hbar}{V_{el}}\right) = 2\pi \frac{V_{el}^2}{\hbar v \lambda_s} \qquad \text{(I. 7)}$$

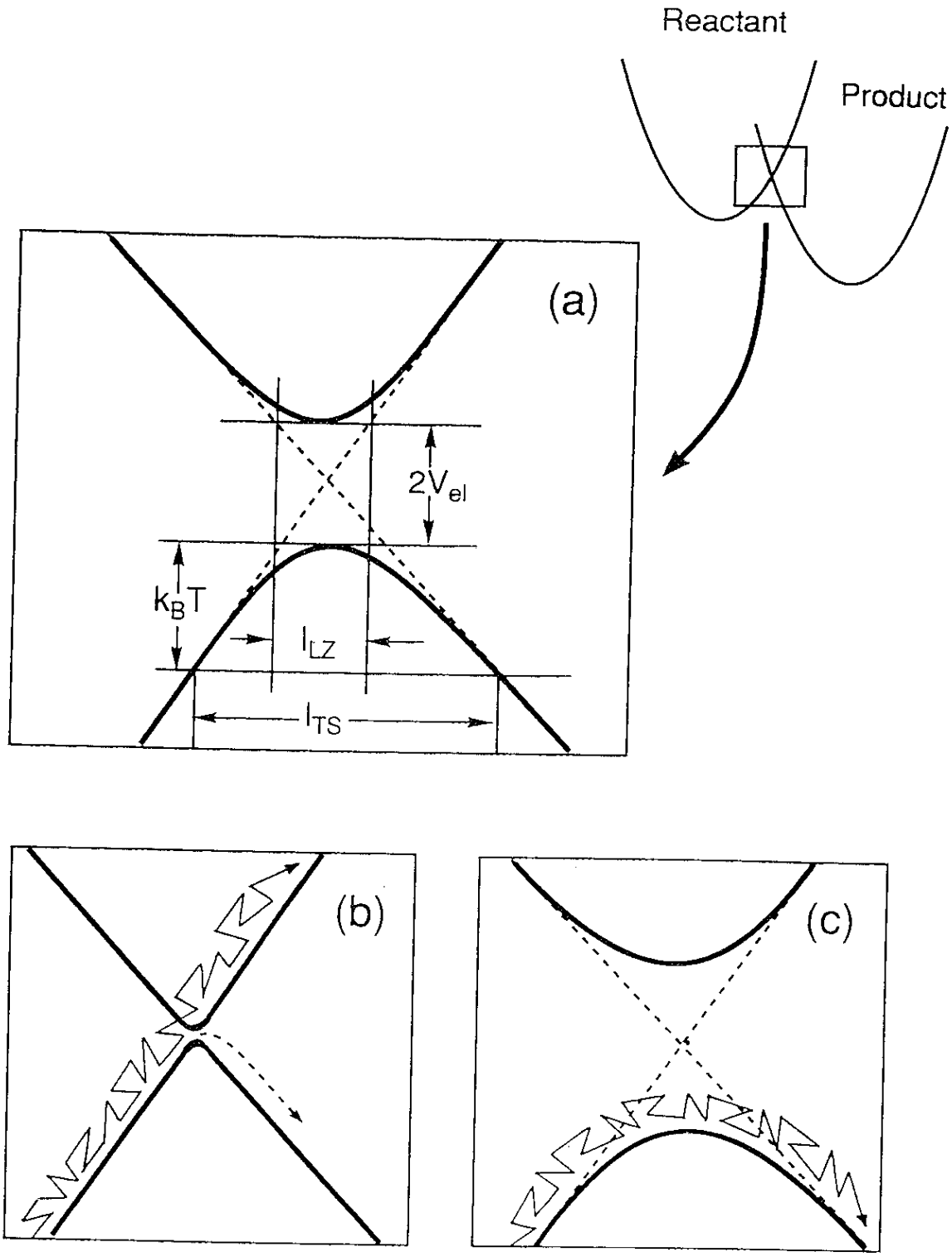

Figure I-2. (a) Definition of the LZ and transition state regions and estimate of the corresponding lengths l_{LZ} and l_{TS}. (b) Shape of the barrier top for non-adiabatic reaction and (c) strongly adiabatic reaction.

where $\hbar$ is Planck's constant, and t_{hop} is treated to be $\hbar/V_{el}$ from the uncertainty principle. Therefore, p depends on V_{el}. In non-adiabatic case, the rate of ET can be written as;[10]

$$k_{NA} = \frac{2\pi}{\hbar} \frac{V_{el}^2}{\sqrt{4\pi\lambda_s k_B T}} \exp(-\frac{\Delta G^*}{k_B T}) \qquad \text{(I. 8)}$$

When reaction is adiabatic ($l_{LZ} >> l_{mfp}$.), p becomes unity, and the velocity v is determined by the solvent fluctuation. As it is shown in Figure I-2 (c), the particle crosses the transition state by Brownian motion. Therefore, the rate for the reactant to cross the transition state will be determined by the length of the transition state l_{TS} and the time for the reactant to stay in the transition state t_{TS};

$$v_{TS} = \frac{l_{TS}}{t_{TS}} \qquad \text{(I. 9)}$$

The transition state is defined as the neighborhood of the activation maximum differing in energy by less than the thermal energy $k_B T$ (see Figure I-2 (a)). The length of this region can be written as;

$$l_{TS} = k_B T \left(\frac{1}{|G'_r|} - \frac{1}{|G'_p|}\right) \cong \frac{2k_B T}{\lambda_s} \qquad \text{(I. 10)}$$

t_{TS} can be written as;

$$t_{TS} = \frac{l_{TS}^2}{2D} \qquad \text{(I. 11)}$$

where D is the diffusion constant for solvent polarization;

$$D = \frac{k_B T}{\eta} \qquad \text{(I. 12)}$$

where η is the coefficient of dielectric friction;

$$\eta = m\omega^2 \tau_s \qquad \text{(I. 13)}$$

where $\omega = (2\lambda_s / m)^{1/2}$, τ_s is the solvent relaxation time. Therefore the adiabatic rate can be written as;[10]

$$k_A = \frac{1}{\tau_s} \sqrt{\frac{\lambda_s}{16\pi k_B T}}\, exp(-\frac{\Delta G^*}{k_B T}) \qquad \text{(I. 14)}$$

The reaction is called solvent-controlled adiabatic reaction, the rate is proportional to the inverse of τ_s. At room temperature, $16\pi k_B T = 1.2$ eV, and the value of λ_s is usually smaller than this. Therefore, the maximum of k_A is about $1/\tau_s$. In TST, solvent fluctuation is treated to be infinitely fast compared to the actual reaction. However, the actual τ_s has a finite value, it is usually in the order of picoseconds. Thus, for ultrafast ET occurring in picosecond time regime, solvent fluctuation should be the limiting step. This kind of effect has become observable only recently with the development of ultrashort pulse lasers.

Recently the dependence of ET rate on diffusive solvation processes has been found in strongly polar solvents.[12~15] Kosower *et al.* examined the excited state intramolecular electron transfer of arylaminonaphthalene sulphonates in alcohol solutions.[12] They found a correlation between the ET rate and the inverse of longitudinal relaxation time τ_L of the solvent as shown in Figure I-3. The τ_L is a solvent

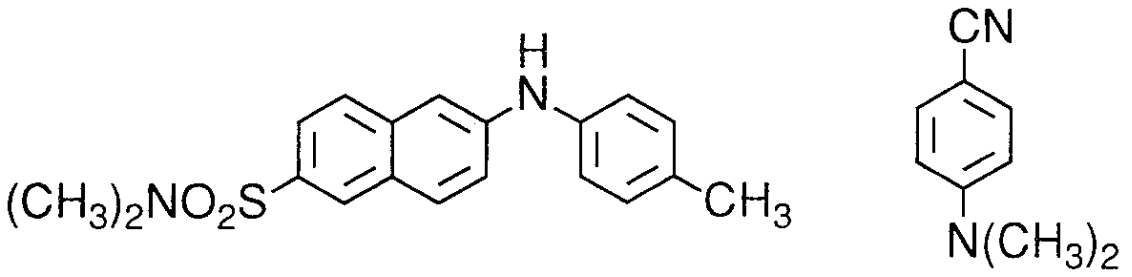

TNSDMA DMABN

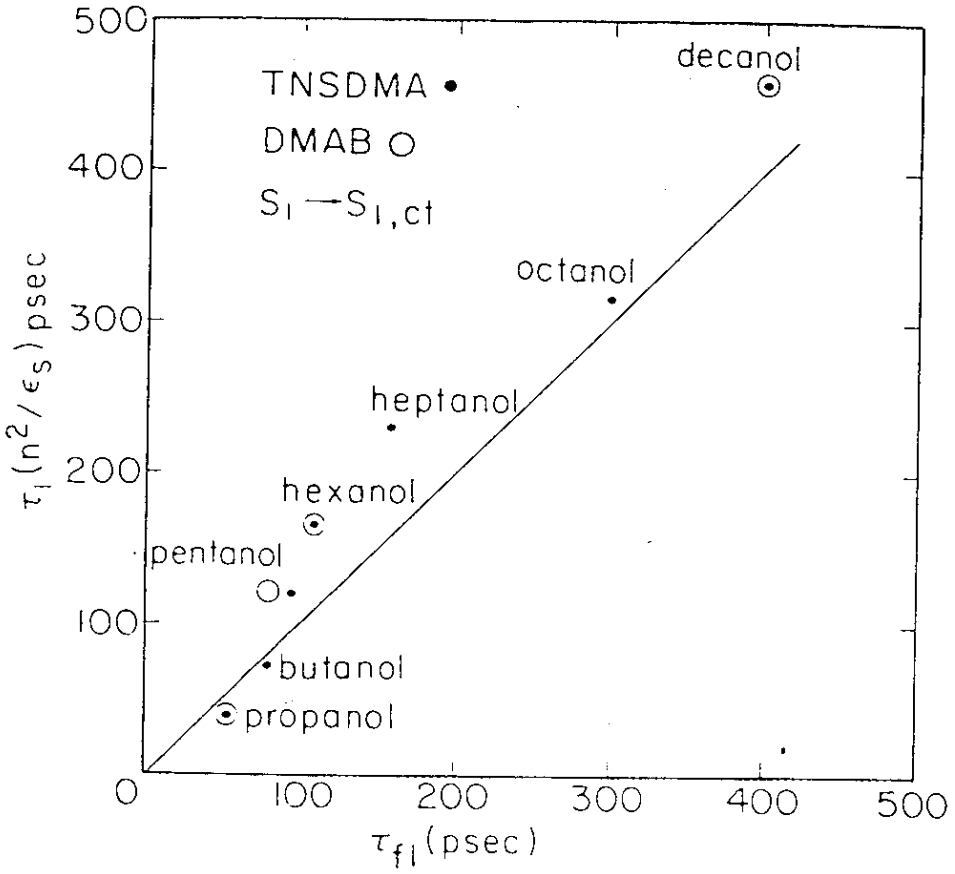

Figure I-3. A plot of the longest longitudinal relaxation times for linear alcohols, $\tau'_l = (\varepsilon / \varepsilon_s)\tau_D$, versus the fluorescence lifetimes for the S_1 state of TNSDMA [6-(4-methylphenyl)amino-2-naphthalenesulfon-N,N-dimethylamide] and the S_1 state of DMABN (*p*-dimethylaminobenzonitrile). The factors, $\varepsilon = n^2$ and ε_S, are the high-frequency and static dielectric constants, respectively. (Kosower *et al.*, *Chem. Phys. Let.*, **96**, 433, (1983))

relaxation time calculated from the Debye relaxation time τ_D, using the following equation;[16]

$$\tau_L = \frac{\varepsilon_\infty}{\varepsilon_0} \tau_D \qquad \text{(I. 15)}$$

where ε_∞ and ε_0 are the high and low frequency dielectric constant, respectively. τ_D is obtained by dielectric measurements. Kang *et al.* studied the charge separation of bianthryl from locally excited state to the charge transferred state.[13] They found this activation-less ET to be solvent-controlled adiabatic reaction. Same kind of adiabatic process was also found for 4-(9-anthryl)-N,N,-dimethylaniline (ADMA).[14,15] The internal conversion from S_2 to S_1 state of ADMA was faster than the system response, however, the following process on the S_1 state was solvent controlled.

I-4. Reactions beyond transition state theory

Predictions made by TST and confirmations made by recent ultrafast experiments were mentioned above. However, very recently, ET reactions much faster than solvation process was found.

Kobayashi *et al.* studied fluorescence decays of electron acceptor dyes in electron donor solvents.[17] They found a fluorescence quenching as fast as ~100 fs for Nile blue A perchlorate (NB) in N,N-dimethylaniline (DMA), and somewhat slower non-exponential fluorescence quenching in aniline (AN) (see Figure I-4). They concluded that the fluorescence quenching is due to intermolecular ET from the solvent to the dye. Kandori *et al.* observed anion of the dye and cation of the solvent by sub-picosecond transient absorption measurement.[18] Usually, τ_L of mono substituted benzenes are in the order of picoseconds, *e.g.*, 4.2 ps for chlorobenzene,[19] 5.7 ps for benzonitrile,[20] 4.8 ps for toluene,[21] and 7.4 ps

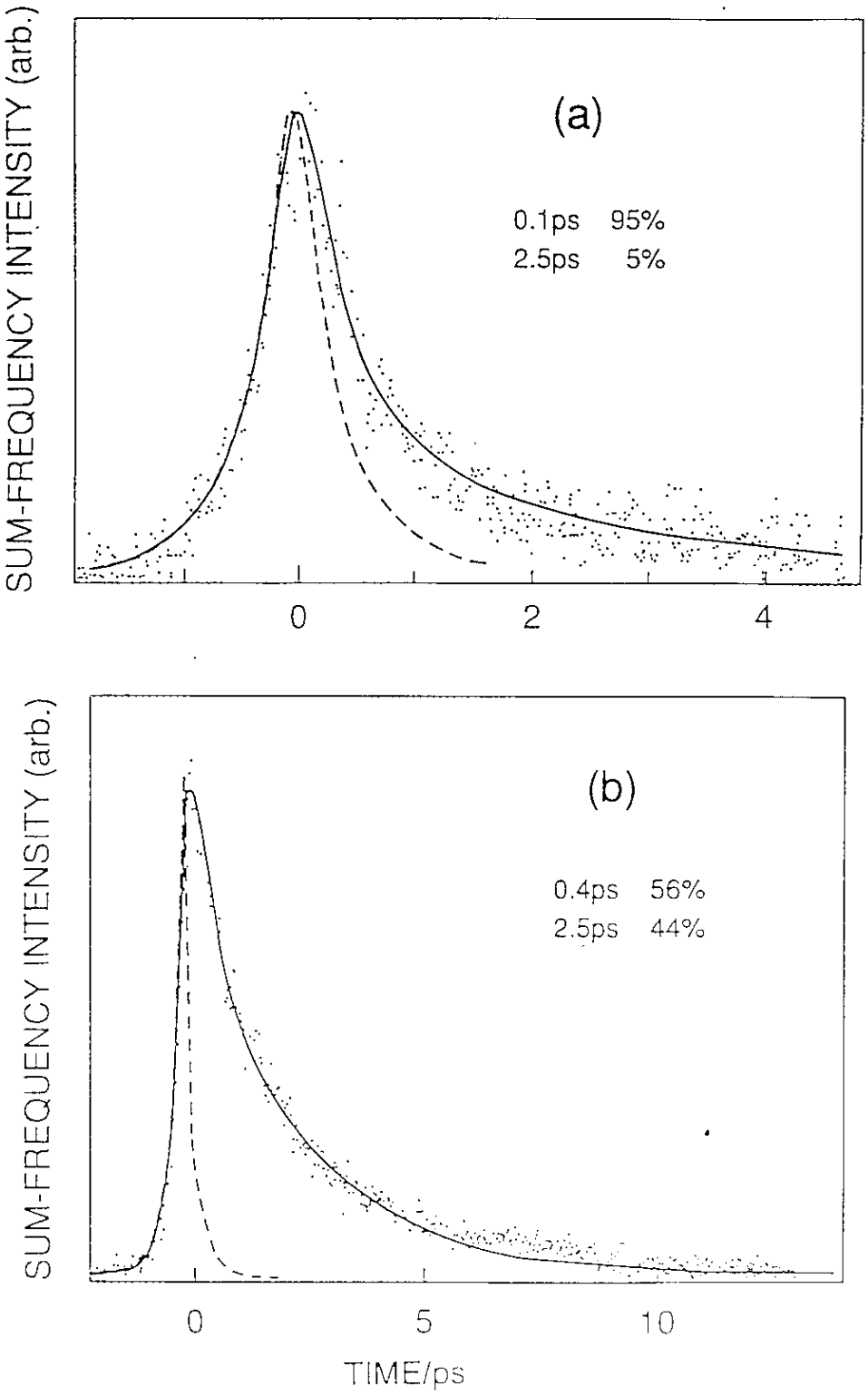

Figure I-4. Fluorescence decays of NB in (a) DMA and (b) AN with a double-exponential fit (solid line). The observation wavelength is 690 nm. The broken line indicates the auto-correlation function of the laser.
(Kobayashi et al., *Chem. Phys. Let.*, **180**, 416, (1991))

for bromobenzene.[19] Therefore, they assumed that the ET of NB in DMA is occurring 50 times faster than the diffusive solvent relaxation process. They concluded that these observations are due to weak polarity of DMA. For weakly polar solvents, the solvent reorganization process becomes less important for the reaction. In such a case, reaction becomes much similar to the ones in the gas phase; the vibrational nuclear reorganization becomes important. The vibrational motion is much faster than the solvent motions, thus the reaction can precede the solvent relaxation process.

Tominaga *et al.* also found ET faster than diffusive solvation process for the intramolecular ET in a metal-metal charge transfer complex.[22] They introduced not only the effect of vibrational motions but also the effect of inertial component of solvation. Inertial solvation component as fast as 60 fs was observed in acetonitrile by Rosenthal *et al.*[23] If the amount of energy relaxation caused by the inertial process is larger than that caused by the diffusive process, it may dominate the rate of ET.

When ET occurs much faster than diffusive solvation process, the distribution on the solvent coordinate may change during the reaction. TST no longer holds in such a case, therefore, non-exponential reaction is often observed. These ultrafast ET can be caused by vibrational motion or inertial process of solvation. The effect of high frequency vibration was first introduced theoretically by Jortner and Bixon,[3] however, it was still based on TST. Sumi and Marcus introduced the effect of classical vibration to the ultrafast ET.[24] The significance of this theory was to divide the reaction coordinate into two coordinates; vibrational nuclear coordinate and solvent coordinate. This theory succeeded in explaining the non-exponential feature of ultrafast ET.

In this thesis, detailed studies of ultrafast ET observed in the system of electron acceptor dyes in donor solvents are carried out. In Chapter II, experimental apparatus, mainly femtosecond up-conversion system, is

described. In Chapter III, measurements of the solvent relaxation times are carried out to confirm that the ET in this system is occurring faster than the solvation process. In Chapter IV, detailed studies of ET, mainly temperature dependence and simulations based on Sumi-Marcus Jortner-Bixon hybrid model[25] are carried out. In Chapter V, substituent effect, energy gap dependence, and chemical timing effect of ET is discussed. In Chapter VI, deuterium isotope effects are discussed.

References for Chapter I

1. S. Glasstone, K. J. Laidler, and H. Eyring, "*The Theory of Rate Processes*", McGraw-Hill Book Company, Inc., Nwew York, (1941).
2. R. A. Marcus, *Discuss. Faraday Soc.*, **29**, 21, (1960).
3. J. Jortner and M. Bixon, *J. Chem. Phys.*, **88**, 167, (1988).
4. M. A. Wasielewski, M. P. Niemczyk, W. A. Svec, and E. B. Pewitt, *J. Am. Chem. Soc.*, **107**, 1080, (1985).
5. J. R. Miller, L. T. Calcaterra, and G. L. Closs, *J. Am. Chem. Soc.*, **106**, 3047, (1984).
6. N. Mataga, T. Asahi, Y. Kanda, T. Okada, and T. Kakitani, *Chem. Phys.*, **127**, 249, (1988).
7. T. Asahi and N. Mataga, *J. Phys. Chem.*, **93**, 6675, (1989).
8. D. Rehm and A. Weller, *Israel J. Chem.*, **63**, 4358, (1975).
9. R. A. Marcus, *J. Chem. Phys.*, **24**, 976, (1956).
10. R. A. Marcus, *J. Chem. Phys.*, **43**, 679, (1965).
11. H. Heitele, *Angew. Chem. Int. Ed. Engl.*, **32**, 359, (1993).
12. E. M. Kosower and D. Huppert, *Chem. Phys. Lett.*, **96**, 433, (1983).
13. T. J. Kang, W. Jarzeba, P. F. Barbara, and T. Fonseca, *Chem. Phys.*, **149**, 81, (1990).
14. K. Tominaga, G. C. Walker, W. Jarzeba, and P. F. Barbara, *J. Phys. Chem.*, **95**, 10475, (1991).
15. K. Tominaga, G. C. Walker, T. J. Kang, P. F. Barbara, and T. Fonseca, *J. Phys. Chem.*, **95**, 10485, (1991).
16. A. Mozumder, *J. Chem. Phys.*, **50**, 3153, (1969).
17. T. Kobayashi, Y. Takagi, H. Kandori, K. Kemnitz, and K. Yoshihara, *Chem. Phys. Lett.*, **180**, 416, (1991).
18. H. Kandori, K. Kemnitz, and K. Yoshihara, *J. Phys. Chem.* **96**, 8042, (1992).

19. D. F. Calef and P. G. Wolynes, *J. Phys. Chem.*. **87**, 3387, (1983).

20. T. Genett, D. F. Milner, and M. J. Weaver, *J. Phys. Chem.*, **89**, 2787, (1985).

21. R. J. Harrison, B. Pearce, G. S. Beddard, J. A. Cowan, and J. K. M. Sanders, *Chem. Phys.*, **116**, 429, (1987).

22. K. Tominaga, D. A. V. Kliner, A. E. Johnson, N. E. Levinger, and P. F. Barbara, *J. Chem. Phys.*, **98**, 1228, (1993).

23. S. J. Rosenthal, X. Xie, M. Du and G. R. Fleming, *J. Chem. Phys.*, **95**, 4715, (1991) .

24. H. Sumi and R. A. Marcus, *J. Chem. Phys.*, **84**, 4894, (1986).

25. G. C. Walker, E. Akesson, A. E. Johnson, N. E. Levinger, and P. F. Barbara, *J. Phys. Chem.*, **96**, 3728, (1992).

CHAPTER II
EXPERIMENTAL

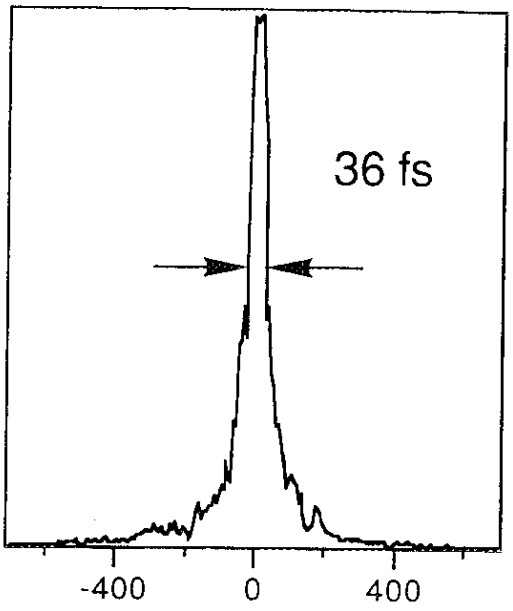

II-1. Femtosecond dye laser system

A homemade passive mode-locked dye laser synchronously pumped by the second harmonic generation (SHG) of Nd YAG laser is shown in Figure II-1. It was used for the experiments of oxazines. The dye laser cavity contains, gain dye jet, saturable absorber jet, and prism pair. This type of femtosecond linear-cavity dye laser was first reported by Dawson *et al.*[1,2] The dye laser was pumped at 532 nm with average power of 1.5 W and repetition rate of 76 MHz. The pump beam was coupled into the gain jet by a focusing mirror with a radius of curvature of 5 cm. The folded focusing section around the gain jet consist of two mirrors, each with a radius of curvature of 7.5 cm. The focusing mirrors for the absorber jet had 3.75 cm radius of curvature. All the mirrors used were normally 100 % reflective around ~600 nm, except the output coupler which had a reflectivity of ~90 %. The thickness of the nozzles, producing a vertical jet stream, were ~400 μm for the gain jet and ~80 μm for the absorber jet. Combination of rhodamine 6G (R6G) and DODCI/DQOCI, or sulforhodamine 101 (SR101) and DQTCI, were used as a gain medium and a saturable absorber, respectively. The dyes were dissolved in ethylene glycol. The solution of the gain dye were changed once a year, and the absorber dye were changed once a weak. The group velocity dispersion (GVD) of the dye laser was compensated by a prism pair inside the laser cavity. The beam had a Brewster's-angle incidence at each surface of the prisms. Spatial cutters between the second prism and the end mirror were used to select the oscillation wavelength.

For R6G, stable oscillation with an output power of ~100 mW and pulse duration of ~80 fs, can be obtained at 583, 605, and 615 nm. The pulse shape is assumed to be hyperbolic secant. The most stable oscillation was achieved at 605 nm. For SR101, stable oscillation with output power of ~80 mW and pulse duration of ~60 fs, were achieved at 675 nm, however, stability was worse than R6G. The record of the shortest pulses achieved, were ~60 fs for R6G and ~35 fs for SR101, however, they were too unstable for any experimental use. The

autocorrelation traces of the pulses achieved by the dye laser are shown in Figure II-4.

Even for the most stable pulse, the pulse duration changed within ~20 minutes. Therefore, dye laser cavity length has to be artificially optimized during the long-time measurement. To minimize the unstability, many efforts have been done. The dye laser is placed on super invar plate to minimize the thermal fluctuation of the cavity length. Active amplitude stabilizer (AAS) is used for the YAG laser to minimize the power fluctuation and pointing unstability. Even when AAS is used, the position of the YAG laser beam changes day by day when it is turned on. Therefore, as is shown in Figure II-1, YAG laser beam spot on the wall penetrated from the third mirror is marked. Everyday, when laser is turned on, the position of the beam is optimized by the first and second mirror to hit the mark on the wall.

II-2. Fluorescence up-conversion measurement using dye laser

Fluorescence decays of oxazines were measured using a femtosecond fluorescence up-conversion system[3,4] shown in Figure II-2. A prism pair outside the dye laser for GVD precompensation was used so that the smallest width of crosscorrelation was achieved. When hyperbolic secant pulse is assumed, the crosscorrelation corresponded to ~80 fs pulse duration at ~605 nm. The angle between the polarization of pump and probe beam was set to the magic angle by $\lambda/2$ plate. The thickness of the BBO crystal (type I) to generate the sum-frequency was 0.3 mm. The up-converted signal was measured with a photon counting system after a monochromator. The principle of this method is shown in Figure II-5.

Oxazine 1 perchlorate (OX1) was obtained from Eastman Kodak Co. and used without further purification. Aniline (AN) and N,N-dimethylaniline (DMA) were distilled under low pressure argon atmosphere right before the experiment. The dye concentration of the sample was 5×10^{-4} M and the

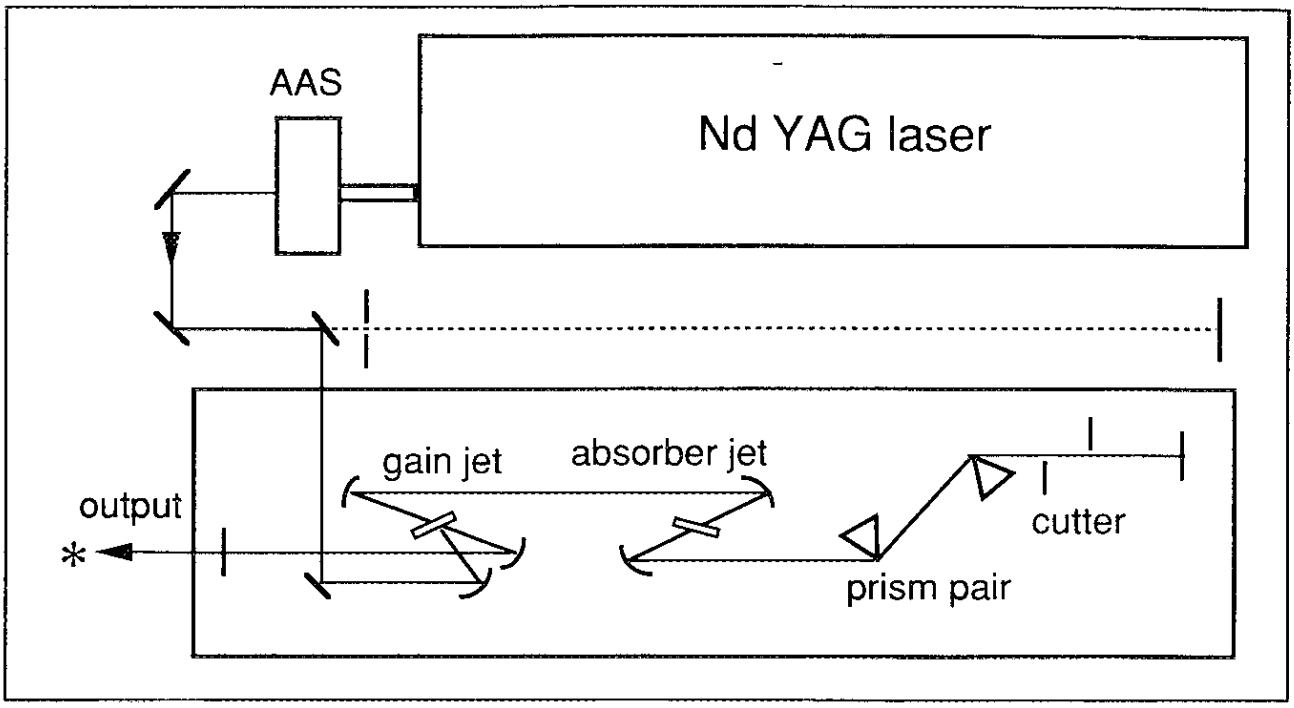

Figure II-1. Homemade passive mode-locked dye laser synchronously pumped by Nd YAG laser. AAS stands for active amplitude stabilizer.

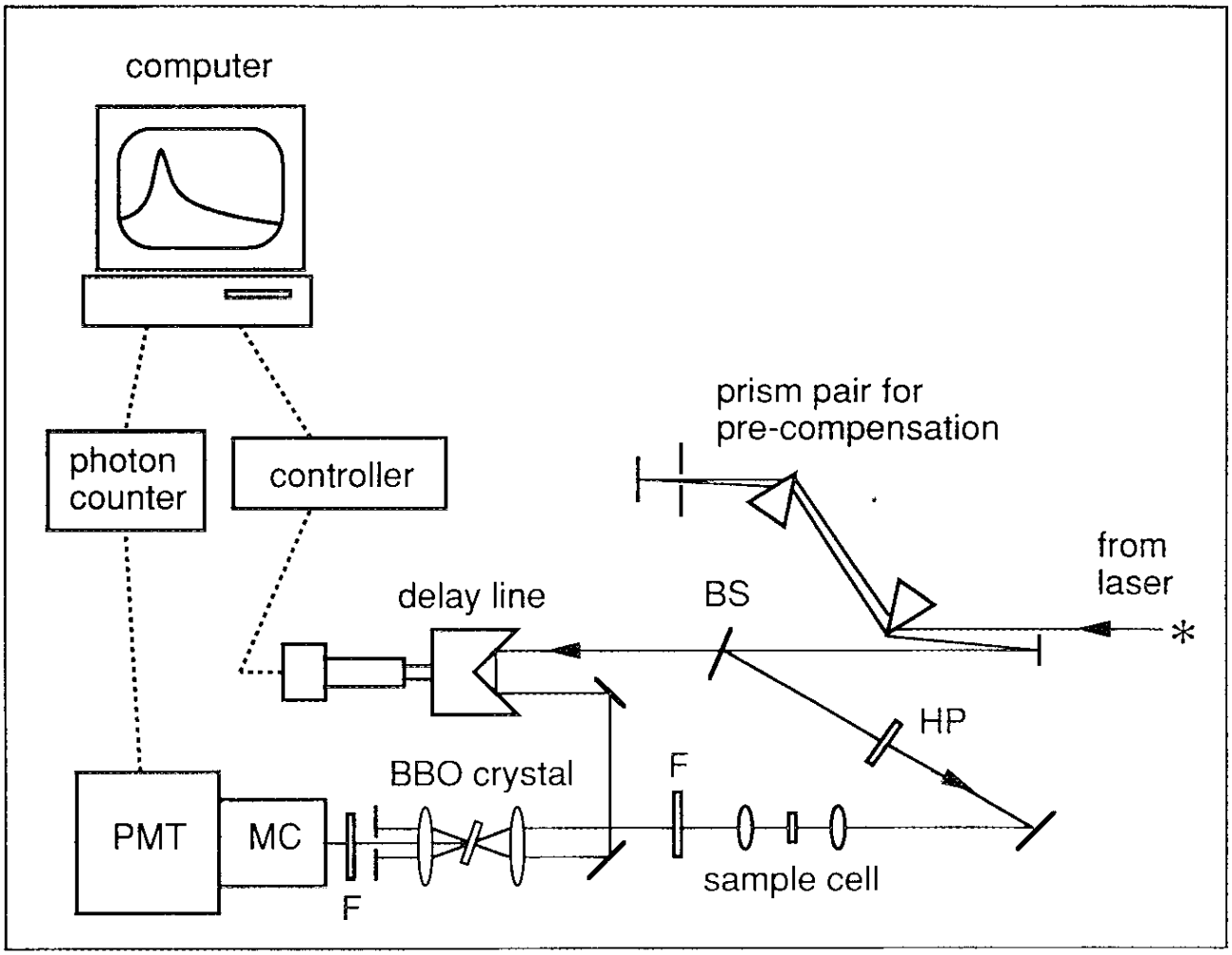

Figure II-2. Fluorescence up-conversion system for the dye laser. BS: beam splitter, HP: half-wave plate, F: filter, MC: monochromator, and PMT: photo multiplier tube.

thickness of the sample cell was 1 mm. Dye solutions were bubbled with argon gas and circulated by micro-pump. For the temperature dependence experiment, samples were heated in oil bath or cooled in ice water during experiments. OX1 was stable in the electron donating solvents at 373 K for ~8 hours.

Analysis of measured kinetics was performed by the "Global Unlimited" fitting program. The crosscorrelation was chosen as a system response function.

II-3. Fluorescence up-conversion measurement using Ti: sapphire laser

Ultrafast fluorescence decays of coumarins were measured using a femtosecond fluorescence up-conversion system shown in Figure II-3. The mode-locked Titanium: sapphire laser oscillates around ~800 nm with a repetition rate of 82 MHz and an average power of ~450 mW. Second-harmonic light (395 nm) was generated in 1 mm BBO crystal (type I), with an average power of ~45 mW, and used to excite the sample. The remaining fundamental was used to up-convert the fluorescence from the sample in a 0.2 mm BBO crystal (type I). The angle between the polarization of pump and probe beam was set to the magic angle by $\lambda/2$ plate. The crosscorrelation measured between SHG pump beam and fundamental probe beam had a full-width-half-maximum of 330 fs. It was reduced to 150 fs when the quartz lenses, which were used to excite the sample and collect the fluorescence, were changed to reflective mirror optics. Some of the crosscorrelation traces are shown in Figure II-4. The up-converted signal was measured with the photon counting system after a monochromator. The dye concentration of the samples were 2×10^{-3} M and the thickness of the sample cell was 1 mm. The samples were circulated by micro-pump and degassed by argon gas during the measurements. Analysis of measured kinetics was performed by the "Global Unlimited" fitting program. The crosscorrelation was chosen as a system response function.

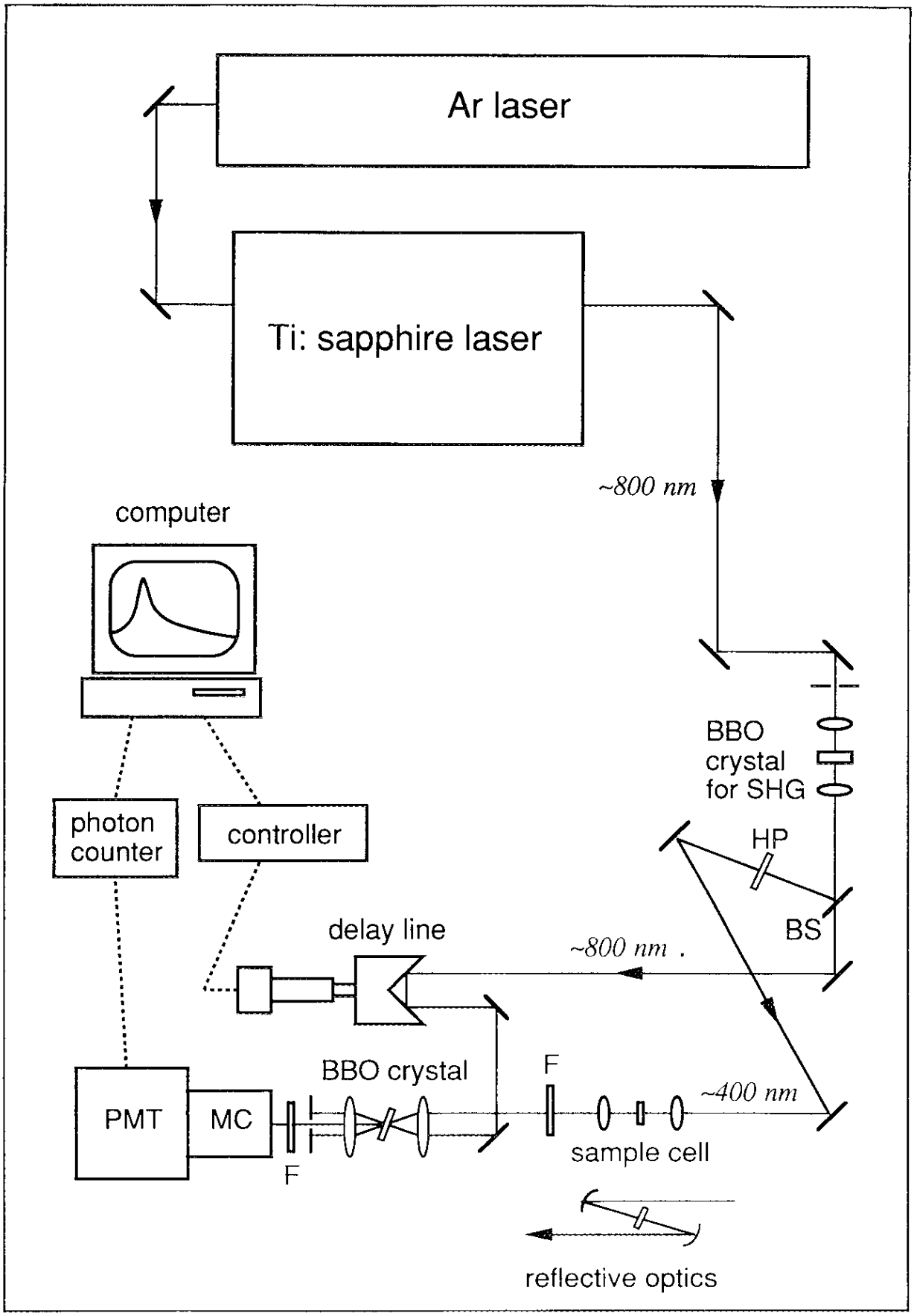

Figure II-3. Fluorescence up-conversion system for the Ti: sapphire laser. SHG: second harmonic generation, BS: beam splitter, HP: half-wave plate, F: filter, MC: monochromator, and PMT: photo multiplier tube.

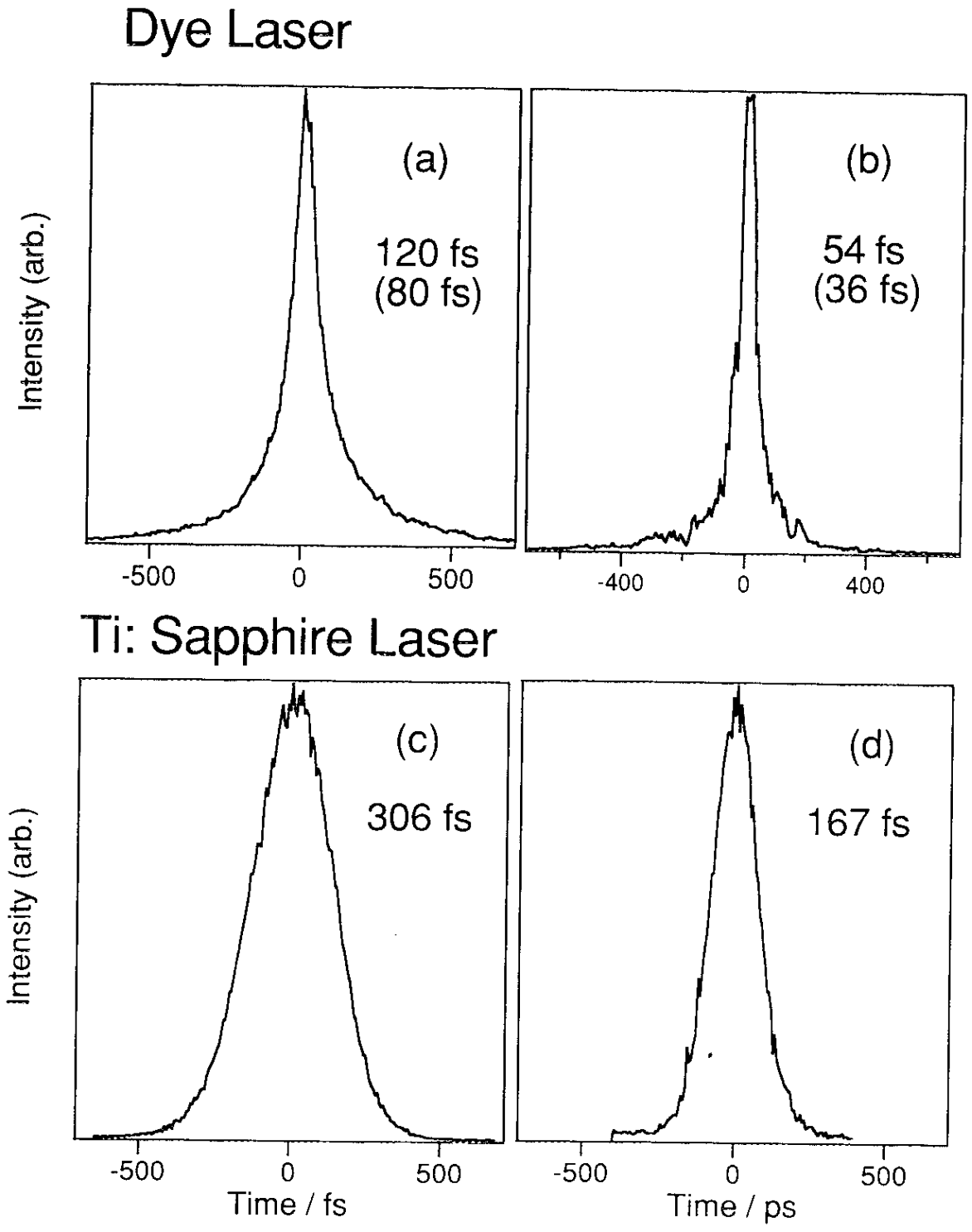

Figure II-4. (a) Typical autocorrelation trace of the dye laser oscillating at 605 nm. (b) Shortest autocorrelation trace for the dye laser at 675 nm. (c) Crosscorrelation between the fundamental and SHG of Ti: sapphire laser measured by up-conversion system with quartz lenses used for the sample excitation and fluorescence collection. (d) Crosscorrelation of Ti: sapphire laser with reflective optics. The value of full-width-half-maximum is shown in each set. The values in ( ) are the pulse durations, when hyperbolic secant pulse shape is assumed.

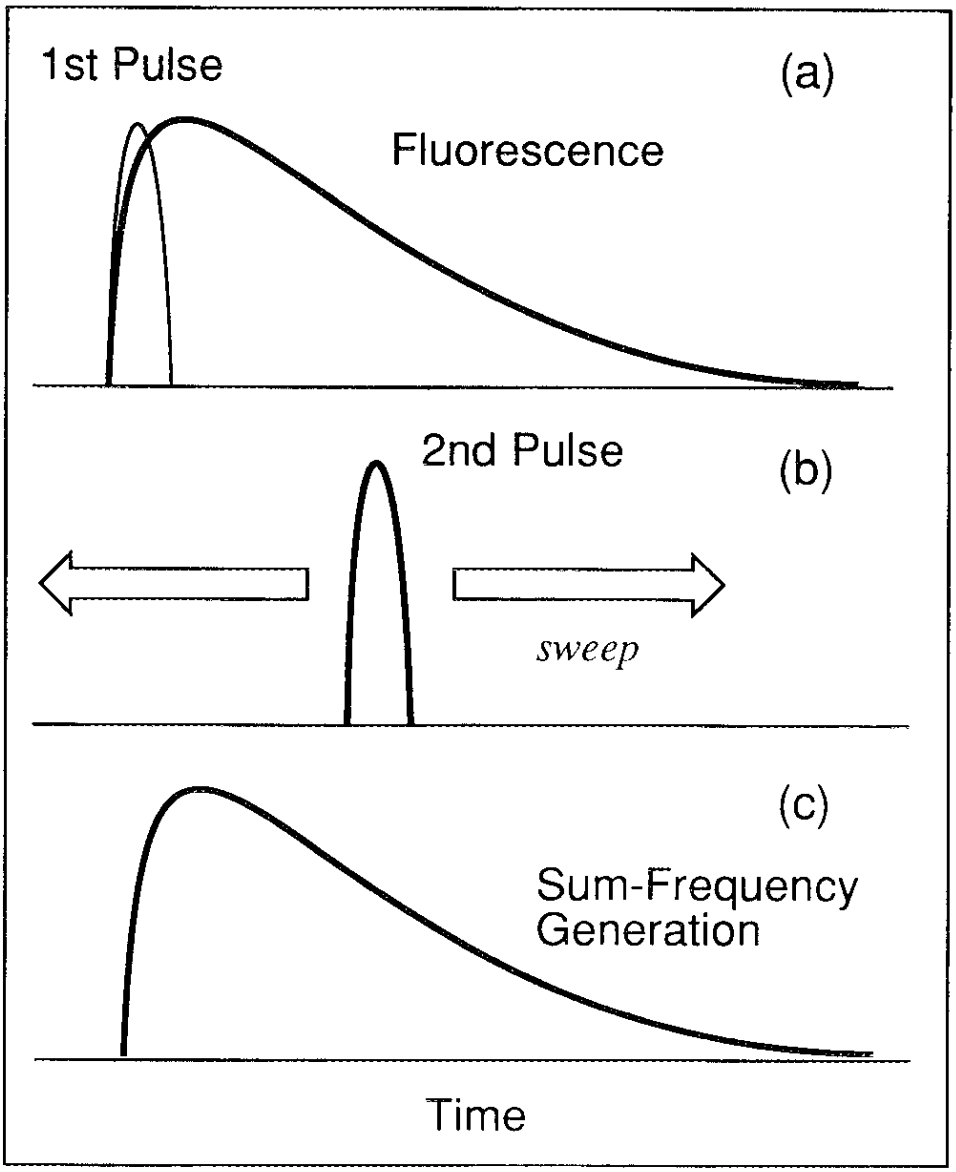

Figure II-5. Principle of fluorescence up-conversion method. (a) Fluorescence is generated by the first pulse. (b) The delay between the first and second pulse is varied. (c) Sum-frequency is generated between the fluorescence and the second pulse. If the intensities of the pulses do not change, the intensity of the sum-frequency will be propotional to the intensity of the fluorescence.

Laser grade coumarin dyes were purchased from Lambda Physik, Eastman Kodak, and Exciton and used without further purification. AN and DMA was distilled at low pressure in argon atmosphere right before measurement.

II-4. Picosecond time-correlated single photon counting and steady-state measurements

Picosecond time-correlated single photon counting measurement was carried out to measure the fluorescence decays of coumarins with long lifetimes. The details of the apparatus have been already reported.[5] The system used in this work employed a CW mode-locked YAG laser to synchronously pump a dye laser with a cavity dumper (4 MHz). Styryl 8 was used for the dye laser to oscillate at 720 nm. Second harmonic at 360 nm was generated in a KTP crystal to excite the sample. The signal was measured with the photon counting system after a monochromator at the magic angle condition. The time resolution of the apparatus was ~50 ps. The concentration of the sample was 1×10^{-5} M and a 1 cm cell was used without circulation.

The steady-state absorption spectra were measured by Shimadzu UV-VIS-NIR recording spectrophotometer UV-3100 and fluorescence spectra by Jasco spectrofluorometer FP-777, respectively.

II-5. Electrochemical measurements

Cyclic voltammetries of oxazines and coumarins were carried out using Pt working, Pt wire auxiliary, and SSCE reference electrodes. The dye concentration of the sample was 2×10^{-3} M. Tetra-n-butylammonium perchlorate purchased from Nacalai Tesque was used as a supporting electrolyte at a concentration of 0.1 M

References for Chapter II

1. M. D. Dawson, T. E. Boggess, D. W. Garvey, and A. L. Smirl, *Opt. Comm.*, **60**, 79, (1986).

2. M. D. Dawson, T. E. Boggess, D. W. Garvey, and A. L. Smirl, *IEEE J. Quant. Elect.*, **23**, 290, (1987).

3. J. Shah, *IEEE J. Quan, Elec.*, **24**, 276, (1988).

4. M. A. Kahlow, W. Jarzeba, T. P. DuBuruil, and P. F. Barbara, *Rev. Sci. Instrum.*, **59**, 1098, (1988).

5. K. Kemnitz, N. Nakashima, and K. Yoshihara, *J. Phys. Chem.*, **92**, 3915, (1988).

CHAPTER III
SOLVENT RELAXATION TIMES OF ELECTRON DONATING SOLVENTS

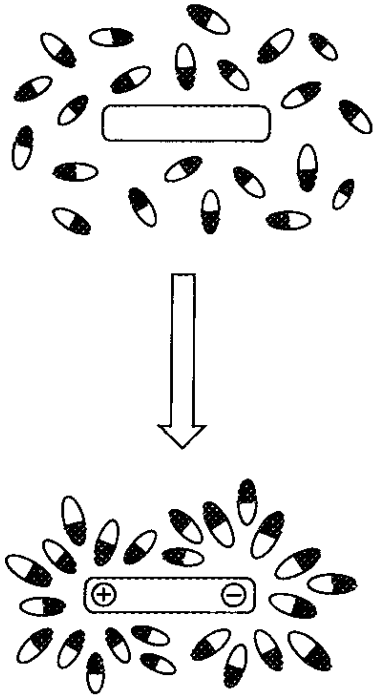

III-1. Solvent relaxation times of electron donating solvents

Kobayashi *et al.* predicted that ET in weakly-polar electron donating solvents occurs much faster than the diffusive solvent relaxation process[1]. To confirm this prediction, the measurement of solvent relaxation time is carried out and it is described in this chapter. The dynamic fluorescence Stokes shift was used to determine solvent relaxation times of the donor solvents (DMA and AN). The idea of this experiment is illustrated in Figure III-1. When a probe dye molecule is photo-excited, the dipole moment of the molecule increases instantaneously. The polarization of the surrounding solvent molecule responds to this change and starts to reorganize. Therefore, the energy relaxation process, caused by the solvent reorganization, shifts the fluorescence spectrum to longer wavelengths. To extract dynamical information of solvent relaxation process, the normalized spectral shift correlation function $C(t)$ was measured;[2]

$$C(t) = \frac{\nu(t) - \nu(\infty)}{\nu(0) - \nu(\infty)} \qquad \text{(III. 1)}$$

where $\nu(t)$, $\nu(\infty)$, and $\nu(0)$ are the fluorescence peak frequencies at times, t, ∞, and 0, respectively. For this method, a probe molecule which undergoes a large instantaneous change of dipole moment upon photo-excitation has to be chosen. Coumarin dyes are often used as probe molecules for this type of experiment.[3~5] Coumarin 102 (C102), which has a lifetime of 2.8 ns in DMA and 1.4 ns in AN, is the choice for this experiment. ET of coumarins will be discussed in Chapter V.

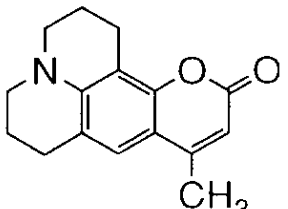

C102

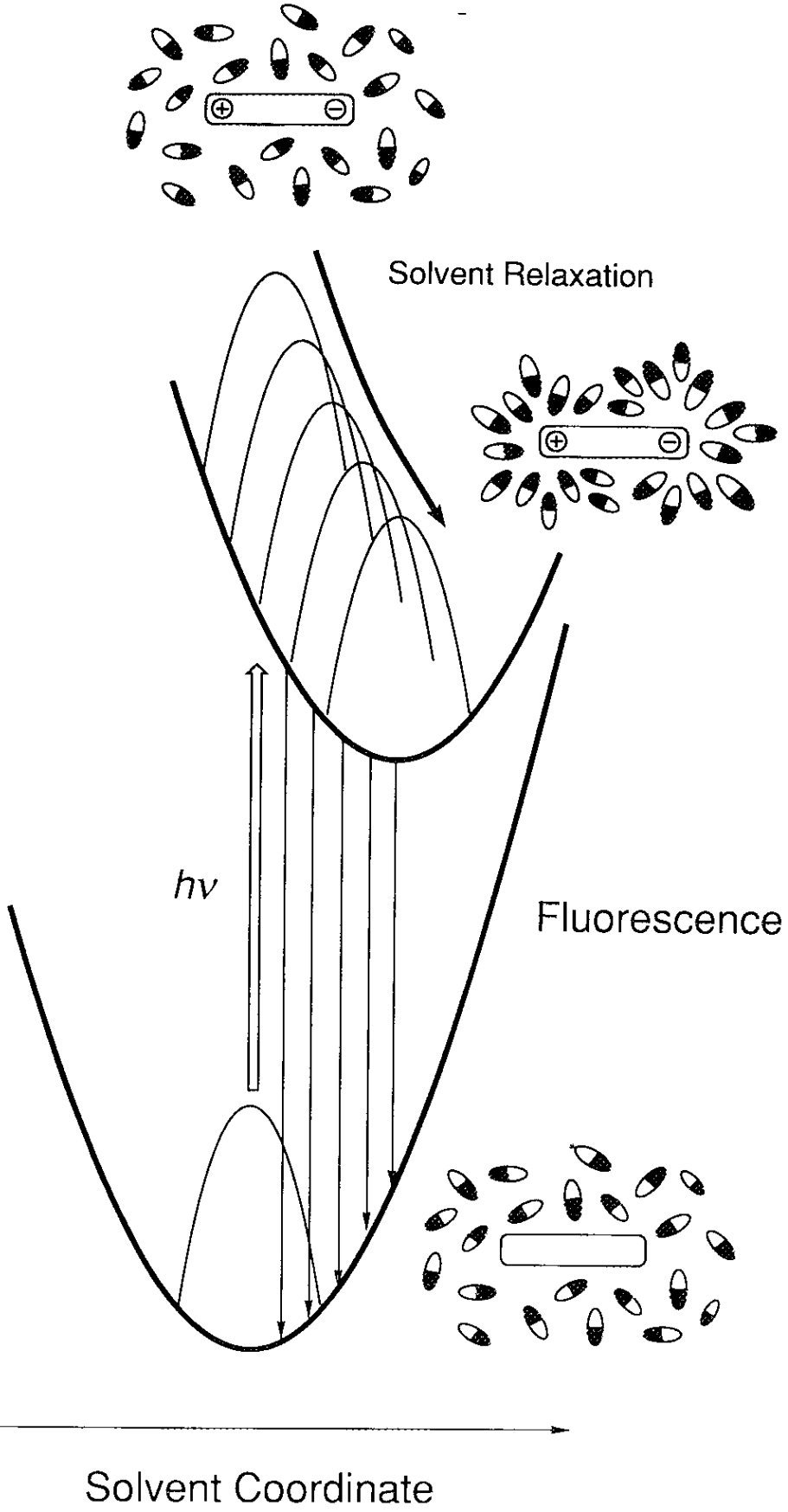

Figure III-1. Dynamic fluorescence Stokes shift caused by solvation process on the excited state free energy surface.

Figure III-2 shows fluorescence decays of C102 observed at different wavelengths. At shorter wavelengths there is a fast decay and at longer wavelengths there is a concurrent rise. This implies that the fluorescence spectrum of C102 is shifting towards red with time. A time-resolved fluorescence spectra would illustrate this red shift.

We have used the spectral reconstruction method to obtain a time-resolved fluorescence spectrum.[3] When the fluorescence up-conversion method is used, the relative intensity between each wavelengths becomes uncertain because the angle of the non-linear crystal has to be tuned at each wavelength of observation. However, the intensity of the fluorescence $I(\lambda, t)$, at a given time t and wavelength λ, can be obtained from the normalized fitted decay series $D(t, \lambda)$ and intensity of the steady-state fluorescence $I_0(\lambda)$;

$$I(\lambda; t) = D(t,\lambda)\, I_0(\lambda) \quad / \int_0^\infty D(t, \lambda)\, dt\,. \qquad \text{(III. 2)}$$

Figure III-3 shows the reconstructed spectrum. The markers correspond to the intensities of the fluorescence at the measured wavelength at a given time t. The lines are the least-square-fits to the points using a log-normal function.[6] The log-normal function describes an asymmetric line shape and is often used to fit broad featureless absorption or fluorescence spectra. It has the form;

$$\varepsilon(\nu) = \frac{\varepsilon_0 b}{a - \nu} \exp(-c^2) \exp\{-\frac{1}{2c^2}[ln(\frac{a - \nu}{b})]^2\}\ ; \quad \nu < a$$

$$\varepsilon(\nu) = 0; \quad \nu \geq a \qquad \text{(III. 3)}$$

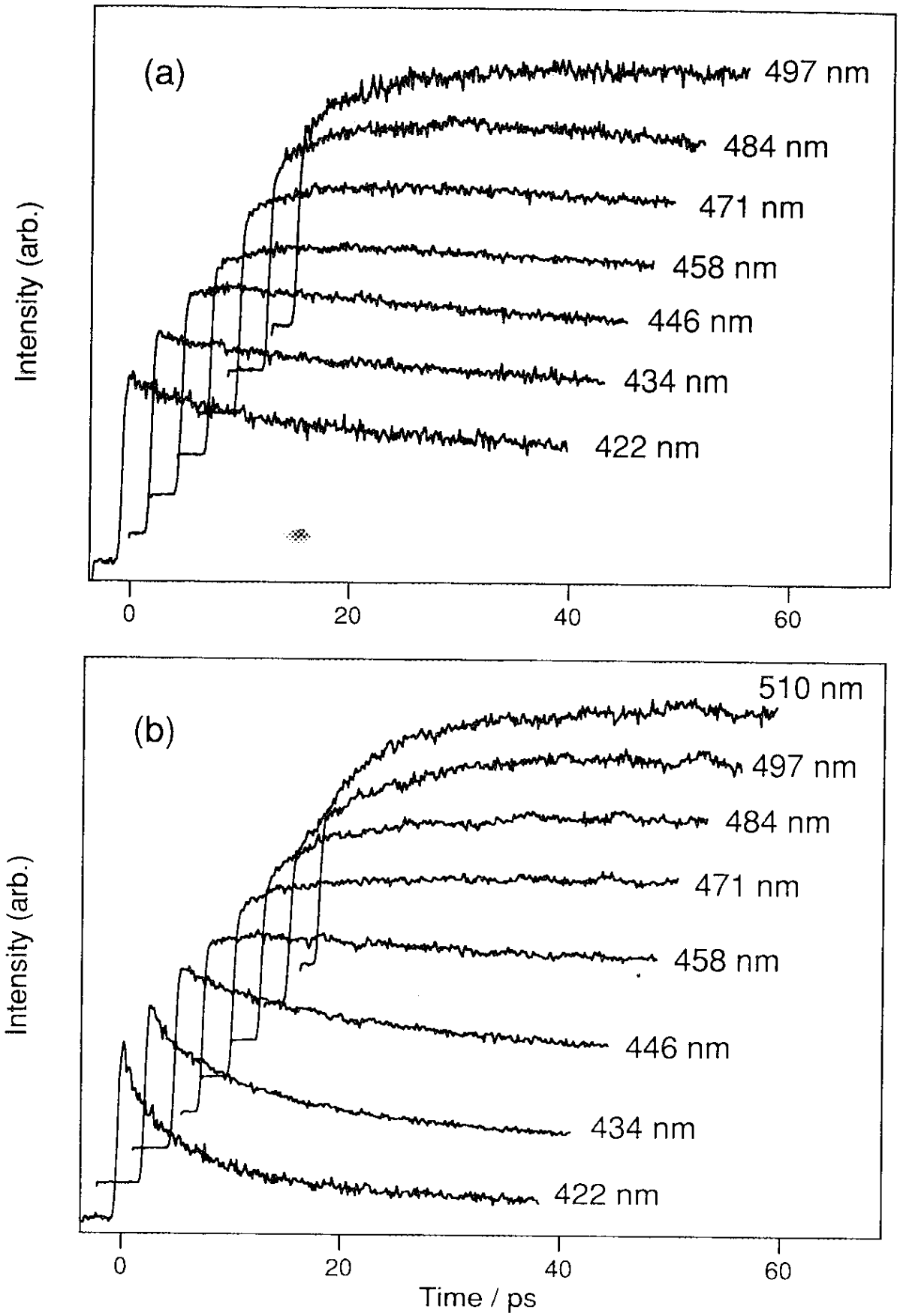

Figure III-2. Fluorescence decays of C102 (a) in DMA and (b) in AN, measured at various wavelengths.

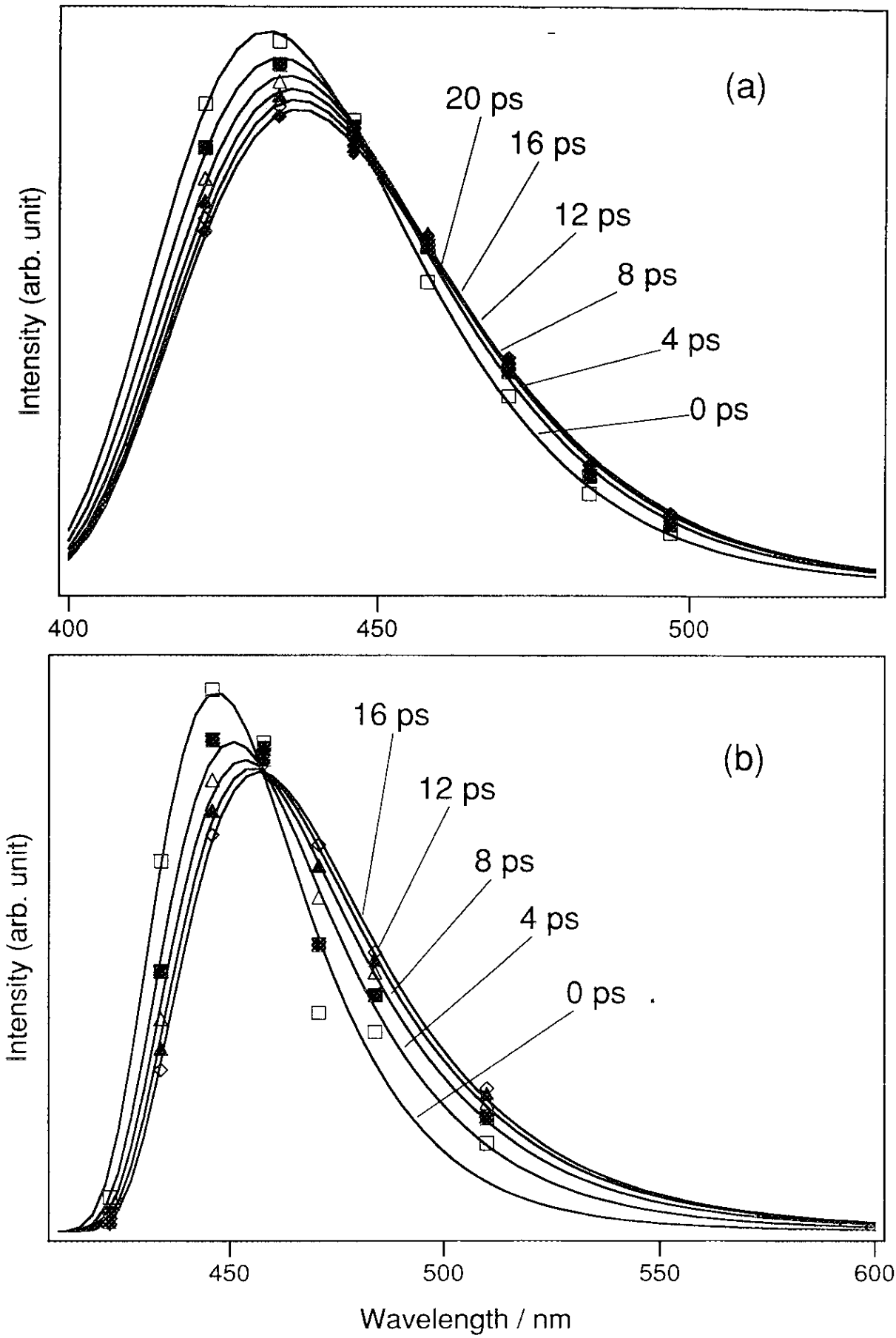

Figure III-3. Reconstructed time-resolved fluorescence spectra of C102 in (a) DMA and (b) AN. The dots correspond to the relative intensities of fluorescence at each wavelength at a specific time. The curves are the log-normal fits to the dots.

where the parameters a, b, and c are related to the frequency of the spectral maximum ν_0, full-width-half-maximum H, and empirical measure of scewness ρ by the expressions;

$$a = \nu_0 + \frac{H\rho}{\rho^2 - 1} \qquad \text{(III. 4a)}$$

$$b = \frac{H\rho}{\rho^2 - 1} exp(c^2) \qquad \text{(III. 4b)}$$

$$c = \frac{ln\rho}{\sqrt{2ln2}} \qquad \text{(III. 4c)}$$

As $\rho \rightarrow 0$, the function approaches the Gaussian asymptotically.

As expected from examinations of the individual fluorescence transients, the peak of the reconstructed spectrum shifts to red with time. At $t = 0$, the peaks are at 432 nm for DMA and 447 nm for AN. They shift to the steady-state values as the time goes on, 436 nm in DMA and 462 nm in AN. The shift is larger for AN which implies a stronger solvent polarity for AN. In Figure III-4, the spectral shift correlation functions $C(t)$ are shown with the results of bi-exponential fitting. The observed solvent relaxation times are 7.9 ps (19 %) and 18.7 ps (81 %) for DMA and 6.7 ps (81 %) and 13.3 ps (19 %) for AN. These are much slower than the fluorescence lifetimes of NB, *i.e.*, 0.1 ps (95 %) and 2.5 ps (5 %) in DMA, and 0.4 ps (56 %) and 2.5 ps (44 %) in AN. Therefore, the prediction made by Kobayashi *et al.* is confirmed, the ET occurs much faster than the diffusive solvation process.

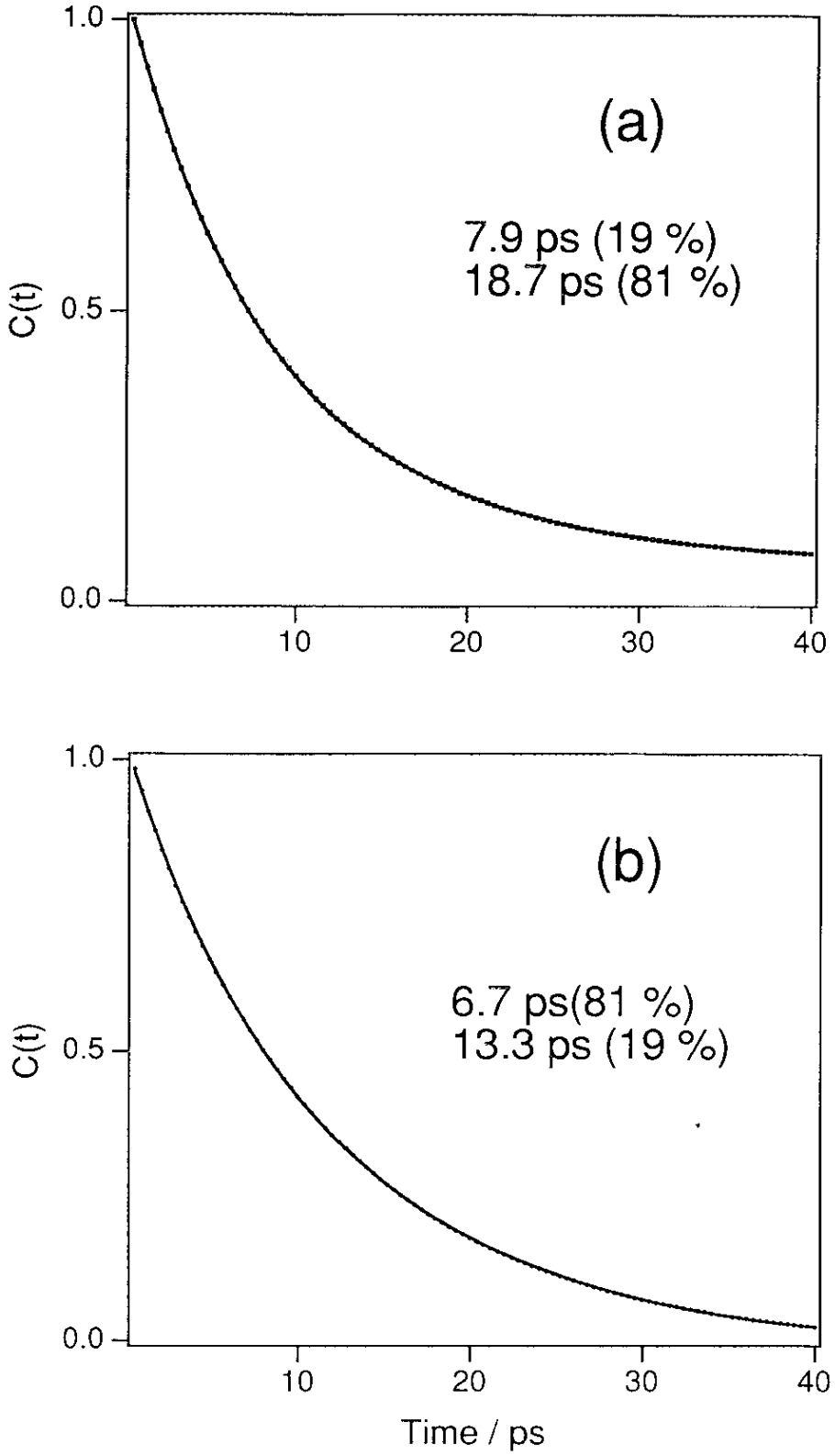

Figure III-4. The normalized spectral shift correlation function *C(t)* of C102 in (a) DMA and (b) AN. Results of bi-exponential fitting are also shown in the figure.

III-2. Temperature dependence of the solvent relaxation time of AN

To obtain temperature dependence of solvent relaxation times, reconstruction of the time-resolved fluorescence spectrum has to be done at each temperature. However, this kind of experiment is too troublesome to carry out. Therefore, a simplified method called "single wavelength method" was applied. This is completely an empirical method first established by Nagarajan *et al.*[7] It is based on an assumption that, "when a fluorescence decay is measured at a certain wavelength of a certain probe molecule, the decay becomes proportional to the spectral shift correlation function *C(t)*." Therefore, this method starts with finding the wavelength where the decay becomes proportional to *C(t)*. Once such a wavelength is found, it can be applied for any other solvent, since the wavelength depends only on the probe molecule. This kind of wavelength is already known for C102 to be 420 nm.[4] Therefore, the temperature dependent measurement of the fluorescence decay of C102 in AN at 420 nm was carried out. A double exponential fitting gives 4.2 ps (67 %) and 37.5 ps (33 %) at room temperature (297 K). The first component was faster than the value obtained from *C(t)*, thus the reliability of this method might be questionable. However, the fluorescence decays at short wavelength should contain information about solvent relaxation. Thus this method may be qualitatively reliable, but not quantitatively. If the solvation time changes with temperature, the decay at this wavelength should also change. The results are shown in Figure III-5, which show no temperature dependence within the experimental error. Therefore, the solvation time of AN seems to be not sensitive to temperature.

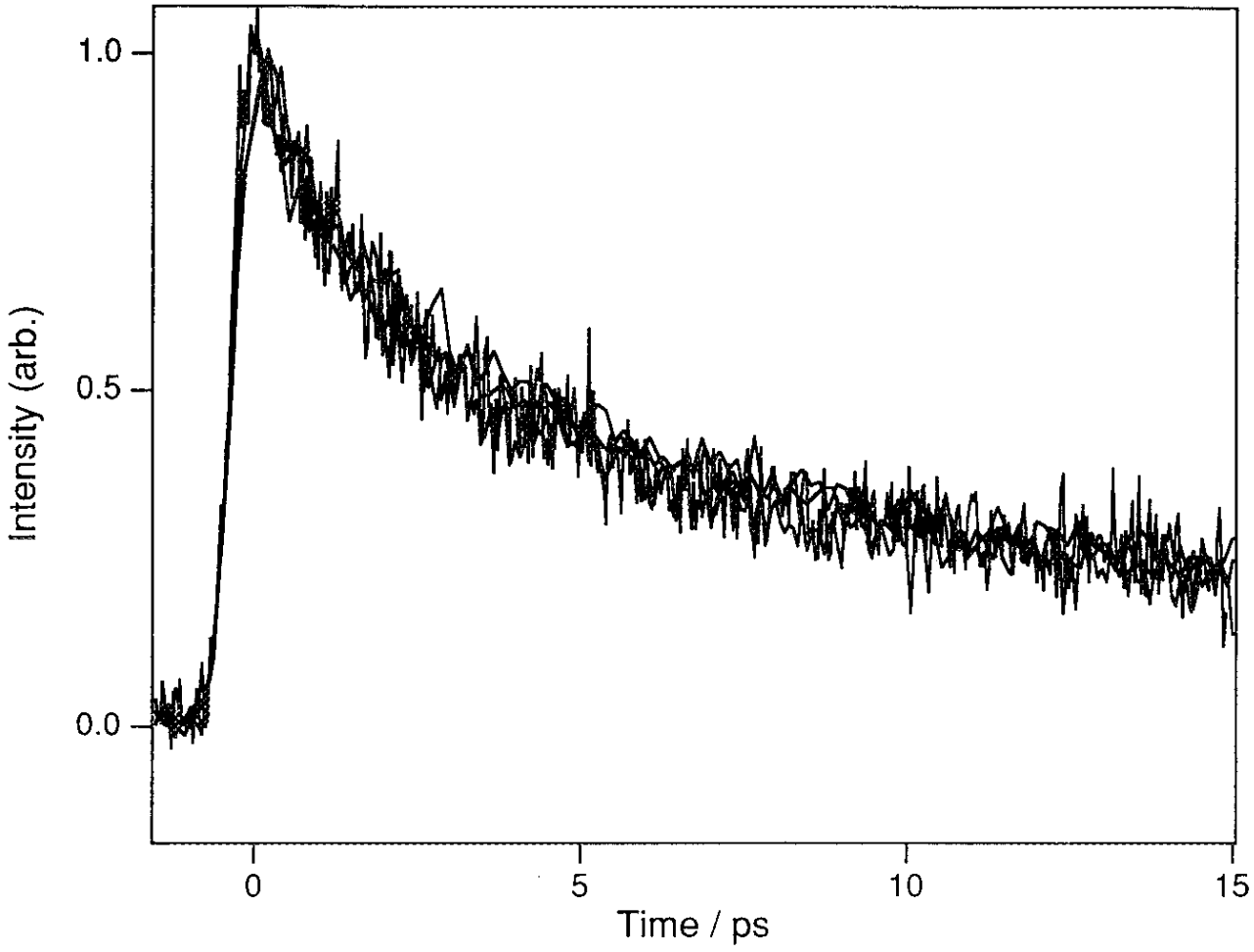

Figure III-5. Temperature dependence of the fluorescence decay of C102 in AN at 420 nm. T = 283, 297, 323, 353 K. No temperature dependence can be seen within the present experimental error.

III-3. Temperature dependence of solvation times calculated from Debye relaxation times

As is mentioned in section I-3, the longitudinal solvent relaxation time can also be calculated from Debye relaxation time obtained by dielectric dispersion and loss measurements. The temperature dependent dielectric measurements of neat AN is reported by Bhattacharyya *et al.*[8] The results they obtained are shown in Table III-1 and Figure III-6. They found two relaxation processes with time constants of 1.08 ps (73 %) and 11.4 ps (27 %) at 45 °C (318 K). To extract longitudinal relaxation times, formula of Bagchi *et al.*[9] is applied.

For solvents with two dispersion regimes, the frequency dependent dielectric constant $\varepsilon(\omega)$ is written as;

$$\varepsilon(\omega) = \varepsilon_\infty + (\varepsilon_0 - \varepsilon_\infty)\left(\frac{C_1}{1 - i\omega\tau_{D1}} + \frac{C_2}{1 - i\omega\tau_{D2}}\right) \qquad \text{(III. 5)}$$

where ε_∞ and ε_0 are optical and static dielectric constants, respectively, τ_{D1} and τ_{D2} are the two Debye relaxation times, and $C_1 + C_2 = 1$. $C(t)$ can be written as;

$$C(t) = A_1 exp(-\frac{t}{\tau_{F1}}) + A_2 exp(-\frac{t}{\tau_{F2}}) \qquad \text{(III. 6)}$$

with time constants;

$$\tau_{F1} = (S_- + 2D)^{-1} \qquad \text{(III. 7(a))}$$

$$\tau_{F2} = (S_+ + 2D)^{-1} \qquad \text{(III. 7(b))}$$

where D is the rotational diffusion constant of the solute,

Table III-1. Temperature dependence of static dielectric constant ε_0, dielectric constant ε', dielectric loss ε'', and two relaxation times τ_1 and τ_2. (Bhattacharyya *et al., J. Phys. Soc. Jap.*, **28**, 204, (1970)).

T (K)	ε_0	ε'	ε''	τ_1 (ps)	τ_2 (ps)
318	6.7	5.57	1.43	1.08 (73 %)	11.4 (27 %)
333	6.4	5.53	1.26	0.85 (72 %)	9.92 (28 %)
348	6.1	5.48	1.15	0.41 (67 %)	7.09 (33 %)

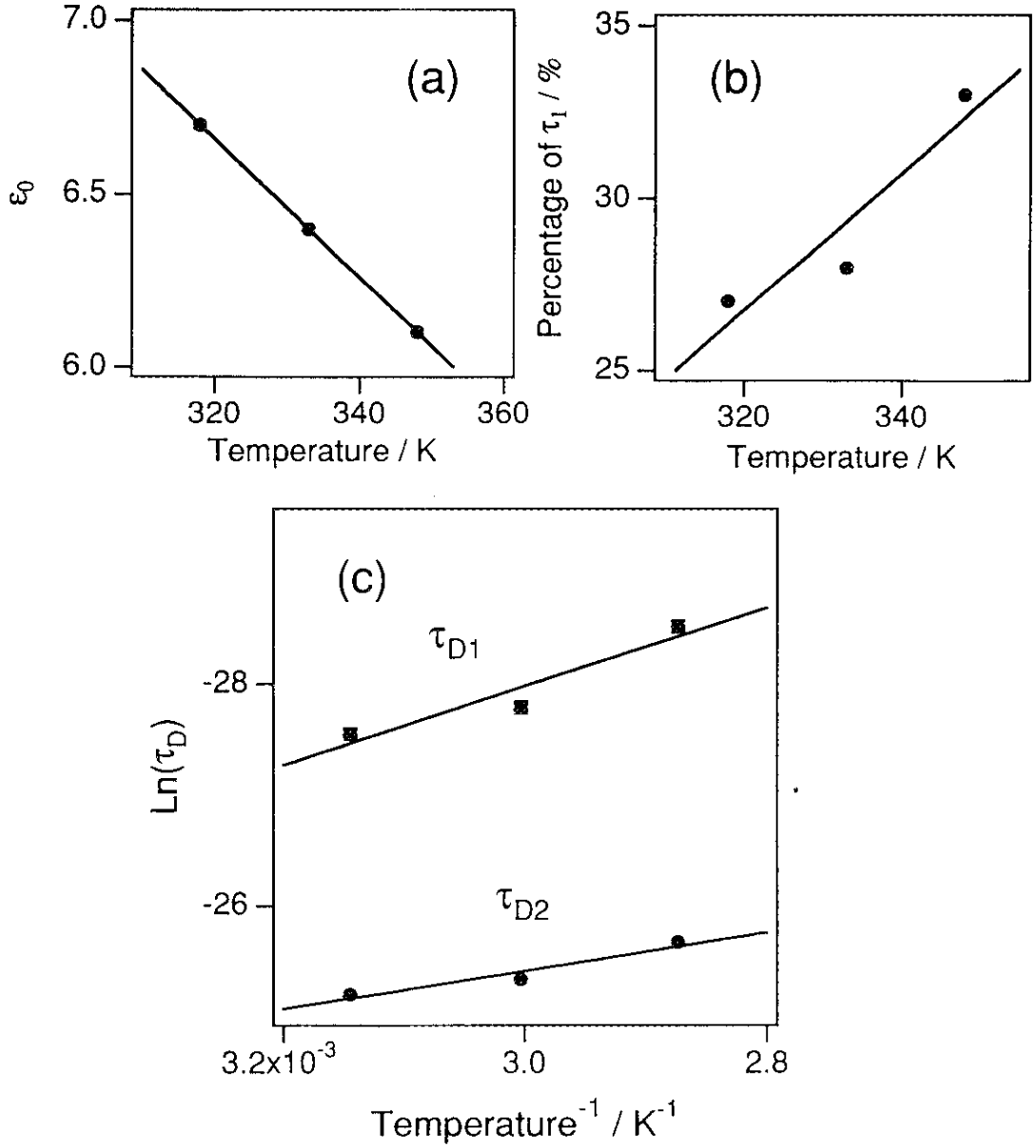

Figure III-6. Temperature dependence of (a) ε_0, (b) percentage of the first Debye relaxation time τ_1 (%), and (c) Debye relaxation times τ_1 and $\tau_2$of AN, plotted from the experimental results of Bhattacharyya *et al.* (*J. Phys. Soc. Jap.*, **28**, 204, (1970)).

$$S_{\pm} = \frac{1}{2}(A \pm \sqrt{B^2 - 4B}) \qquad \text{(III. 8)}$$

$$A = \frac{(\tau_{D1} + \tau_{D2})(2\varepsilon_\infty + \varepsilon_c) + 2(\varepsilon_0 - \varepsilon_\infty)(C_1\tau_{D2} + C_2\tau_{D1})}{\tau_{D1}\tau_{D2}(2\varepsilon_\infty + \varepsilon_c)} \qquad \text{(III. 9)}$$

$$B = \frac{2\varepsilon_0 + \varepsilon_c}{\tau_{D1}\tau_{D2}(2\varepsilon_\infty + \varepsilon_c)} \qquad \text{(III. 10)}$$

where ε_C is the dielectric constant of the solute molecule and

$$A_1 = (\frac{S_+S_-}{S_+ - S_-})(C_1\tau_{D2} + C_2\tau_{D1} - \frac{1}{S_+}) \qquad \text{(III. 11a)}$$

$$A_2 = (\frac{S_+S_-}{S_+ - S_-})(\frac{1}{S_+} - C_1\tau_{D2} - C_2\tau_{D1}) \qquad \text{(III. 11b)}$$

The results of calculation using these formulas are shown in Table III-2 and Figure III-7. For this calculation, it is assumed that the rotational diffusion of the solute is negligibly slow ($D = 0$) and, $\varepsilon_C = 0$. A larger ε_C's give longer relaxation times, however, they were not quite sensitive to ε_C. The activation energies obtained from these results are, 6.0 kcal / mol for τ_{F1}, and 3.7 kcal / mol for τ_{F2}. Battacharyya *et al.* did not somehow measure the values at room temperature. Therefore, The values at room temperature (24 °C) were extrapolated. The fittings to the results shown in Figure III-7 give 1.0 ps and 15.2 ps. However, the percentages cannot be obtained from these fittings. Therefore, the values of ε_0, C_1, τ_{D1}, and τ_{D2} at room temperature were estimated from Figure III-6 (a), (b), and (c), respectively. They were, $\varepsilon_0 = 7.12$, $C_1 = 0.779$, $\tau_{D1} = 2.59$ ps, and $\tau_{D2} = 17.4$ ps. The obtained longitudinal relaxation times were 1.1 ps (92.7 %) and 15.2 ps (7.3 %). The fast component changes from 1.1 ps to 210 fs when temperature is changed from 24 °C to 75 °C. It becomes five times

Table III-2. Temperature dependence of solvation times τ_{F1} and τ_{F2} calculated from the Debye ralaxation times of AN measured by Battacharyya *et al.*

T (K)	τ_{F1} (ps)	τ_{F2} (ps)
318	0.48 (89 %)	9.6 (11 %)
333	0.40 (88 %)	8.3 (12 %)
348	0.21 (84 %)	5.8 (16 %)

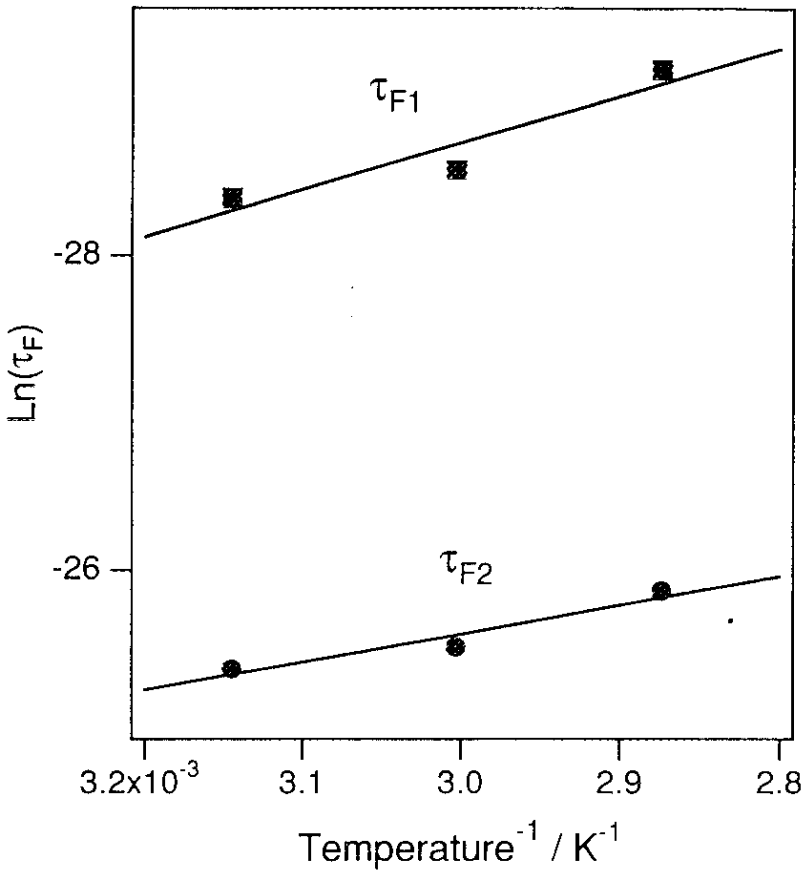

Figure III-7. Temperature dependence of solvation times τ_{F1} and τ_{F2} calculated from the Debye relaxation times of AN measured by Battacharyya *et al.* The activation energy becomes 6.0 kcal / mol for τ_{F1} and 3.7 kcal / mol for τ_{F2}.

shorter. Such a large change should be observed in the temperature dependent decays of Figure III-5, however, it was not observed. The temperature dependence of the longitudinal relaxation times will be discussed again in Chapter IV. It had no relation with the temperature dependence of ET.

References for Chapter III

1. T. Kobayashi, Y. Takagi, H. Kandori, K. Kemnitz, K. Yoshihara, *Chem. Phys. Lett.*, **180**, 416, (1991).

2. B. Bagchi, D. W. Oxtoby, and G. R. Fleming, *Chem. Phys.*, **86**, 257, (1984).

3. M. Maroncelli and G. R. Fleming, *J. Chem. Phys.*, **86**, 6221, (1987).

4. M. A. Kahlow, T. J. Kang, and P. F. Barbara, *J. Chem. Phys.*, **88**, 2372, (1988).

5. M. A. Kahlow, W. Jarzeba, T. J. Kang, and P. F. Barbara, *J. Chem. Phys.*, **90**, 151, (1989).

6. D. B. Siano and D. E. Metzler, *J. Chem. Phys.*, **51**, 1856, (1969).

7. V. Nagarajan, A. M. Brearley, T. J. Kang, and P. F. Barbara, *J. Chem. Phys.*, **86**, 3183, (1987).

8. J. Bhattacharyya, A. Hasan, S. B. Roy, and G. S. Kåstha, *J. Phys. Soc. Jap.*, **28**, 204, (1970).

9. B. Bagchi, D. W. Oxtoby, and G. R. Fleming, *Chem. Phys.*, **86**, 257, (1984).

CHAPTER IV
TEMPERATURE DEPENDENCE OF ELECTRON TRANSFER

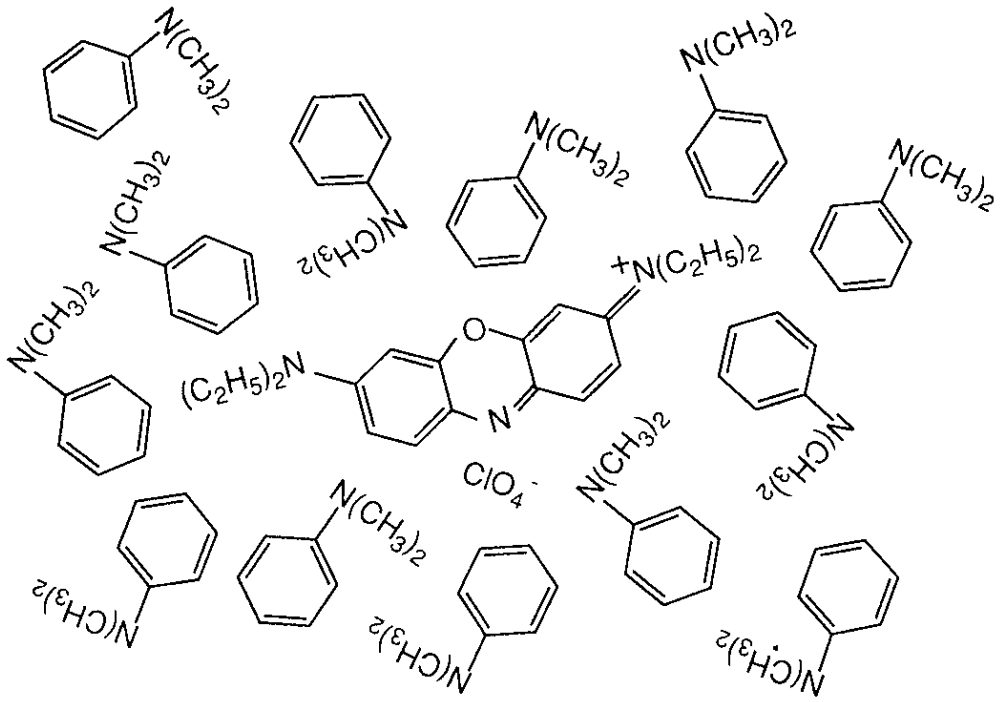

IV-1. Fluorescence quenching of oxazines by electron transfer

Oxazines, shown in Figure IV-1, are usually strong fluorescent substances and often used as laser dyes. However, when they are dissolved in electron donating solvents, such as AN or DMA, the fluorescence is severely quenched. Figure IV-2 shows absorption and fluorescence spectra of OX1 in DMA and in 1-chloronaphthalene (1-CN). 1-CN is a solvent which has a similar physical properties to DMA, however, it is not an electron donor. The fluorescence intensity of OX1 in DMA is more than 1000 times weaker than the one in 1-CN. This kind of strong fluorescence quenching was also observed for NB. In the previous studies,[1,2] it was concluded that fluorescence quenching of NB was due to intermolecular ET from the solvent to the dye. The reaction products, namely, neutral radical of NB with the cations of the solvents, were observed by sub-picosecond transient absorption measurement.[2]

The fluorescence decays of NB and OX1 in the donor solvents are shown in Figure IV-3 and IV-4, respectively. The pump wavelength is 605 nm of R6G dye laser. The fluorescence decays of NB in these solvents are already reported by Kobayashi *et al.*[1] However, the time resolution is much better for the present experiment, *i.e.*, *c.a.* 300 fs for Kobayashi *et al.* and 80 fs for the present case. The fluorescence intensity is plotted in the logarithmic scale. The decay of OX1 in DMA shows a linear decay, indicating a single exponential function with a lifetime of ~280 fs. Whereas, OX1 and NB in AN gave a non-exponential decay. The signal of NB in DMA was very weak due to its ultrashort lifetime and low solubility in DMA. Fittings were made by single exponential function for the decays in DMA and triple exponential function for the ones in AN. The fitting parameters are shown in Figure IV-3 and IV-4.

The cyclic voltammograms of oxazines in AN are shown in Figure IV-5, which show two pairs of strong reduction waves. The first pair is

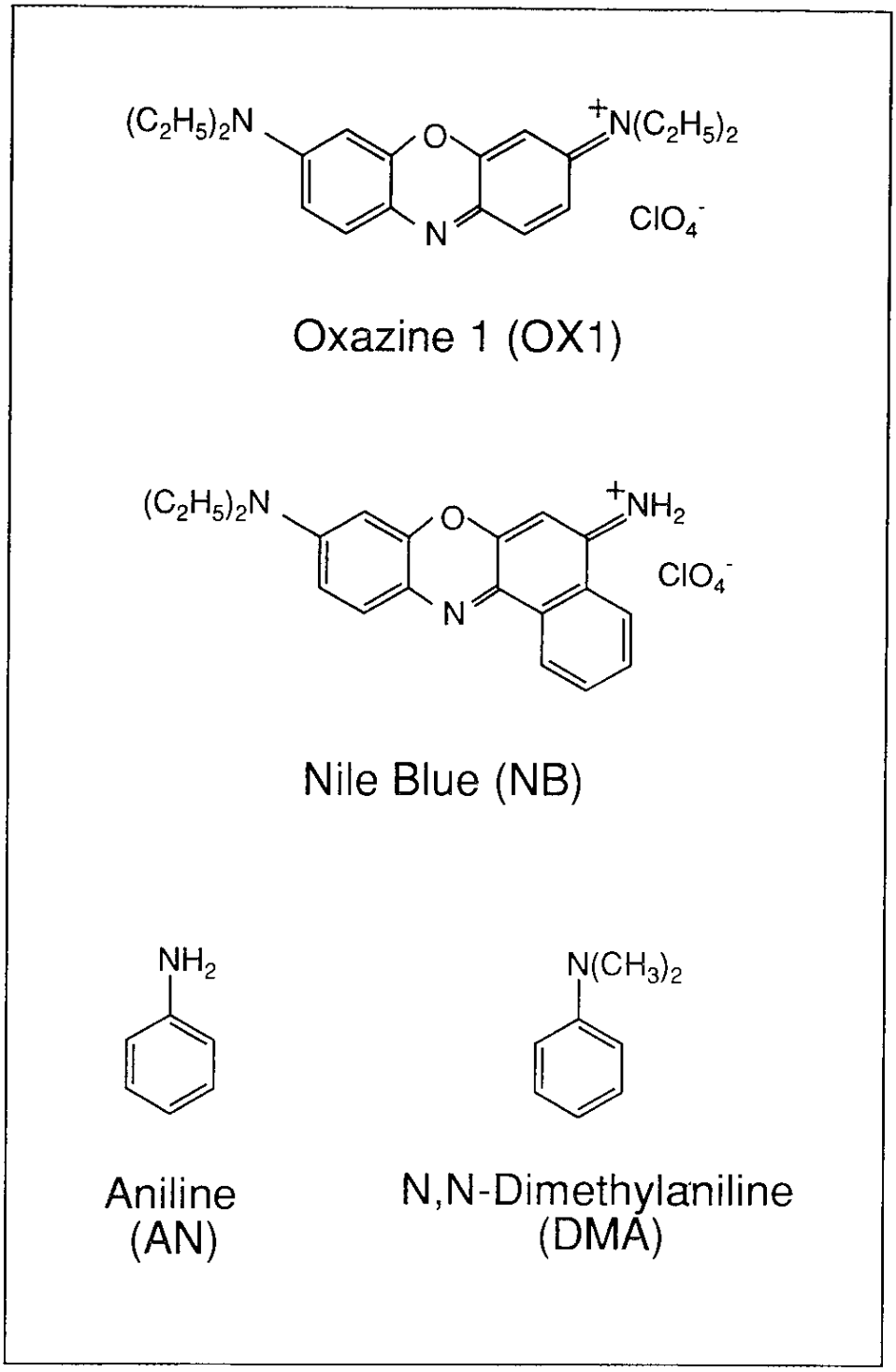

Figure IV-1. Structures of oxazines and donor solvents.

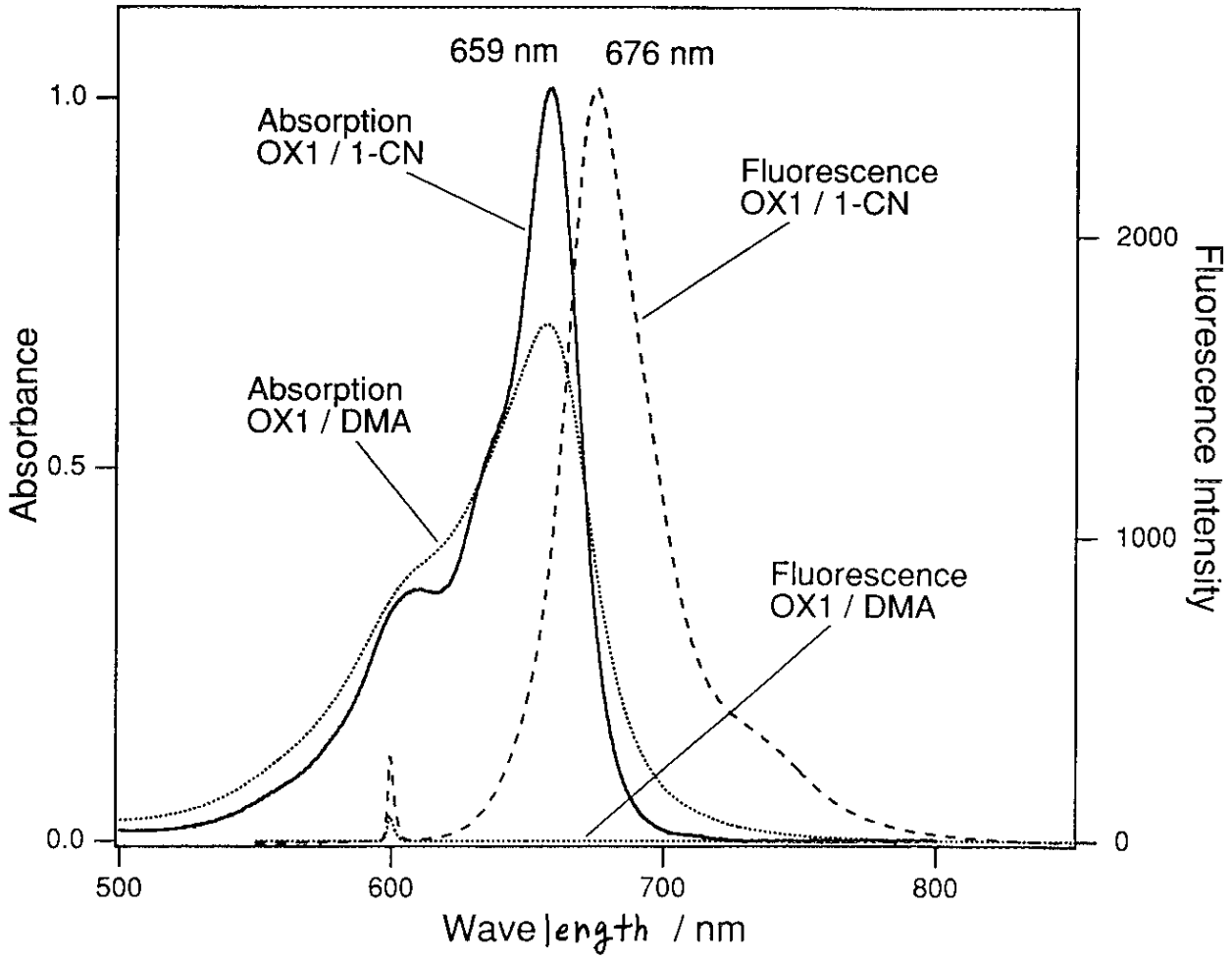

Figure IV-2 Absorption and fluorescence spectra of OX1 in DMA and 1-CN. Concentrations are 1×10^{-5} M.

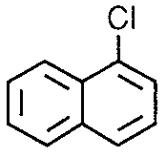

1-chloronaphthalene (1-CN)

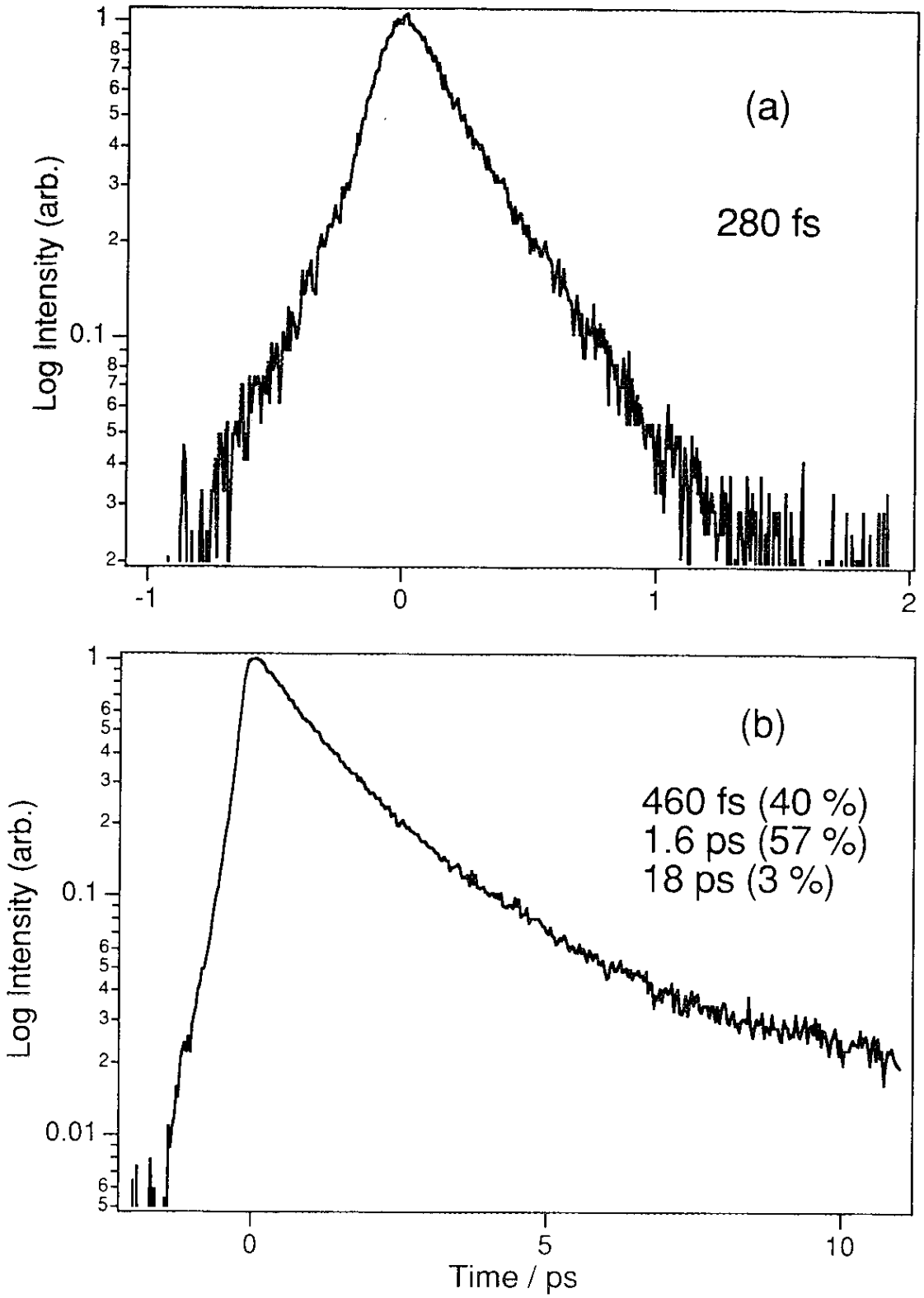

Figure IV-3. Fluorescence decays of OX1 in (a) DMA and (b) AN observed at 725 nm. Results of the fitting is also shown in the figure. Single and triple exponential functions were used to fit (a) and (b), respectively.

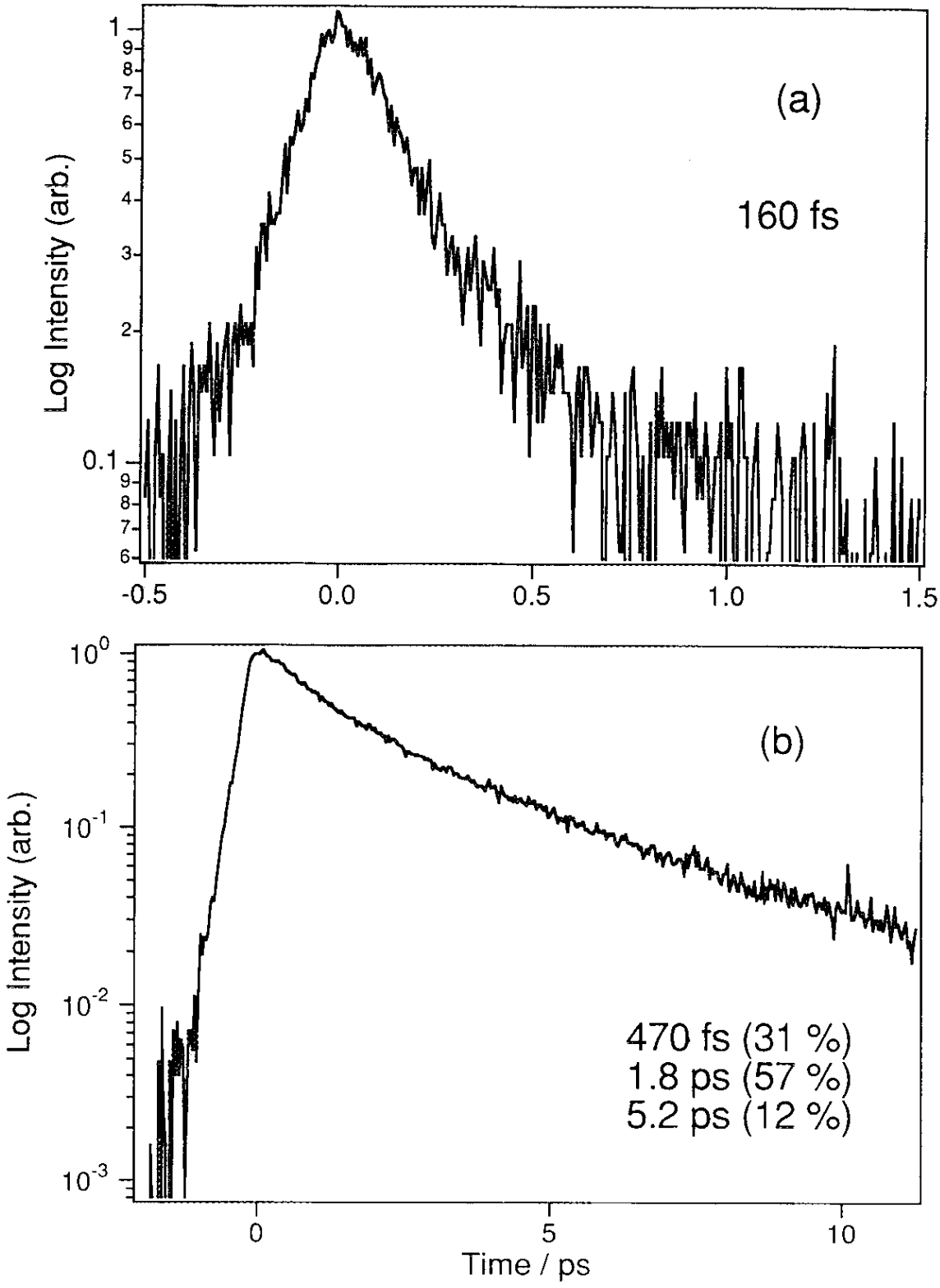

Figure IV-4. Fluorescence decays of NB (a) in DMA observed at 700 nm and (b) in AN observed at 690 nm. Results of the fitting is also shown in the figure. Single and triple exponential functions were used to fit (a) and (b), respectively.

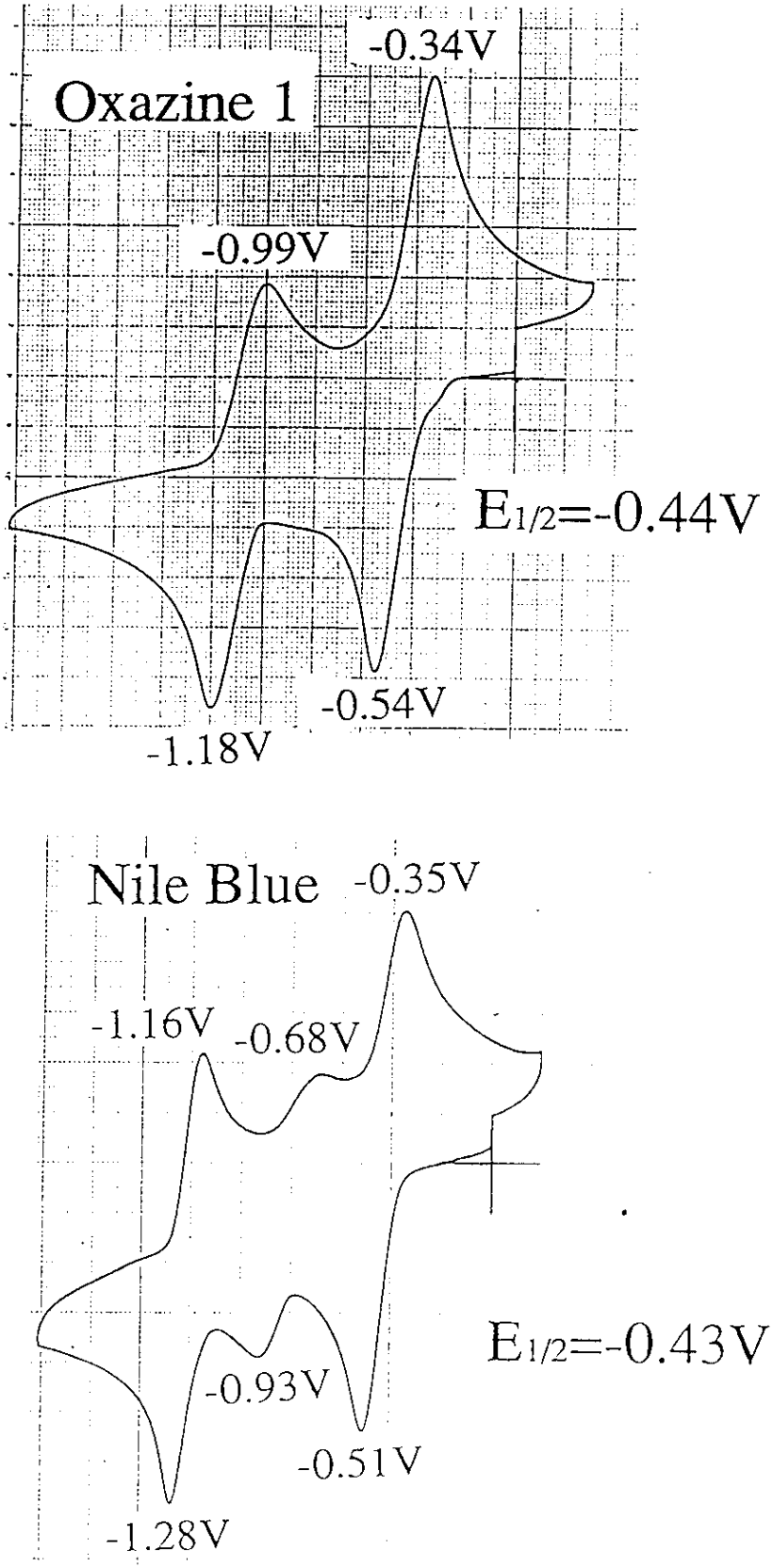

Figure IV-5. Cyclic voltammograms of oxazines in AN. Concentration is $1x10^{-3}$ M.

due to the first reduction potential and the second is to the second reduction potential. A pair of small waves between the two strong pairs, observed for NB, may be due to dimers, but it is not clear yet. The first reduction potential $E_{1/2}$ was obtained by calculating the average of the two peaks in the first pair. OX1 and NB shows a similar value of reduction potential, *i.e.*, $E_{1/2}$ = -0.43 V, which means that OX1 and NB have a similar value of electron affinity. Therefore, it can be confirmed that the strong fluorescence quenching of OX1 is also due to ET form the donor solvent to the dye.

The ET of oxazines in donor solvents are proposed in Figure IV-6. When dye is photo-excited, ET occurs from the solvent to the excited state of the dye. The back ET occurs successively from the neutral radical of the dye to the solvent cation, and the system goes back to the ground state again. The lifetime of the radical ion pair of NB and DMA was 4.0 ps,[2] and that of OX1 and DMA was 4.7 ps.[3] NB has an NH_2 substituent which could also cause an excited state proton transfer to the solvent. However, OX1 cannot show this kind of reaction, since the amino groups of OX1 are all substituted by ethyl groups.

The absorption spectra of OX1 in Figure IV-2, shows a broadening in DMA compared to the one in 1-CN, which may be indicating a formation of a weak charge-transfer complex between OX1 and DMA. A same kind of phenomenon was also observed for NB. However, it was not observed with coumarins which will be discussed in Chapter IV.

The excited-state lifetimes of these dyes are very long (a few nanoseconds) in normal non-reactive solvents. Therefore, the inverse of the ultrashort lifetimes shown in Figure IV-3 and IV-4 can be regarded as an ET rate. However, there are a few other phenomena which can occur in the same time scale, they are (1) intramolecular vibrational redistribution (IVR) and (2) solvent relaxation process. To investigate these possibilities,

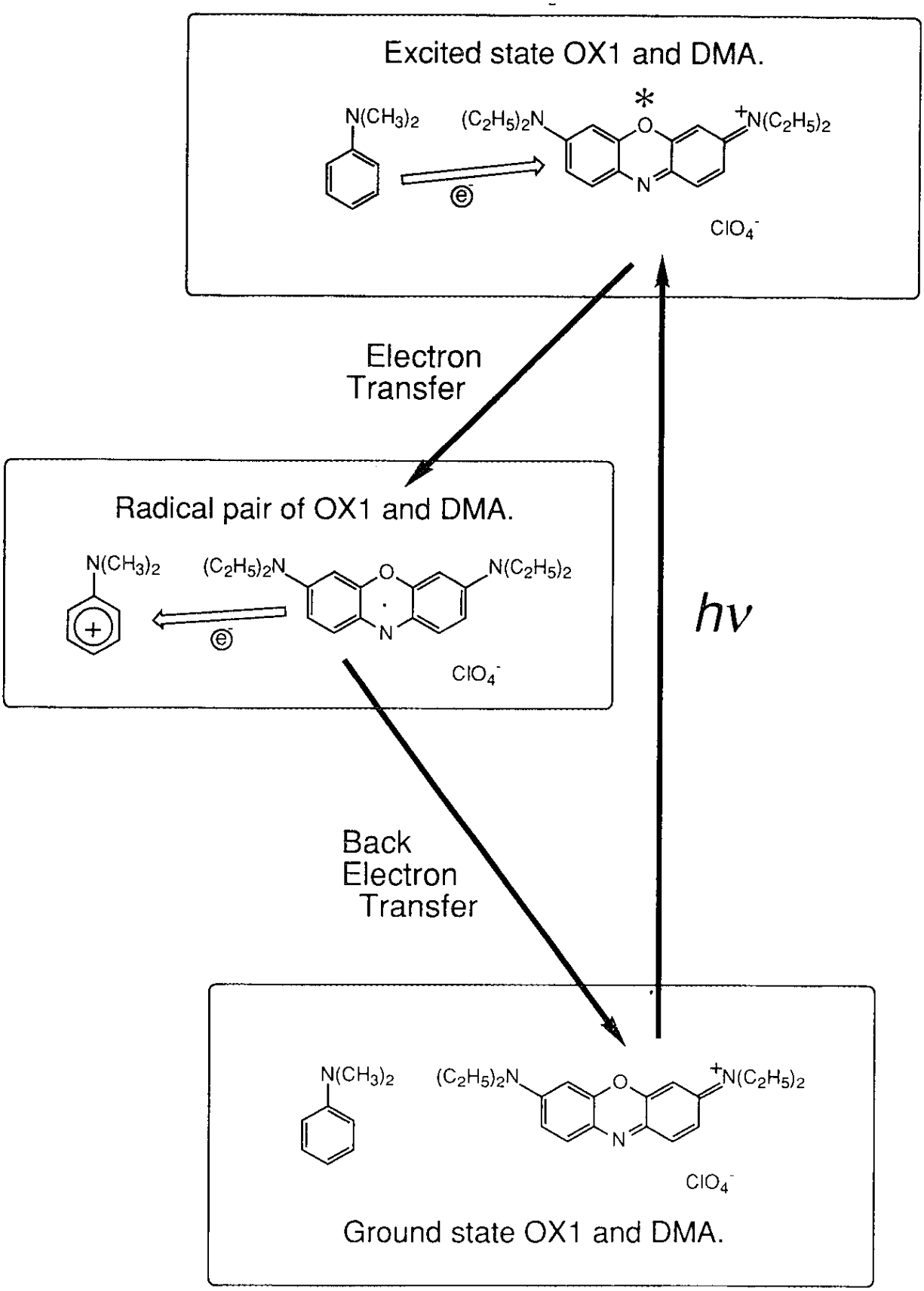

Figure IV-6. Reaction of OX1 in DMA.

studies on excitation and observation wavelength dependence were carried out.

IV-2. Excitation-wavelength dependence of fluorescence decay

The excitation wavelength for the experiments shown in Figure IV-3 and IV-4 is 605 nm, which excites the blue side of the absorption spectra of oxazines. Experiments using 675 nm light were also carried out to excite the red side of the absorption spectra. The energy difference between 605 and 675 nm light is 0.21 eV. The fluorescence decays excited at 675 nm are shown in Figure IV-7 and IV-8 (solid line) with the ones excited at 605 nm (broken line), for comparison. The signal-to-noise (S/N) ratio is poor for the 675 nm excited decay of OX1 in DMA, however, it looks identical with the one excited at 605 nm within the experimental error. Therefore, there is no effect of excess energy in this case. The fluorescence decay of NB in DMA was too weak to measure. The decays of OX1 in AN, excited at 605 and 675 nm, deviated at the slower part of the kinetics, as is shown in Figure IV-8. The result of three exponential fitting is 400 fs (42 %), 1.7 ps (51 %), and >30 ps (7 %). The first and second component are identical with the ones for 605 nm excitation within the experimental error, however, the third component became longer. For NB in AN, this kind of effect seems minor, although S/N ratio is worse than the one obtained for OX1 in AN.

Several reasons can be considered for the slow component observed in the decay of OX1 in AN with 675 nm excitation. It can be (1) the effect of IVR, (2) hole burning of the distribution on the solvent coordinate, or (3) a contamination of fluorescent substances. Mokhtari *et al.* observed a time-dependent fluorescence bandwidth broadening of NB in methanol with a time constant of ~400 fs.[4] They assigned this broadening to a vibrational relaxation process. If ET is occurring faster than such a

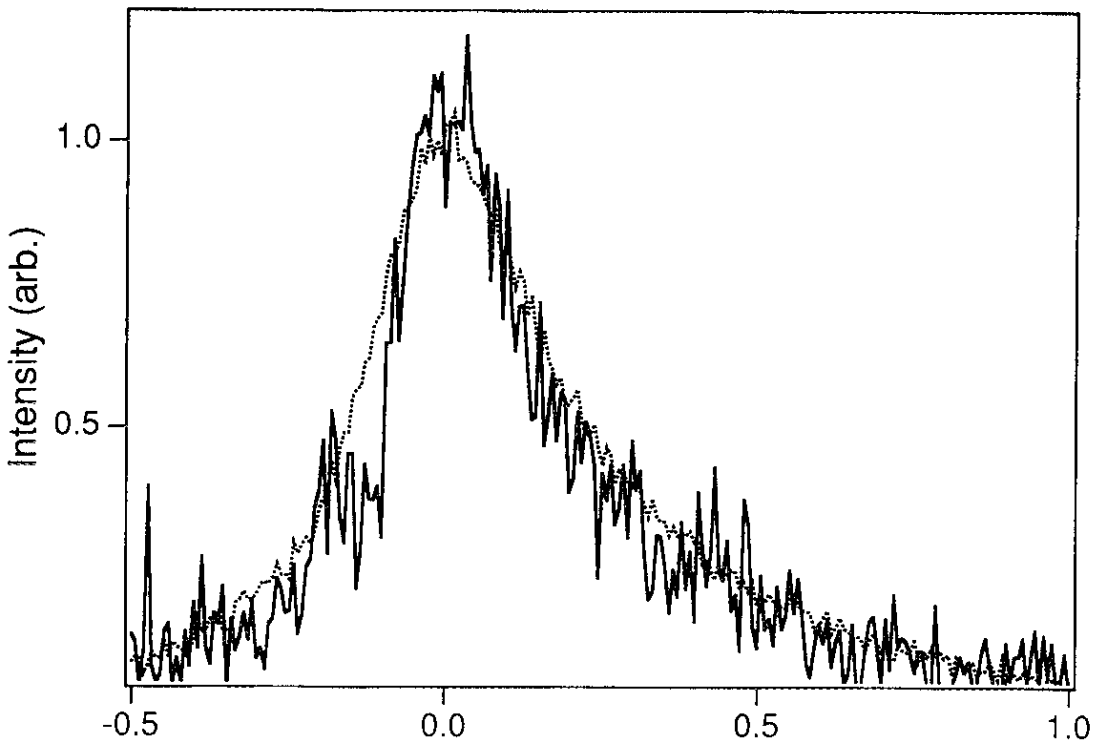

Figure IV-7. Fluorescence decays of OX1 in DMA, solid line; excited at 675 nm and observed at 770 nm, broken line; excited at 605 nm and observed at 725 nm.

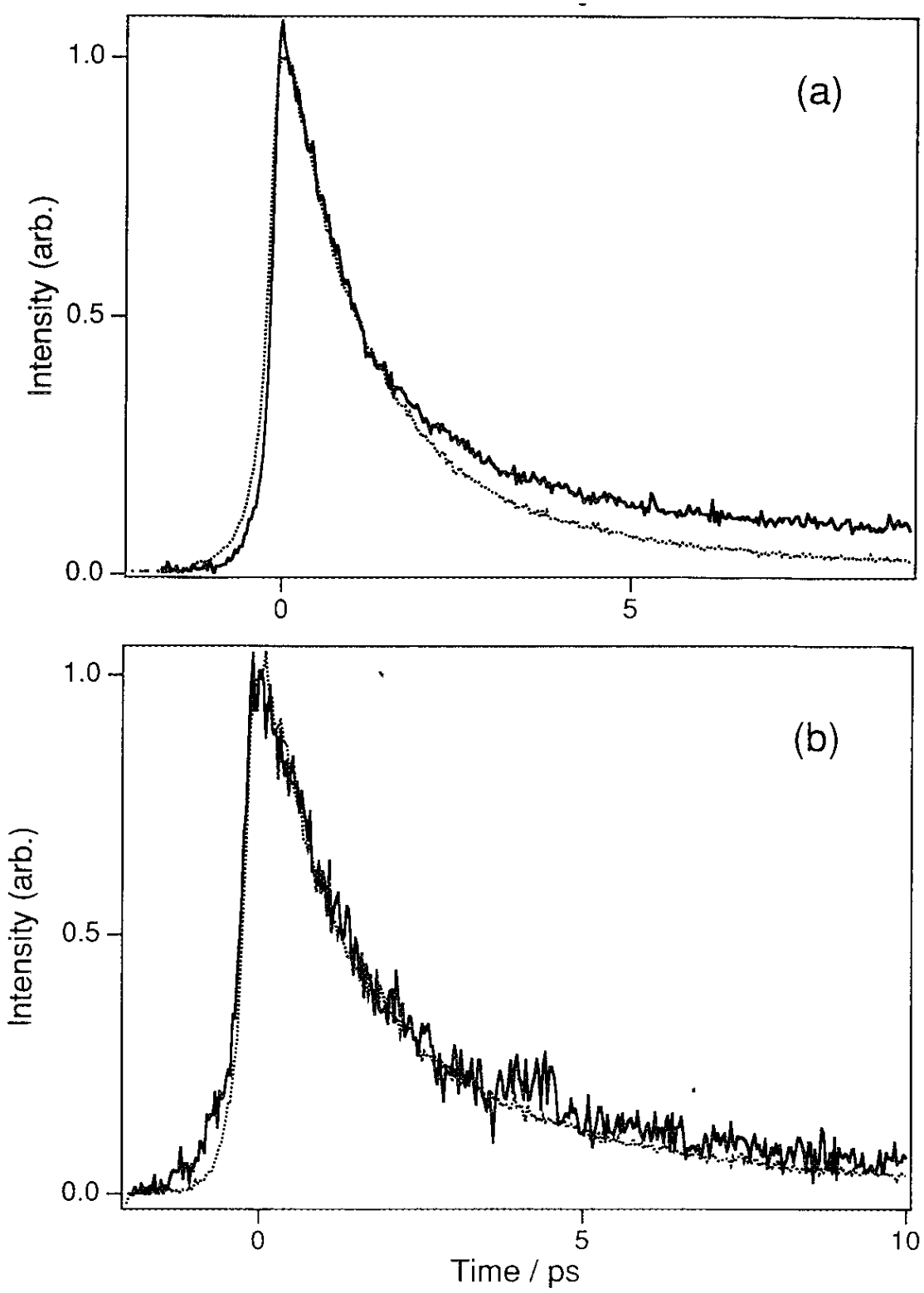

Figure IV-8. Fluorescence decays of (a) OX1 and (b) NB in AN, excited at 675 nm and observed at 770 nm (solid line). Fluorescence decays, excited at 605 nm and observed at 725 nm, are also shown for comparison(broken line).

vibrational relaxation, excitation at shorter wavelength will give the molecule an excess vibrational energy for the reaction. Shank *et al.* carried out a femtosecond hole burning experiment for a similar oxazine dye, cresyl violet in ethylene glycol.[5] They used a 60 fs pulse with a bandwidth of 8 nm to produce a hole and a 10 fs pulse with a bandwidth of 100 nm to probe the absorption spectrum. The lifetime of the hole was about ~150 fs. If the inhomogeneous broadening of the absorption spectrum of oxazines are mainly caused by a distribution of solvent organization, excitation at different wavelength can excite a dye with a different solvent organization. As a result, the rate constants of ET may change according to the solvent organization of the excited dye.

However, these phenomena should affect not only the slow part but also the fast part of the reaction. Moreover, the ET of coumarin did not show any excitation wavelength dependence, which will be discussed in the next chapter. Therefore, the slow decay component of OX1 in AN excited at 675 nm, seems to be caused by contamination. The samples are treated with great care, however, they are very sensitive to light and air. The circulating cell for the experiment is quite difficult to clean up. There is also a possibility of a formation of small amount of dimers by the dye. The fluorescence we are observing is very weak, therefore, the decay can be easily affected by a small contamination of fluorescent substances.

IV-3. Observation-wavelength dependence of fluorescence decay

The fluorescence decays of oxazines observed at various wavelengths are shown in Figure IV-9 and IV-10. No wavelength dependence was observed, every decay gives a similar lifetimes for each dye. The reconstructed time-resolved fluorescence spectra of OX1 in AN are shown in Figure IV-11. Markers corresponds to the fluorescence intensities at given wavelength and time, and lines are the results of fitting

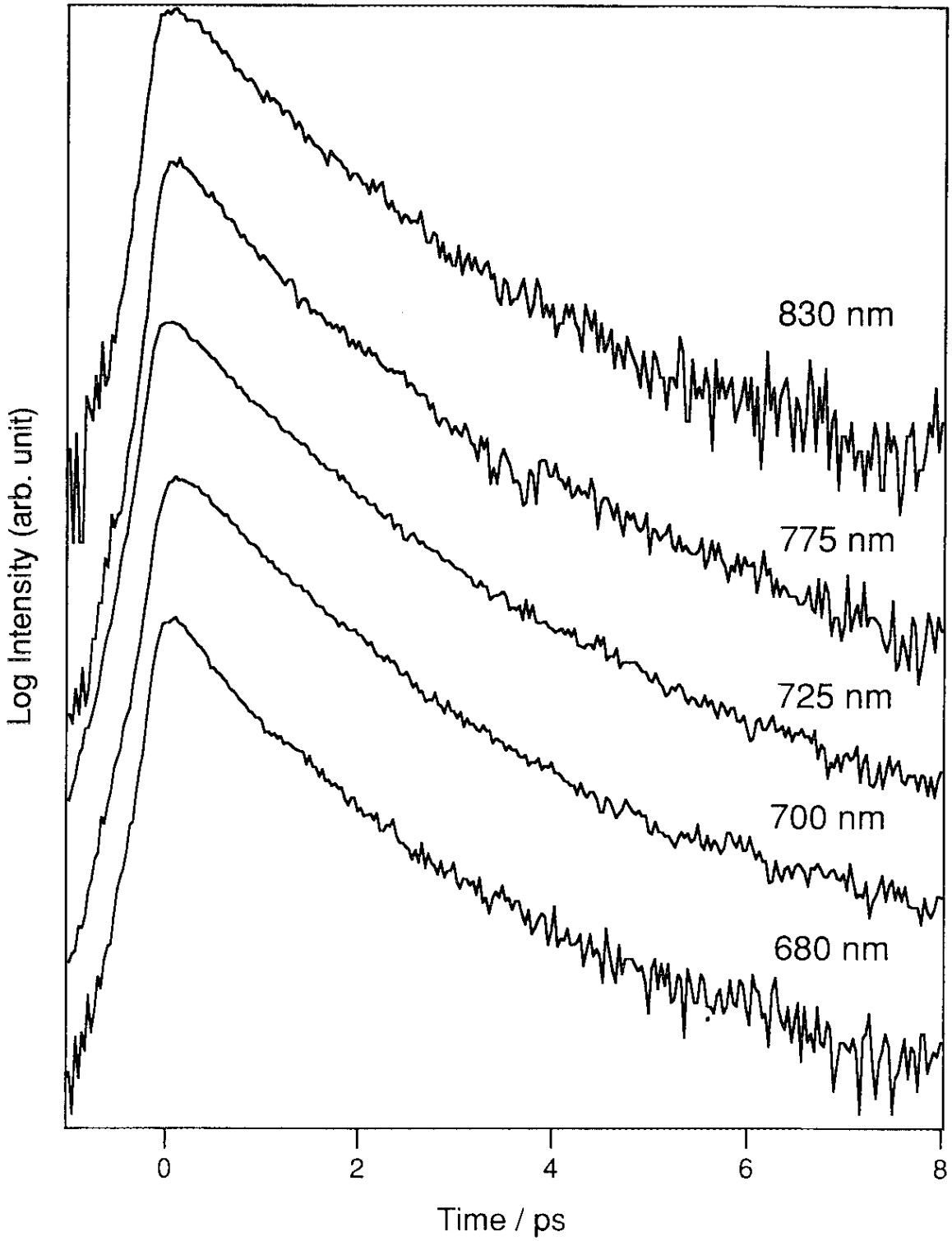

Figure IV-9. Fluorescence decays of OX1 in AN excited at 605 nm and measured at various wavelengths.

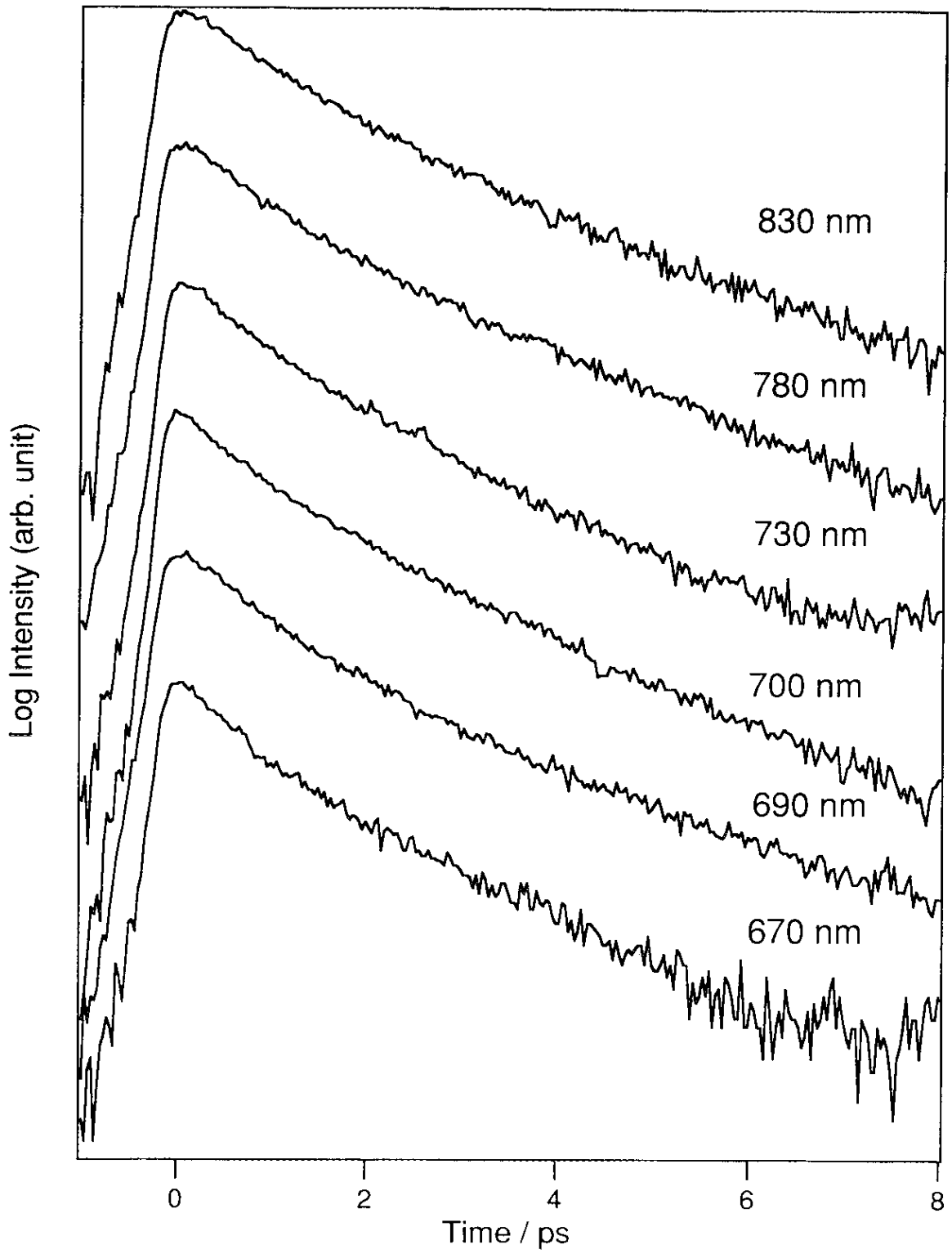

Figure IV-10. Fluorescence decays of NB in AN excited at 605 nm and measured at various wavelengths.

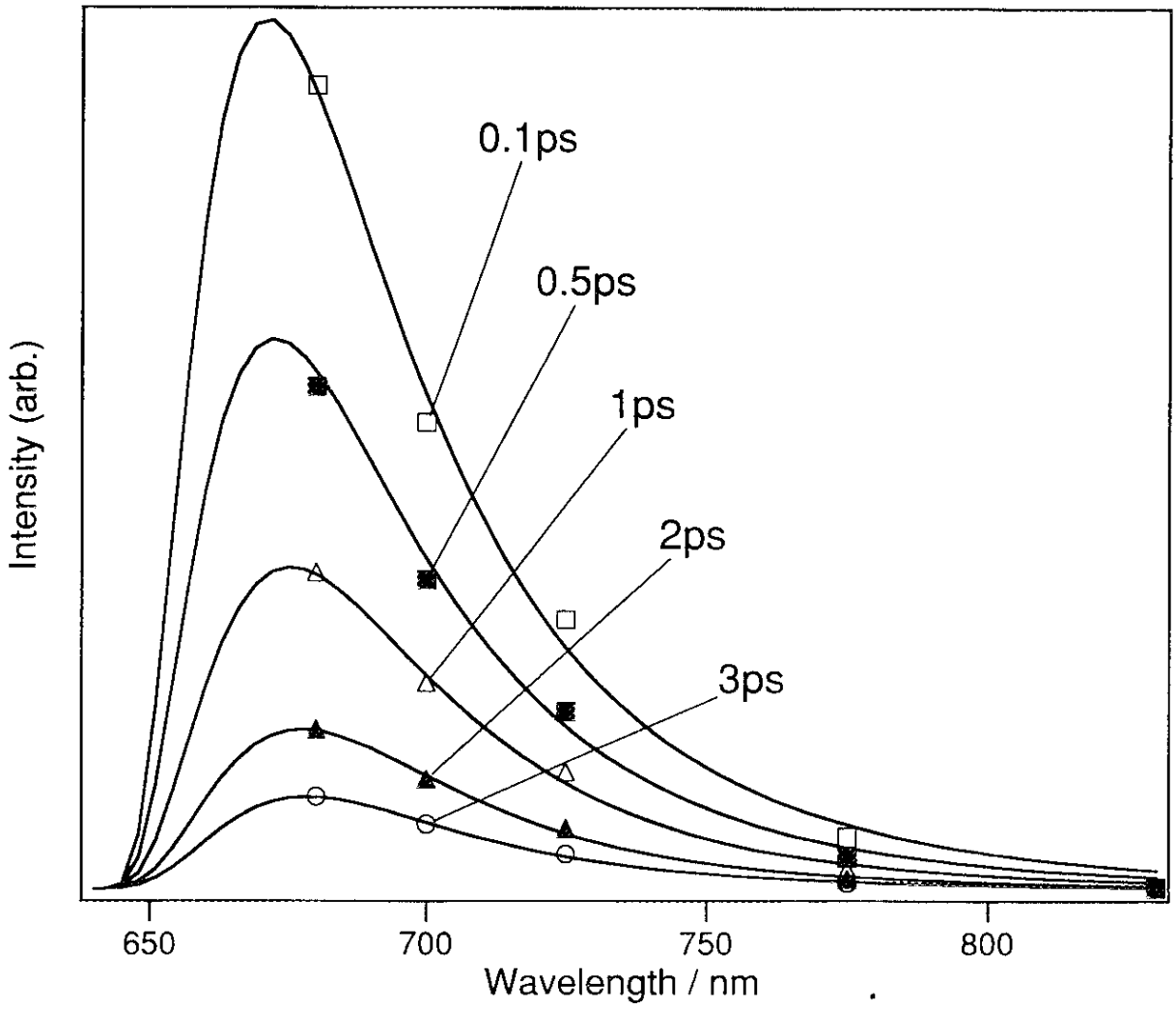

Figure IV-11. Reconstructed time-resolved fluorescence spectra of OX1 in AN. Markers corresponds to the fluorescence intensity at given wavelength and time. Lines are the results of fitting using log-normal function.

to these markers using a log-normal function. Details of this method are already mentioned in Chapter III. The fluorescence decreases without changing the shape of the spectrum, no dynamic Stokes shift can be seen.

For many dye molecules, the dynamic fluorescence Stokes shift caused by solvent relaxation process have been observed. If the dipole moment of excited state differ from the one of the ground state, the initial distribution on the free energy surface, caused by photo-excitation, will not be in equilibrium. The organization of solvent molecules surrounding the dye, has to change to a new organization appropriate for a new dipole. Therefore, this energy relaxation process can be observed as a red shift of the fluorescence spectral peak. The dynamic fluorescence Stokes shift of coumarins are often used to measure solvent relaxation times.[6~8] The fluorescence Stokes shift of NB in methanol is also reported.[9] However, for the case shown in Figure IV-9~11, there seems to be no Stokes shift. The solvent relaxation times for AN are estimated to be 6.7 ps (81 %) and 13.3 ps (19 %) from the dynamic Stokes shift of C102 (see Chapter III). The ET is occurring much faster than the solvation process of AN. In other words, ET is occurring before the distribution relaxes to the equilibrium for the excited state. Therefore, it seems that the population of the excited dye vanishes before the Stokes shift occurs. However, the Stokes shift of OX1 is very small compared to coumarins, *e.g.* 380 cm^{-1} for OX1 in 1-CN, while, 3450 cm^{-1} for C153 in 1-CN. The change in dipole moment of OX1, on photo-excitation, seems to be small compared to coumarins. Therefore, the initial distribution of OX1 on the excited state energy surface, seems to be already close to the equilibrium.

IV-4. Temperature dependence of fluorescence decay

The temperature dependence of fluorescence decays of OX1 in anilines are shown in Figure IV-12. The ultrafast single exponential decay

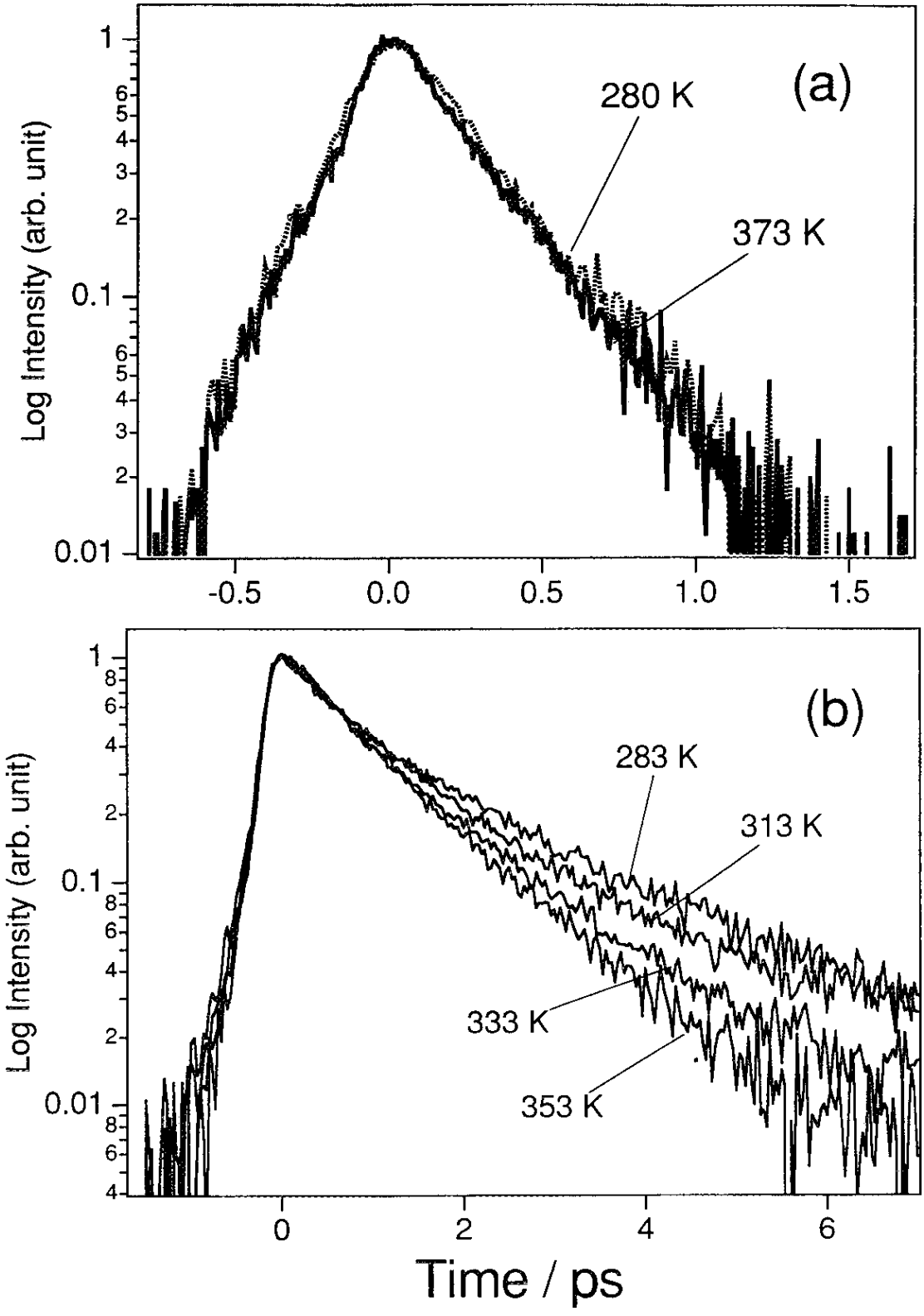

Figure IV-12. Temperature dependence of fluorescence decays of OX1 (a) in DMA and (b) in AN. The samples were excited at 605 nm and observed at 700 nm.

(280 fs) of OX1 in DMA does not show any temperature dependence from 280 K (7 °C) to 373 K (100 °C). In AN, however, a clear temperature dependence was observed in its non-exponential decay. As the temperature increases from 283 K (10 °C) to 353 K (80 °C), the decay become faster. The results of the triple exponential fittings at different temperatures are shown in Table IV-1, and Arrhenius plots of the first and second components are shown in Figure IV-13. The first component (~430 fs) does not show a temperature dependence but the second component shows a dependence which gives an activation energy of 1.0 kcal / mol. This value is much smaller than the activation energies of the longitudinal relaxation times of AN (see Chapter III-3). They were 6.0 kcal / mol for the fast longitudinal relaxation time τ_{F1} and 3.7 kcal / mol for the second one τ_{F2}. Therefore, it seems to be no relation between ET and the longitudinal relaxation times obtained from Debye relaxation times.

IV-5 Effect of solvent dynamics on electron transfer and Sumi-Marcus two-dimensional model

In the present measurements, several interesting features are observed; (1) ET in both solvents is much faster than the diffusive solvation process. Especially in DMA, ET seems to occur more than twenty times faster than the fastest component of the solvation process. (2) OX1 in DMA shows an extremely fast single exponential ET, but in AN, it shows a somewhat slower non-exponential ET. (3) In DMA, there is no temperature dependence, while in AN, there is one for the slower part of the reaction which gives an activation energy of 1.0 kcal / mol.

It is clear from the results mentioned above that, in the present system, the ET occurs much faster than the diffusive solvation process. Weakly polar nature of the solvents seems to be the major reason of the

Table IV-1. Results of triple exponential fitting of the fluorescence decays of OX1 in AN at different temperature.

T (K)	τ_1 (ps)	τ_2 (ps)	τ_3 (ps)
283	0.42 (49 %)	1.62 (42.6 %)	4.4 (9.3 %)
297	0.46 (40 %)	1.64 (57 %)	18 (3 %)
313	0.43 (41.2 %)	1.44 (57.5 %)	>10 (1.3 %)
333	0.39 (39.5 %)	1.3 (60 %)	>10 (0.5 %)
353	0.47 (24 %)	1.11 (75.6 %)	> 10 (0.4 %)

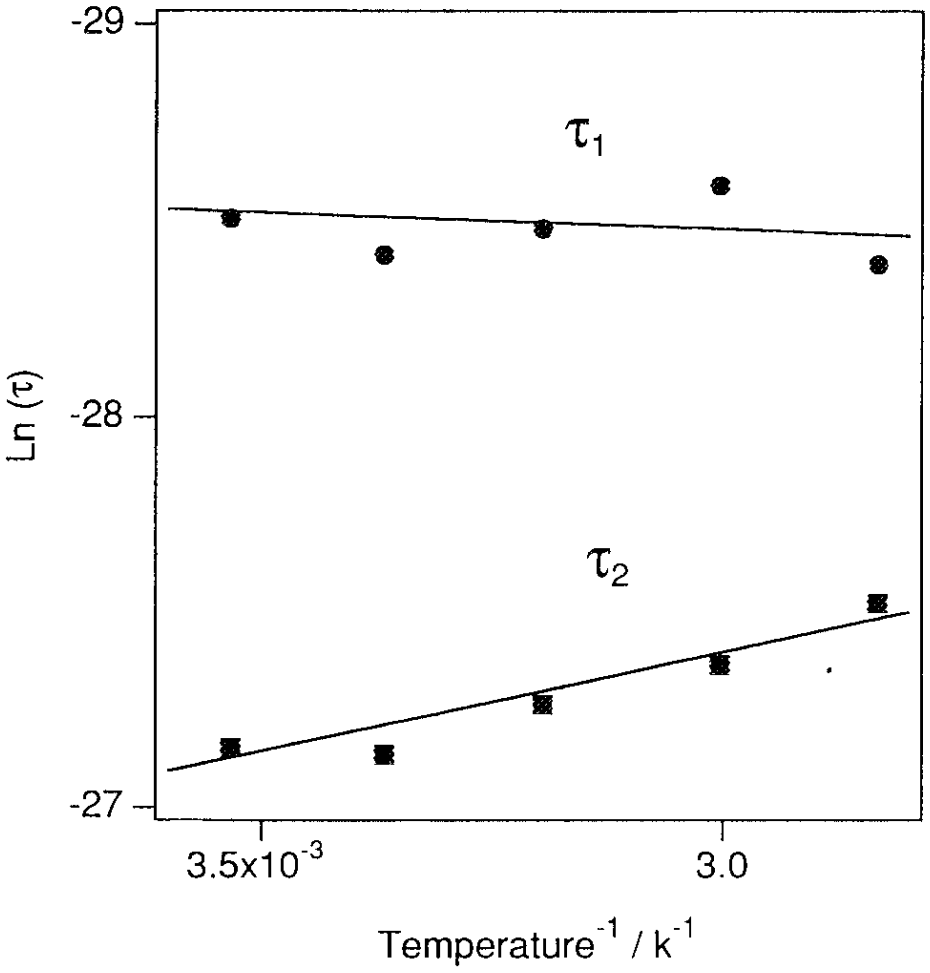

Figure IV-13. Arrhenius plots of the fluorescence lifetimes of OX1 in AN. The first component does not show a temperature dependence, while the second component shows a dependence which gives an activation energy of 1.0 kcal / mol.

very fast ET. However, we cannot neglect a possibility of a much faster solvation process. If such process occurs faster than 100 fs, we may not see it because of the limit of our system response. Inertial contributions to solvation dynamics were observed to be as fast as 60 fs in acetonitrile.[10] However, in the present system, we think that the solvation process itself is not so important because of the weak polarity of these solvents. As is shown in Table IV-2, dielectric constants (ε) are only 5.01 and 6.89 for DMA and AN, respectively. These values are quite small compared to polar solvents such as acetonitrile (ε = 37.5) and methanol (ε = 32.6). In polar solvents ET rates can be controlled by the solvent dynamics, because the energy relaxation process by solvation becomes important. On the other hand, in weakly polar solvents, this effect will become much smaller and the solvation process will not dominate the reaction. Instead, intramolecular vibrational dynamics will be more important for the reaction. In this case, ET can become much faster than solvation dynamics.

In polar solvents, where the ET reactions are dominated by the solvation process, the solvent polarization is the important degree of freedom. In weakly polar solvents, where reactions can proceed much faster than the solvation process, a second coordinate which describes the intramolecular reorganization of the nuclear has to be introduced. One example of this type of two-dimensional model has been proposed and analyzed theoretically by Sumi, Nadler, and Marcus.[11,12]

To explain exponential and non-exponential kinetics of ET faster than the diffusive solvation process, the idea of Sumi-Marcus two-dimensional reaction coordinate is used. In this treatment, instead of the usual one dimensional reaction coordinate (solvent coordinate), two coordinates are used, *i.e.*, the solvent coordinate and the vibrational nuclear coordinate. Free energy surface drawn in a two-dimensional plane

Table IV-2. Solvent properties of the donor solvents. The solvent reorganization energy is calculated for NB.

	DMA	AN
Solvation Time (ps)	7.9 (19 %) 18.7 (81 %)	6.7 (81 %) 13.3 (19 %)
Dipole Moment (D)	1.61	1.51
Dielectric Constant	5.01	6.89
Refractive Index	1.558	1.586
Viscosity(cP)	1.29	3.77
Ionization Energy (eV)	7.12	7.68
Solvent Reorganization Energy (eV)	0.28	0.34
H-bonding	No	Yes

spanned by the solvent coordinate, X, and the nuclear coordinate, q, is shown in Figure IV-14. The contours of the surface for the reactant are on one side of the transition state curve C, and that of the product are on the other side. There are two minima on the surface, located at O for the reactant and O' for the product. For simplicity, it is assumed that both the reactant and the product surfaces are quadratic functions, diagonal in the X and q coordinates and that the force constants are the same for the reactant and for the product.

The nuclear coordinate represents all of the changes in bond lengths and angles between the product and the reactant. The solvation coordinate describes the polarization of the solvent molecule which is related to the solvation process. In the Sumi-Marcus treatment, the vibrational nuclear motion is assumed to be infinitely fast, but the solvent motion is assumed to be diffusive. Thus, although the distribution along X may evolve in time, the distribution along q is always at equilibrium. Therefore, one can define a rate constant $k(X)$ at each X with a suitable averaging over the population in the q coordinate;

$$k(X) = \nu_q \, exp[- \frac{\Delta G^*(X)}{k_B T}] \qquad \text{(IV. 1)}$$

where $\Delta G^*(X)$ is the activation energy for the reaction observed at a point X and ν_q is the pre-exponential factor.

If the motion of the solvent is effectively frozen, the time-dependent full population on the reactant surface $P(t)$ will be given by the sum of each population $p(X, t)$ at each X;

$$P(t) = \int p(X, 0) \, exp[- k(X)t] dX \qquad \text{(IV. 2)}$$

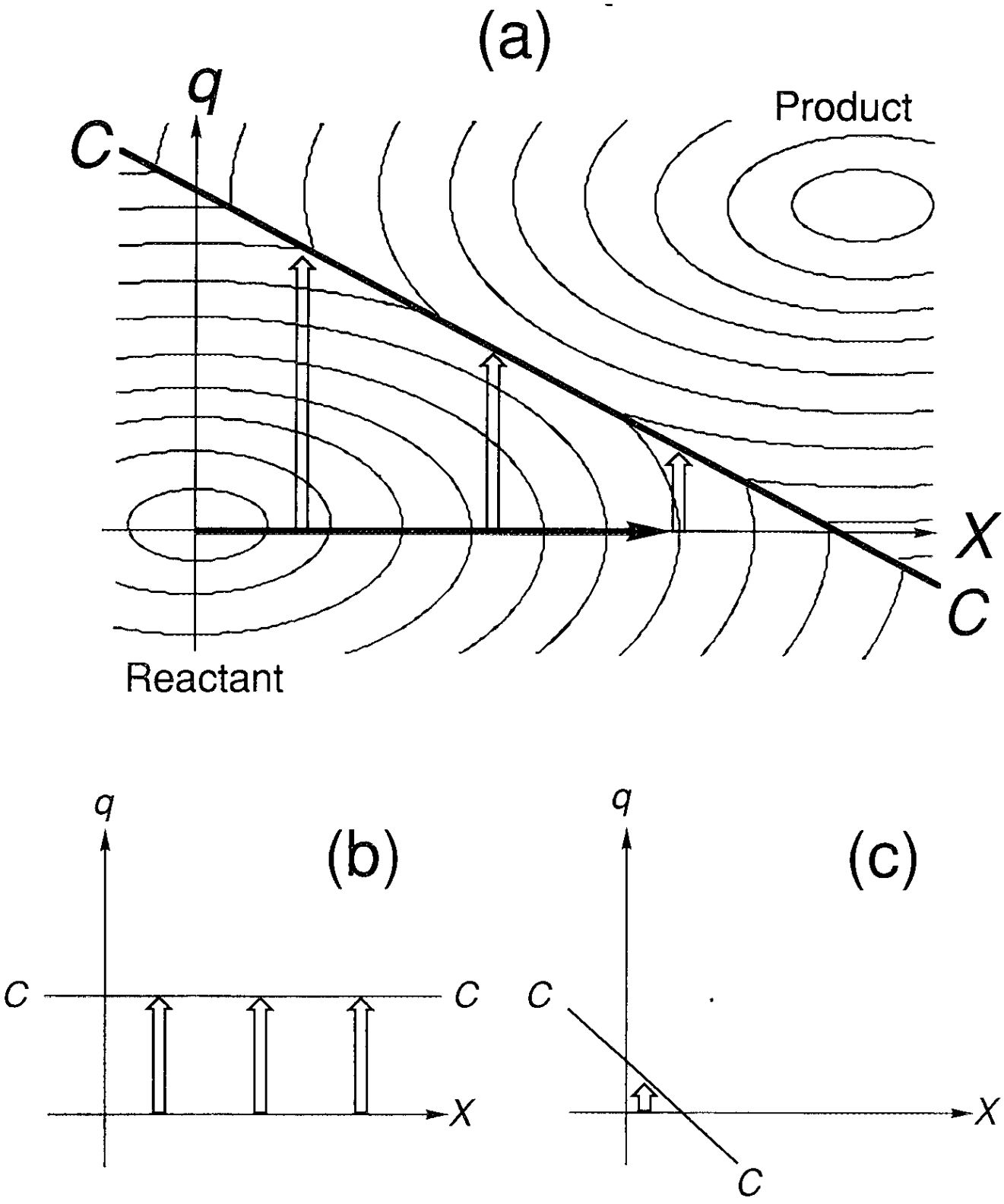

Figure IV-14. (a) A free energy surface drawn in a two-dimensional plane spanned by solvent coordinate *X* and nuclear vibrational coordinate *q*. (b) A simplified scheme with transition state curve *C* parallel to *X* axis. (c) A simplified scheme with almost no energy barrier.

The main point of this assumption is that the different reaction rate $k(X)$ at each X changes the distribution of the reactant during the reaction and give rise to non-exponentiality. If the solvent is not frozen, the population dynamics can be described with a diffusion-reaction equation;

$$\frac{\partial p(X,t)}{\partial t} = D\frac{\partial}{\partial X}\left[\frac{\partial}{\partial X} + \frac{1}{k_B T}\frac{dV(X)}{dX}\right] p(X,t) - k(X)\, p(X,t) \qquad \text{(IV. 3)}$$

where D is the diffusion constant and $V(X)$ is the free energy surface on the solvent coordinate. D is given by $D = k_B T / (2\lambda_s \tau_s)$, where λ_s is the solvent reorganization energy. The first term on the right hand side represents the slow diffusion along the solvent coordinate X and the last term represents the fast reaction along the nuclear coordinate q.

Sumi and Marcus discussed the non-exponentiality of the reaction in terms of the width of the "reaction window". The width of the reaction window can be determined by the ratio between inner-sphere reorganization energy λ_i and solvent reorganization energy λ_s. For the case of $\lambda_i / \lambda_s >> 1$, the reaction takes place through a "wide window" and for $\lambda_i / \lambda_s << 1$, it takes place through a "narrow window". If the transition state curve C is parallel to the X axis (Figure IV-14 (b)), the energy barrier $\Delta G^*(X)$ will be the same at any X and the full decay of the reactant population will be exponential ("wide reaction window" case). On the other hand, if curve C is not parallel to the X axis as shown in Figure IV-14 (a), the energy barrier $\Delta G^*(X)$ will be different at each X. In such a case, the reaction becomes non-exponential ("narrow reaction window" case). At the beginning of the reaction, the population distributed near the "reaction window" will react along the q coordinate over the low energy barrier and the reactants near the bottom of the well will be left behind. There are two pathways for the remaining reactants near the bottom of the well to react. (1) Cross directly the high energy barrier along the nuclear

coordinate q, or (2) first move along the solvent coordinate X to a better position and then cross the lower reaction barrier along q axis. In such a case, the distribution of the reactant will change during the reaction.

There are some literature reports of applications and extensions of the Sumi-Marcus model.[13~16] Walker *et al.*[13] combined it with the Jortner-Bixon model and introduced the effect of a quantum mechanical high frequency vibration. Tominaga *et al.*[14] introduced the effect of an inertial component of solvation dynamics to try and understand how that affects very fast ET kinetics.

In a qualitative application of the treatment of Sumi and Marcus to our experimental results, the reaction of OX1 in DMA might be thought to have a wider reaction window than that of OX1 in AN. As is mentioned in Chapter III, the Stokes shift shown in Figure III-3 implies a slightly stronger solvent polarity for AN than DMA. This may cause a larger solvent reorganization energy λ_S for AN than DMA. An independent estimate of λ_s can be also determined from the size of the molecules and dielectric constants. Kobayashi *et al.* calculated these values for NB.[1] However, the difference was not so large; 0.28 eV for DMA and 0.34 eV for AN. For inner-sphere reorganization energy λ_i, similar values for both systems are also expected, since same electron acceptor OX1 is used. For the ET of NB, $\lambda_i = 0.31$ eV was estimated by Kobayashi *et al.* Therefore, the ratio becomes similar for both solvents; $\lambda_i / \lambda_s \approx 1$. The "width of reaction window" does not seem like a plausible explanation for the large difference between the ET of OX1 in DMA and AN.

The physical properties of the two solvents are listed in Table IV-2. There are several interesting differences: (1) viscosity, (2) ionization potential, and (3) hydrogen bonding ability. The amino group of AN can form hydrogen bonds with the solute molecule or with solvent molecules themselves but that of DMA cannot. The hydrogen bonding between

solvent molecules may be the reason for high viscosity of AN relative to DMA. The high viscosity can slow down the solvent dynamics and therefore can slow down the reaction. However, the observed solvent relaxation time is even somewhat longer in DMA. Therefore difference in viscosity may not be suitable to explain the difference in the two systems.

The remaining difference which should be noted is the difference in ionization potential. The difference was calculated to be 0.17 eV between DMA and AN, from the ionization potential in the gas phase I_{vap}, using the next formula;[17]

$$\Delta I_{cond} = I_{vap}^{AN} - I_{vap}^{DMA} - (1 - \frac{1}{\varepsilon_{AN}}) \frac{e2}{2r_{AN}} + (1 - \frac{1}{\varepsilon_{DMA}}) \frac{e2}{2r_{DMA}} \qquad \text{(IV. 4)}$$

where ε is the dielectric constant, e the electronic charge, and r the radius of the charged solvent molecule. This difference will cause a difference in the free energy gap for the reaction, and, thereby, the free energy barrier for the reaction. This could explain the faster reaction in DMA and the observed temperature dependence, if the reaction in DMA is barrierless and the reaction in AN has a small activation energy.

It seems that the faster reaction in DMA than in AN can be readily explained by the difference in energy gap. On closer examination, it seems that this difference in energy gap can also be the cause of the difference in exponentiality. As is shown in Figure IV-14 (a), if there is a energy barrier, the reactants populated near the "reaction window" will react first and the ones populated near the bottom will be left behind. Therefore, the distribution of the reactant will be altered by the reaction, and non-exponential reaction take place. On the other hand, if there is no reaction barrier, the reactant can react very rapidly without this kind of effect and exponential kinetics may occur (Figure IV-14 (c)). Thus, the difference in energy gap may be the major reason for the different ET kinetics in AN

and DMA. To support this conclusion, we have performed simulations using a modified Sumi-Marcus diffusion-reaction equation, described in the next section.

IV-6. Simulation of electron transfer process based on Sumi-Marcus Jortner-Bixon hybrid model

The Sumi-Marcus model treats both the solvent and intramolecular mode classically. However, the actual system should have not only the classical modes but also quantum mechanical high-frequency modes. Jortner and Bixon have developed an ET model which introduces the effect of the quantum mechanical high frequency modes.[18] In this model, the reactant surface crosses not only with the vibrational ground state of the product but also with vibrationally excited states of the product. Therefore, reaction occurs to several free energy surfaces of the product, each of which is characterized by a different vibrational quantum number. The effect of high frequency modes become remarkable in the inverted region, which makes the bell-shape energy gap dependence asymmetric. The reaction of oxazines in DMA are activationless, which means that the reaction is not in the inverted region but very close to it. Therefore, for the simulation, we use hybrid model of Sumi-Marcus and Jortner-Bixon developed by Walker *et al.*[13] In this model, the intramolecular vibration is separated into the quantum mechanical high frequency mode and classical low frequency mode. Walker *et al.* obtained a modified diffusion-reaction equation;

$$\frac{\partial p(X,t)}{\partial t} = D \frac{\partial}{\partial X}\left[\frac{\partial}{\partial X} + \frac{1}{k_B T}\frac{dV(X)}{dX}\right] p(X,t) - \sum_n k(n,X)\ p(X,t) \qquad \text{(IV. 5)}$$

where $k(n, X)$ is the reaction rate between the vibrational ground state of the reactant and vibrational state n of the product. The non-adiabatic formula is used for $k(n, X)$;

$$k(n, X) = \frac{2\pi}{h} V_{el}'^2 (4\pi\lambda_l k_B T)^{-1/2} exp(- \frac{\Delta G^*(n, X)}{k_B T}) \qquad \text{(IV. 6)}$$

where λ_l is the reorganization energy for the classical low frequency mode. V'_{el} is the electronic matrix element concerning the effect of Franck-Condon factor which can be written as

$$V_{el}'^2 = \frac{S^n}{n!} exp(-S) V_{el}^2 \qquad \text{(IV. 7)}$$

where the electron-vibrational coupling strength is $S = \lambda_h^2/2$. λ_h is the reorganization energy for the high-frequency mode. $\Delta G^*(v_r, X)$ is the activation energy which depends on the quantum number of the vibrational state n and the solvation coordinate X;

$$\Delta G^*(n, X) = (\lambda_s + \Delta G - 2X\lambda_s + nh\nu_h + \lambda_l)^2 / 4\lambda_l \quad . \qquad \text{(IV. 8)}$$

For D, the time dependent diffusion coefficient $D(t)$ is used;[20]

$$D(t) = - \frac{k_B T}{2\lambda_s} \frac{1}{C(t)} \frac{dC(t)}{dt} \qquad \text{(IV. 9)}$$

where

$$C(t) = a_1 exp(- t / \tau_1) + a_2 exp(- t / \tau_2) \qquad \text{(IV. 10)}$$

τ_1, is the first and τ_2 is the second solvation time, and $a_1 + a_2 = 1$.

This model contains many parameters, some of them are difficult to obtain experimentally. But we tried to fit the experimental data using as realistic parameters as possible. Firstly we estimated that the minimum of the S_0 and S_1 free energy surface of OX1 are located at the same point. This means that the excited state dipole and ground state dipole moment of OX1 does not change drastically. This approximation makes the initial distribution produced by the excitation an equilibrium one. As is mentioned in section IV-3, the Stokes shift of OX1 is very small, therefore, this approximation seems quite reasonable. Secondly, it is assumed that the reaction occurs only from the lowest vibrational state of the reactant. This approximation seems quite reasonable, as is mentioned in section IV-2, there is no excitation wavelength dependence. We used 0.12 eV for the solvent reorganization energy λ_s, and 0.38 eV for the reorganization energy of the classical low frequency mode λ_l. We had to use a smaller value for λ_s than the one listed in Table III-2 to make the reaction window rather wide ($\lambda_l / \lambda_s \approx 3$). We used 0.015 eV for the electronic matrix element V_{el}, which is smaller than the value estimated by Kobayashi *et al.*[1] (0.036 eV). If the value of Kobayashi *et al.* is used, the reaction becomes too fast. Double solvation time of 7 ps (50%) and 15 ps (50%) which are close to the observed solvation time for AN and DMA are used. 0.13 eV and 1400 cm^{-1} are used for the reorganization energy λ_h and the frequency ν_h of the high frequency mode, respectively.

The results of the simulations are shown in Figure IV-15. The normalized population of the reactant $P(t)$ is plotted against time (ps) on a logarithmic scale. The energy gaps $-\Delta G$ are 0.50 eV for Figure IV-15 (a) and 0.33 eV for Figure IV-15 (b). Temperature is changed in each set, from 273 K to 373 K with an assumption that the physical properties of the solvent do not change drastically with temperature. The longitudinal relaxation time changed drastically with temperature, as is mentioned in

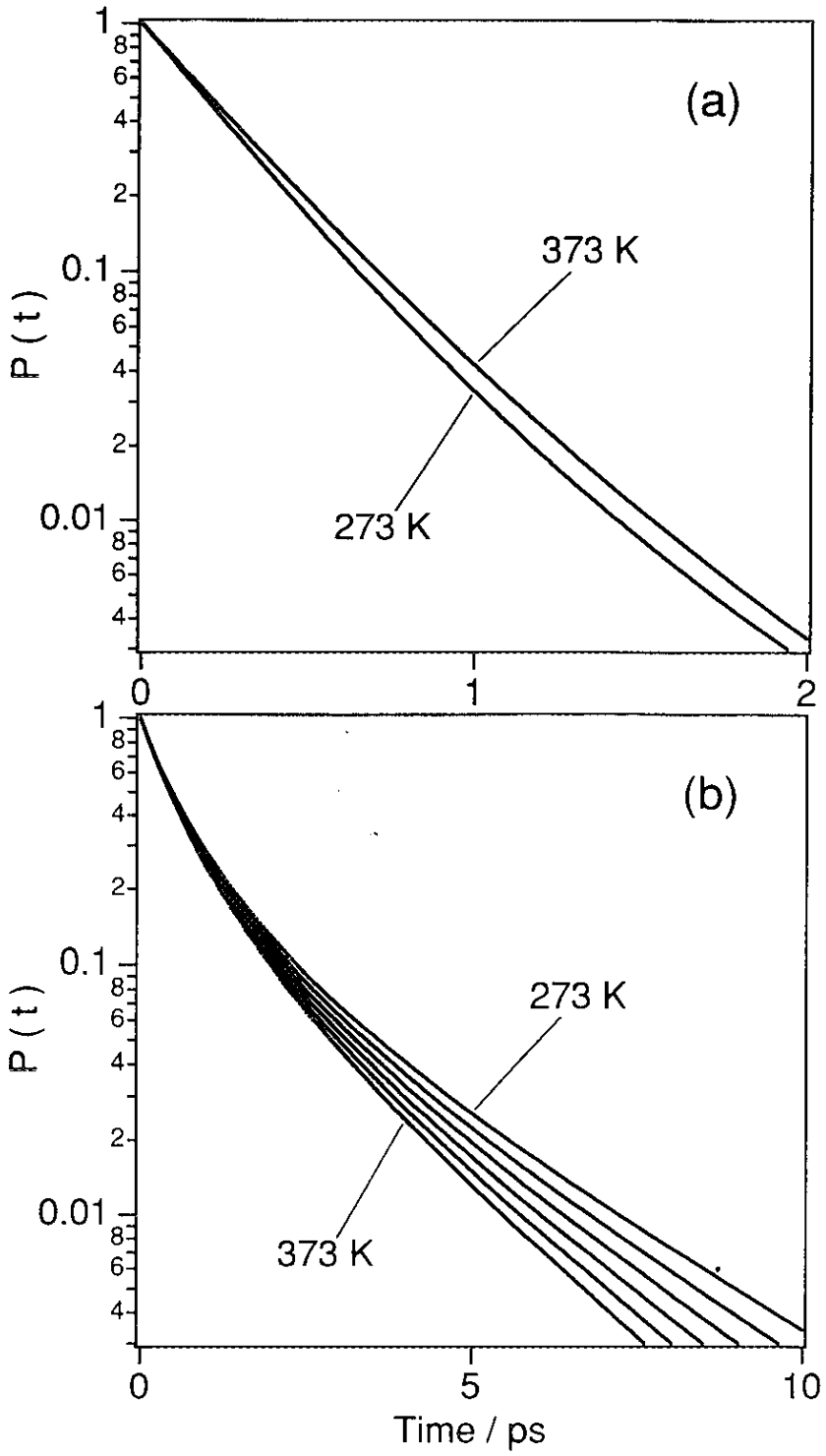

Figure IV-15. Results of simulation using Sumi-Marcus Jortner-Bixon hybrid model. (a) $-\Delta G = 0.50$ eV, $T = 273$ and 373 K. (b) $-\Delta G = 0.33$ eV, $T = 273$, 293, 313, 333, 353, and 373 K.

Chapter III. The activation energies were 6.0 kcal / mol for the first longitudinal relaxation time τ_{F1} and 3.7 kcal / mol for the second one τ_{F2}. However, it is not realistic to use these parameters to simulate the reaction of OX1, which only shows an activation energy of 1.0 kcal / mol for the slow part of the kinetics in AN. As is shown in Figure III-5, the fluorescence decay of C102 in AN did not show any temperature dependence. Therefore, it is assumed that relaxation time of the donor solvents do not change drastically with temperature. Another property of the solvent which changes with temperature is the dielectric constant. From Table III-1 and IV-3, the static dielectric constant ε_0 changes from 6.89 at room temperature to 6.1 at 75 °C (348 K). The solvent reorganization energy λ_s will change with ε_0. Their relation is;[19]

$$\lambda_s = e^2\left(\frac{1}{n^2} - \frac{1}{\varepsilon_0}\right)\left(\frac{1}{2r_D} + \frac{1}{2r_A} - \frac{1}{L}\right) \qquad \text{(IV. 11)}$$

where n is the refractive index, r the radius of donor and acceptor molecule, and L the distance between donor and acceptor. Therefore, if λ_s is 0.13 eV at room temperature, it becomes 0.12 eV at 75 °C. This difference is small enough to neglect.

Figure IV-15 (a) corresponds to the ET of OX1 in DMA, where there is no activation barrier. The free energy surface for the lowest vibrational state of the product crosses the bottom of the reactant surface. Such a situation occurs when $-\Delta G = \lambda_I + \lambda_s = 0.50$ eV. The simulated reaction shown in Figure IV-15 (a) is almost exponential, which coincides with the experimental result of OX1 in DMA shown in Figure IV-3 (a). The exponentiality of the reaction increases when ΔG is somewhat larger. On the other hand, it decreases when the reaction window is narrower ($\lambda_I / \lambda_s \leq 1$).

In Figure IV-15 (a), the reaction becomes slower at higher temperature. When the reaction window is located near the bottom of the reactant well, a higher temperature causes a wider distribution which spreads the population further from the reaction window. However, no temperature dependence was observed for OX1 in DMA within the experimental error.

In Figure IV-15 (b), $-\Delta G_0$ is 0.17 eV smaller than Figure IV-15 (a). This difference corresponds to the difference in ionization potential between DMA and AN in condensed phase. Although the size of the reaction window is not changed, the reaction shows non-exponential kinetics, which agrees with the experimental result of OX1 in AN. The reaction becomes faster as the temperature increases and the change is rather large at the slower part of the reaction than the fast part. The results of fitting to these simulations are shown in Table IV-3, and Arrhenius plots obtained from these fittings are in Figure IV-16. The first component (~420 fs) shows almost no activation barrier (0.1 kcal / mol), whereas the second component has an activation barrier of 0.4 kcal / mol. This value is somewhat smaller than the experimental result (1.0 kcal / mol), however it still coincides quite well with the actual experiment.

IV-7. Summery of Chapter IV

Intermolecular ET faster than the solvation process, was found for the system with oxazines in weakly-polar electron donating solvents. Especially in DMA, the reaction occurs more than an order of magnitude faster than the solvation process. The reaction of OX1 in DMA shows clear single exponential kinetics with no activation energy. ET with non-exponential kinetics occurs in AN. The slower part of the non-exponential kinetics is temperature dependent, indicating an activation energy of 1.0 kcal / mol. The difference in energy gap seems to explain the observed

Table IV-3. The results of triple exponential fitting (τ_1, τ_2, and τ_3) of the simulated ET shown in Figure III-18 (b)

T (K)	τ_1 (ps)	τ_2 (ps)	τ_3 (ps)
273	0.45 (61.7 %)	1.71 (37.4 %)	>10 (0.9 %)
293	0.44 (62.1 %)	1.64 (37.1 %)	>10 (0.8 %)
313	0.44 (62.3 %)	1.58 (37.1 %)	>10 (0.6 %)
333	0.43 (62.3 %)	1.52 (37.2 %)	>10 (0.5 %)
353	0.43 (62.2 %)	1.46 (37.4 %)	>10 (0.4 %)
373	0.42 (61.9 %)	1.41 (37.6 %)	>10 (0.5 %)

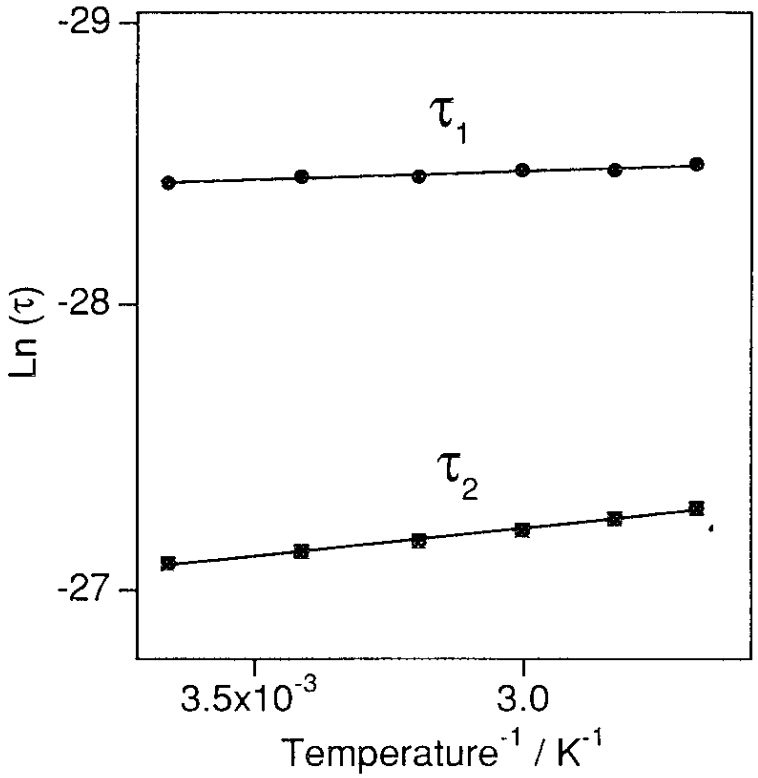

Figure IV-16. Simulated Arrhenius plots of first component τ_1 and the second component τ_2 when $-\Delta G = 0.33$ eV. The activation energies obtained from the slopes are 0.1 kcal / mol for τ_1 and 0.4 kcal / mol for τ_2.

phenomena, including the difference in exponentiality of the kinetics. This conclusion can be explained using a two dimensional reaction coordinate, *i.e.*, the solvent coordinate and nuclear vibrational coordinate. Simulations using a modified Sumi-Marcus diffusion-reaction equation were also carried out. When the reaction window is wide ($\lambda_i / \lambda_s = 3$), the kinetics of the reaction changes from non-exponential to exponential as the activation energy decreases.

References for Chapter IV

1. T. Kobayashi, Y. Takagi, H. Kandori, K. Kemnitz, and K. Yoshihara, *Chem. Phys. Lett.* **180**, 416, (1991).

2. H. Kandori, K. Kemnitz, and K. Yoshihara, *J. Phys. Chem.*, **96**, 8042, (1992).

3. K. Yoshihara, Y. Nagasawa, A. Yartsev, S. Kumazaki, H. Kandori, A. E. Johnson, and K. Tominaga, submitted to *J. Photchem. Photobiol. A.*

4. A. Mokhtari, J. Chesnoy, and A. Laubereau, *Chem. Phys. Lett.*, **155**, 593 (1989).

5. C. H. Brito Cruz, R. L. Frok, W. H. Knox, and C. V. Shank, *Chem. Phys. Lett.* **132**, 341, (1986).

6. M. Maroncelli and G. R. Fleming, *J. Chem. Phys.*, **86**, 6221, (1987).

7. M. A. Kahlow, T. J. Kang, and P. F. Barbara, *J. Chem. Phys.*, **88**, 2372, (1988).

8. M. A. Kahlow, W. Jarzeba, T. J. Kang, and P. F. Barbara, *J. Chem. Phys.*, **90**, 151, (1989).

9. A. M. J. Cesnoy and A. Laubereau, *Chem. Phys. Lett.*, **155**, 593, (1989).

10. S. J. Rosenthal, X. Xie, M. Du and G. R. Fleming, *J. Chem. Phys.*, **95**, 4715, (1991) .

11. H. Sumi and R. A. Marcus, *J. Chem. Phys.*, **84**, 4894, (1986).

12. W. Nadler and R. A. Marcus, *J. Chem. Phys.*, **86**, 3906, (1987).

13. G. C. Walker, E. Akesson, A. E. Johnson, N. E. Levinger, and P. F. Barbara, *J. Phys. Chem.*, **96**, 3728, (1992).

14. K. Tominaga, D. A. V. Kliner, A. E. Johnson, N. E. Levinger, and P. F. Barbara, *J. Chem. Phys.*, **98**, 1228, (1993).

15. S. Su and J. D. Simon, *J. Chem. Phys.*, **89**, 908, (1988).

16. D. K. Phelps and M. J. Weaver, *J. Phys. Chem.*, **96**, 7187, (1992).

17. T. Tani and S. -I. Kikuchi, *Rept. Inst. Ind. Sci. Univ. Tokyo*, **18**, 51, (1968).

18. J. Jortner and M. Bixon, *J. Chem. Phys.*, **88**, 167, (1988).

19. R. A. Marcus, *J. Chem. Phys.*, **24**, 988, (1956).

20. J. T. Hynes, *J. Phys. Chem.*, **90**, 3701, (1986).

CHAPTER V
SUBSTITUENT EFFECT AND ENERGY GAP DEPENDENCE OF ELECTRON TRANSFER

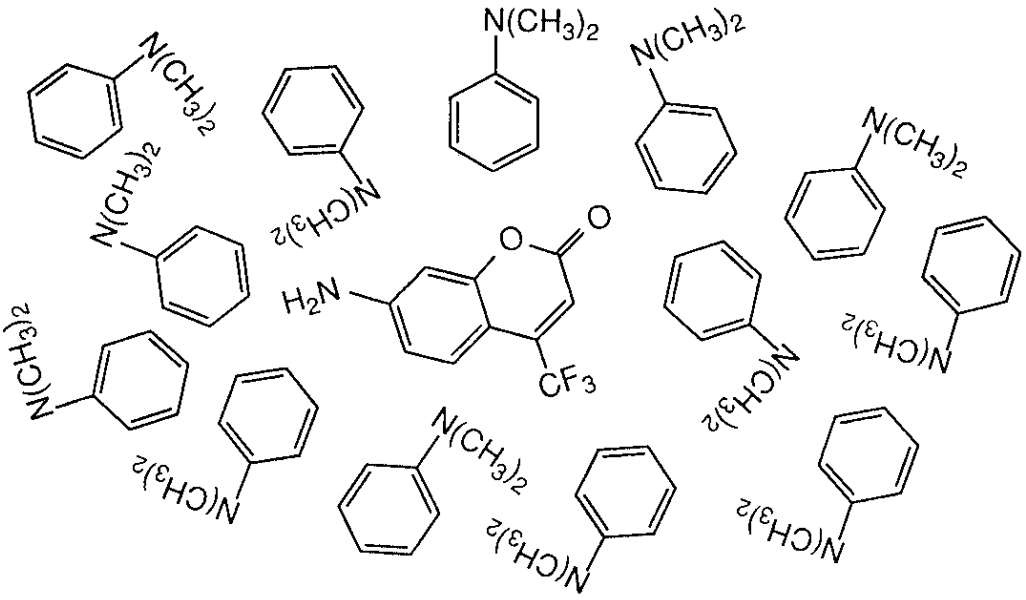

V-1. Fluorescence quenching of coumarins by electron transfer

7-aminocoumarin dyes, shown in Figure V-1, are usually strong fluorescent substances used as laser dyes.[1,2] Their fluorescence yield is almost unity in usual non-reactive solvents, however, when they are dissolved in electron donating solvents, such as AN or DMA, the fluorescence is strongly quenched. In Figure V-2, the absorption and fluorescence spectra of coumarin 151 (C151) in DMA and in ethyl acetate (EtAc) are shown. Both solvents have a similar value of $E_T(30)$, an empirical parameter of solvent polarity, which is 38 kcal / mol.[3] However, the fluorescence intensity of C151 in DMA is more then 1000 times weaker than the one in EtAc. The sharp peaks appearing in the fluorescence spectra of C151 in Figure V-2 (b) are Raman bands of the solvent, the intensity of the former being much weaker than the latter. When these Raman bands are subtracted, with taking into consideration of the effect of self-absorption, fluorescence peak appears around 410 nm which can be seen in the inset of Figure V-2 (b). This is much blue shifted compared to the fluorescence peak in EtAc (449 nm, Figure V-2 (a)). The details of the fluorescence peak shifts will be discussed in section V-4.

This kind of strong fluorescence quenching was also observed in the case of Nile blue A perchlorate (NB) and oxazine 1 (OX1), as is mentioned in Chapter IV. In the previous studies,[4~7] it was concluded that these fluorescence quenchings are due to ET from the solvent to the excited dye. The radical anion of these dyes with the cations of the solvents were observed by the subpicosecond transient absorption measurements.[5] Therefore, this strong fluorescence quenching of coumarins can be also regarded as an ET form the donor solvent to the excited dyes. The reaction of this system is proposed in Figure V-3. When dye is photo-excited, ET from the solvent occurs. The back electron transfer from the radical anion of

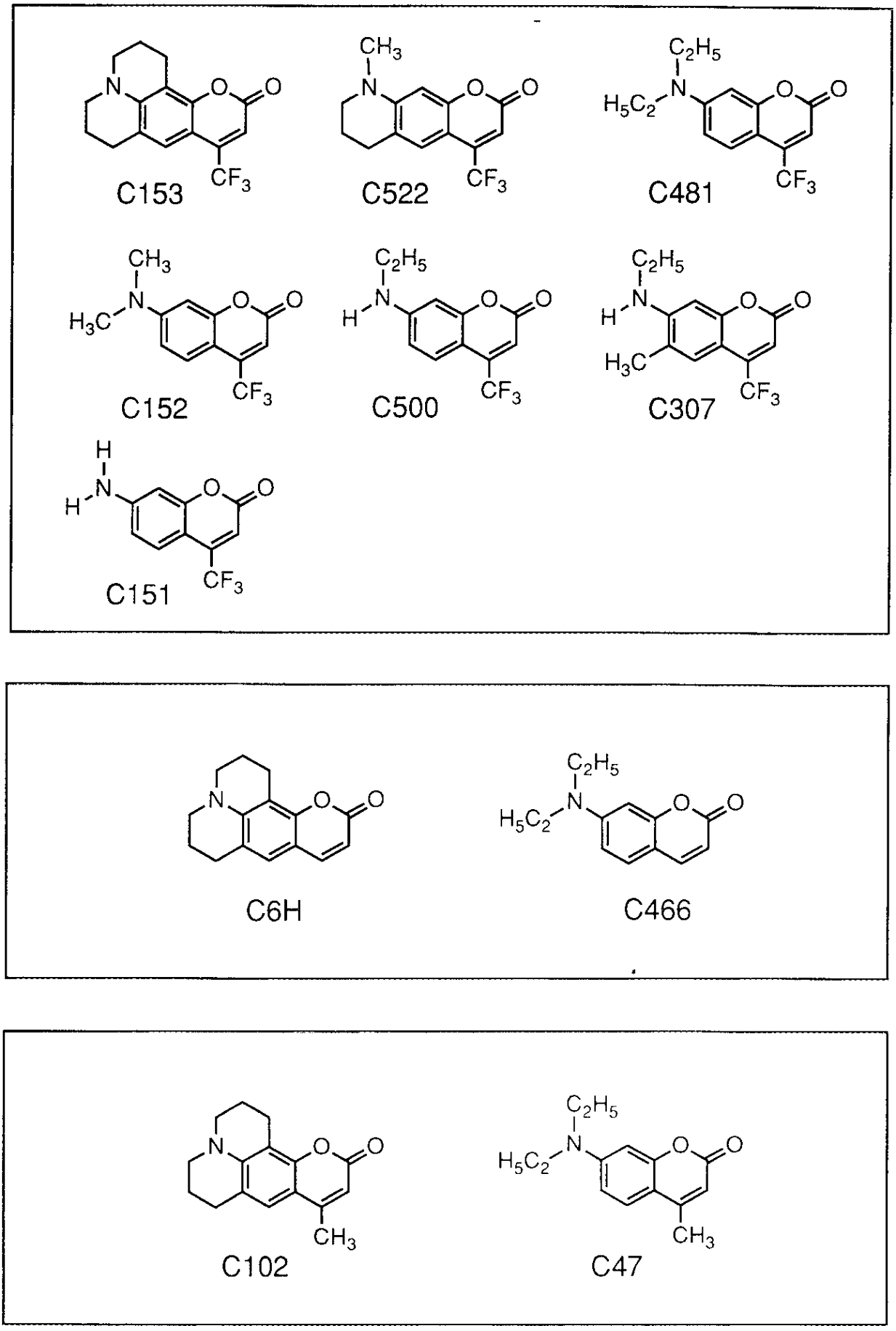

Figure V-1. Structures of coumarins.

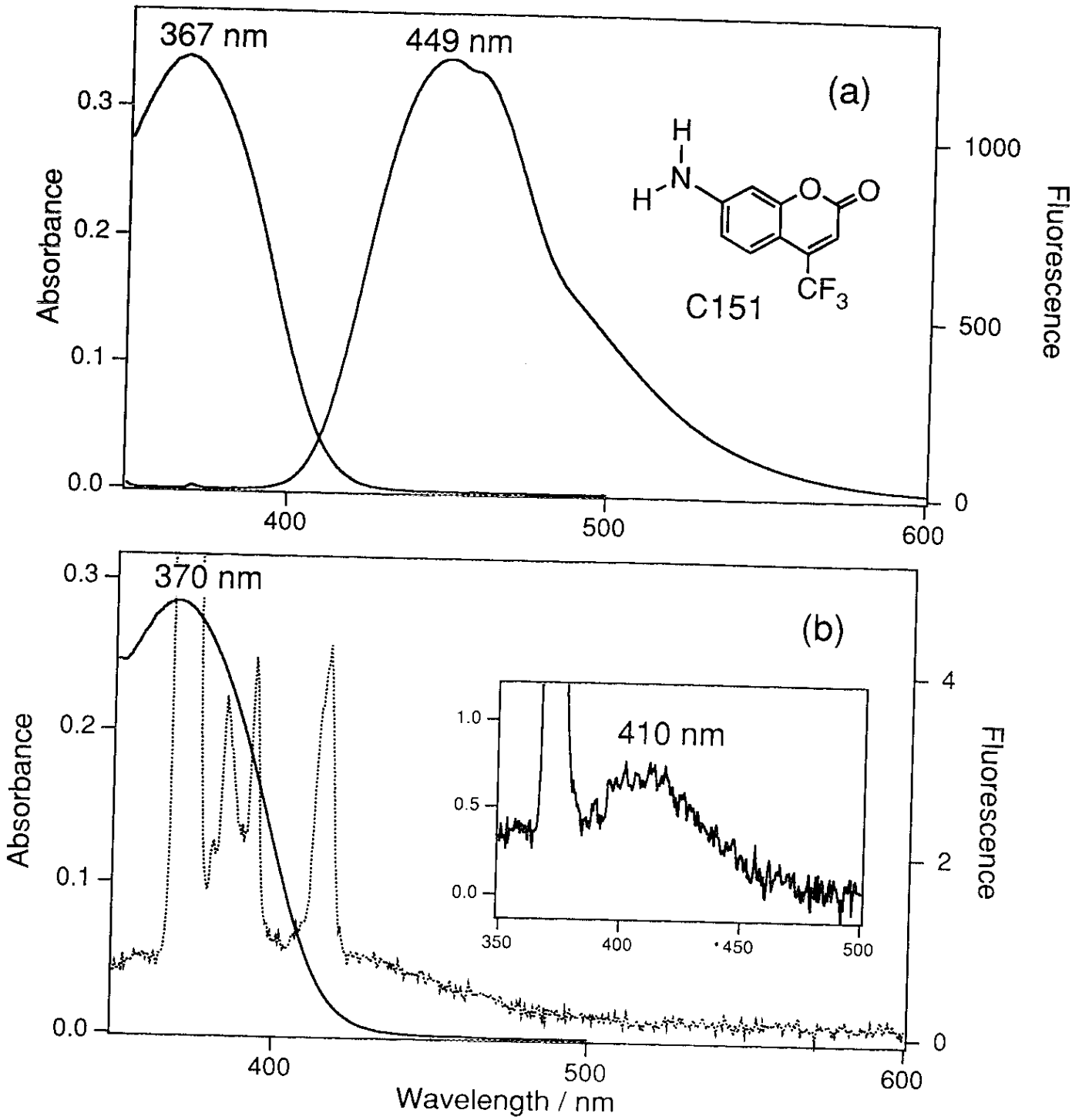

Figure V-2. Absorption and fluorescence spectra of C151 excited at 370 nm, (a) in ethyl acetate and (b) in DMA. The sharp peaks appearing in (b) are the Raman bands of the solvent. The fluorescence spectrum obtained by subtracting these bands is shown in the inset of (b).

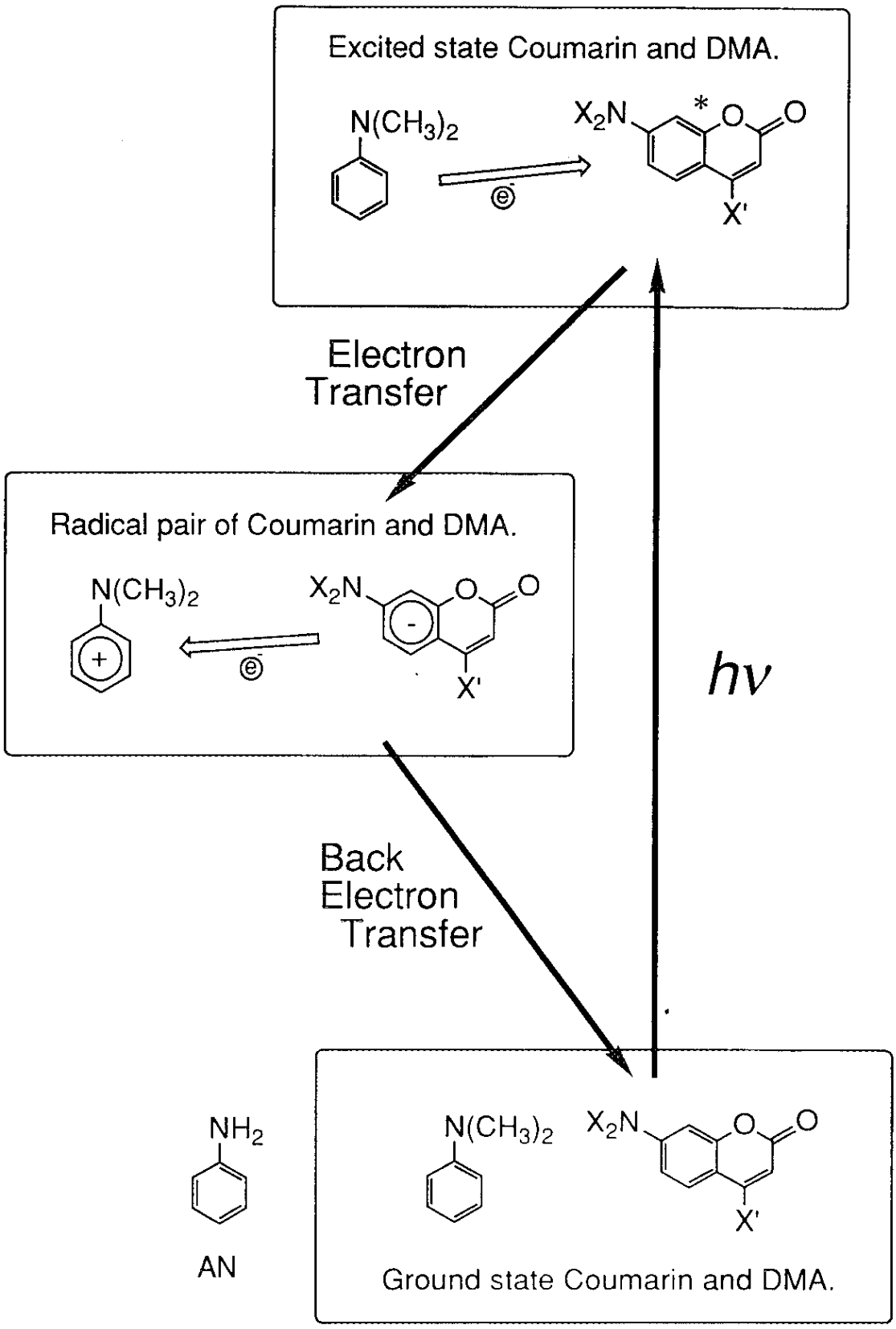

Figure V-3. Reaction of coumarins in electron donating solvents.

the dye to the solvent cation occurs successively, and the system comes back to the ground state.

Broadening of the absorption spectrum was observed for OX1 in DMA (Figure IV-2), which might indicate formation of a charge transfer complex. However, in the case of coumarins, such broadening was not observed.

The amount of fluorescence quenching depends on the structure of coumarin. Fluorescence of some coumarins were strongly quenched, like the ones shown in Figure V-2 (b), however some showed only a weak fluorescence quenching. These observation indicates that the rate constants of ET should be spread over various regions, form the nanosecond to femtosecond domain. Therefore, fluorescence decay measurements were carried.

V-2. The effect of substituent groups on electron transfer

For the studies of the strongly quenched fluorescence, the femtosecond fluorescence up-conversion technique was applied.[8,9] For the study of weakly quenched coumarins, the picosecond photon counting method was used.[10] The fluorescence decays of 4-CF_3 coumarins are shown in Figure V-4, V-5, and V-6. The decays of coumarins with no substitution in 4-position is shown in Figure V-7, and the decays of 4-methyl coumarins are shown in Figure V-8. The results of fittings are shown in Table V-1 and V-2. The observed wavelength was set close to the maxima of the fluorescence to avoid the effect of dynamic fluorescence Stokes shift.

In these series of measurements, there are several interesting observations. (1) Most of the ET of 4-CF_3 coumarins are faster than the diffusive solvation process, (2) and most of them shows non-exponential fluorescence decay. The results of analysis shown in Table V-1 are tentatively made with a double exponential function, except for the single exponential function (ca. 210 fs) for the fastest system of C151 in DMA. (3)

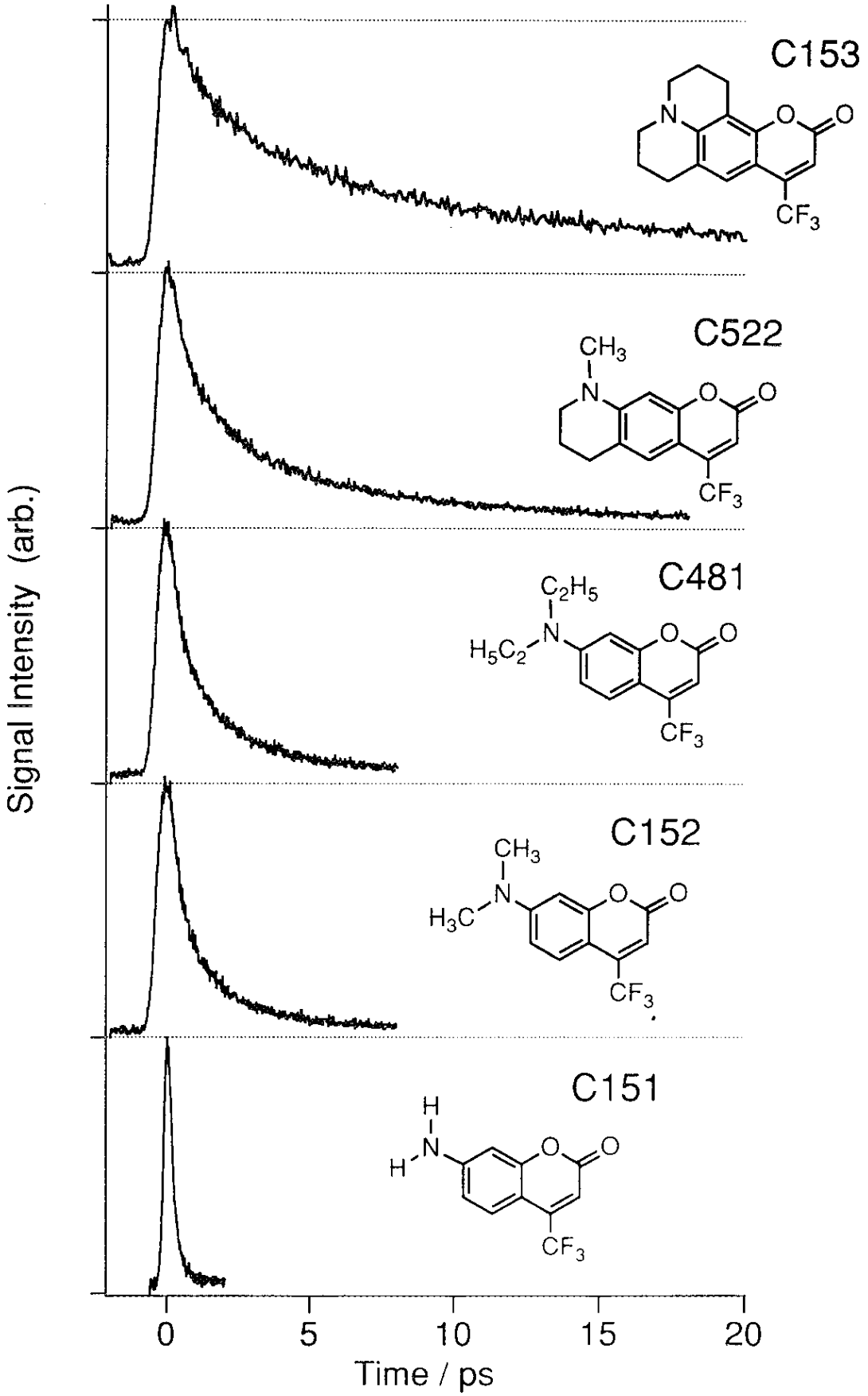

Figure V-4. Fluorescence quenching of 4-CF_3 coumarins in DMA, excited at 395 nm and observed at 510 nm. Concentartions are $2x10^{-3}$ M.

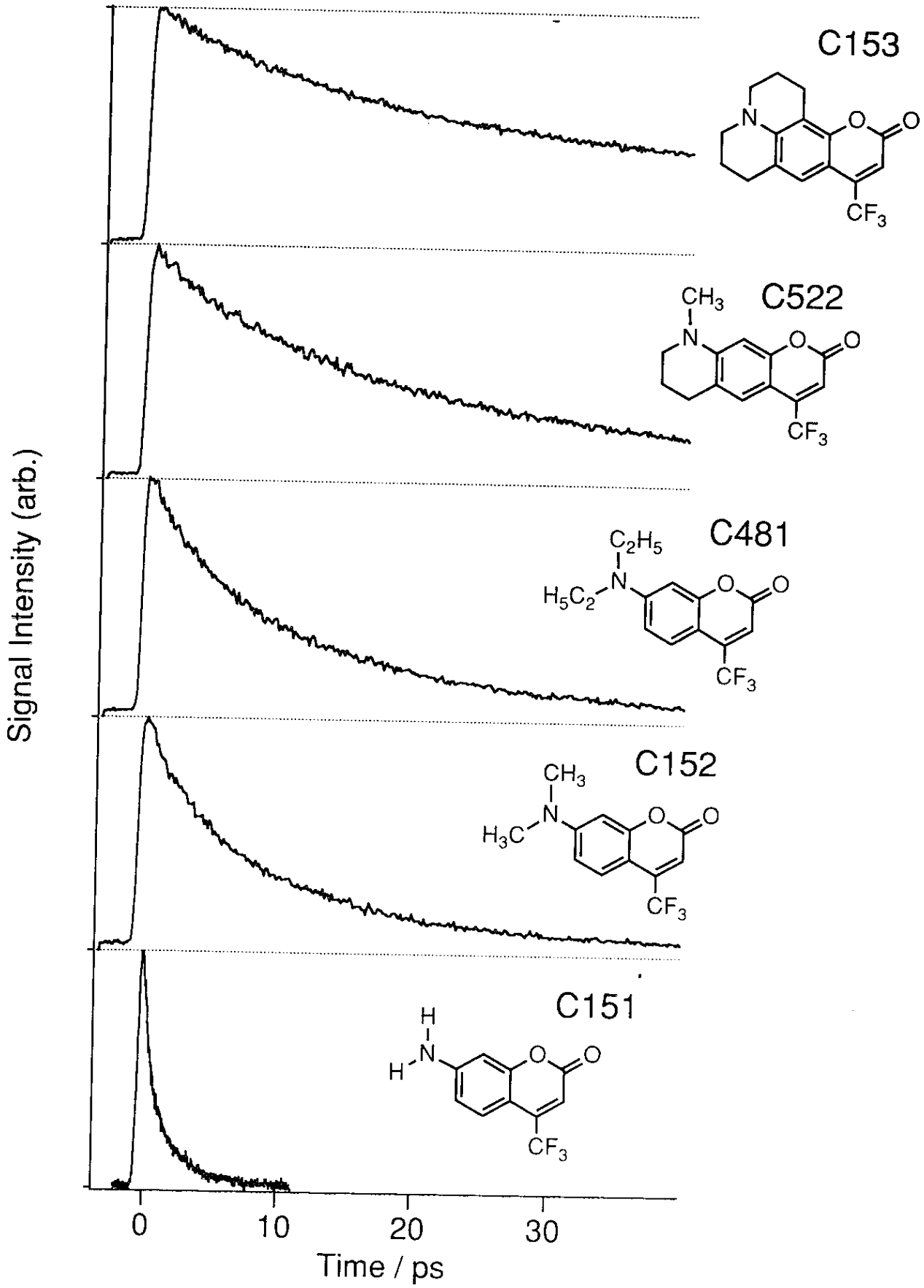

Figure V-5. Fluorescence quenching of 4-CF_3 coumarins in AN, excited at 395 nm and observed at 510 nm. Concentartions are $2x10^{-3}$ M.

Table V-1. Absorption λ_{abs} and fluorescence λ_{flu} maximum, Stokes shift Δv, reduction potential $E_{red}(dye^{0/-})$, relative energy gap ΔG_{rel}, and fluorescence lifetimes τ_{ET} of 4-CF_3 coumarins.

	in DMA						in AN					
	λ_{abs} nm	λ_{fl} nm	$\Delta\nu$ cm^{-1}	$E_{red(dye^{0/-})}$[a] V	ΔG_{rel}[b] eV	τ_{ET}[c] ps	λ_{abs} nm	λ_{fl} nm	$\Delta\nu$ cm^{-1}	$E_{red(dye^{0/-})}$[a] V	ΔG_{rel}[b] eV	τ_{ET}[c] ps
C153	416	504	4200	-2.4	0.00	3.1 {67%} 19.4 {33%} [8.5]	435	526	3990	-1.76	0.17	17 {59%} 285 {41%} [127]
C522	408	463	2910	-2.2	-0.26	0.8 {69%} 4.0 {31%} [1.8]	422	512	4170	-1.72	0.04	10 {39%} 34 {61%} [25]
C481	400	448	2680	-2.2	-0.32	0.57 {80%} 2.9 {20%} [1.0]	413	505	4410	-1.69	-0.05	4.1 {37%} 15.2 {63%} [11]
C152	397	446	2770	-2.1	-0.44	0.46 {89%} 2.7 {11%} [0.71]	408	504	4670	-1.68	-0.10	3.7 {41%} 12.4 {59%} [8.8]
C151	370	410	2630	-2.1	-0.67	0.21 {100%}	376	450	4370	-1.75	-0.29	0.59 {50%} 1.9 {50%} [1.2]

a) Reduction (peak) potentials from irreversible waves.
b) Relative values of energy gap. C153 in DMA is fixed to 0 eV.
c) Values in [ ] are the average lifetimes; $\langle\tau\rangle = A_1\tau_1 + A_2\tau_2$.

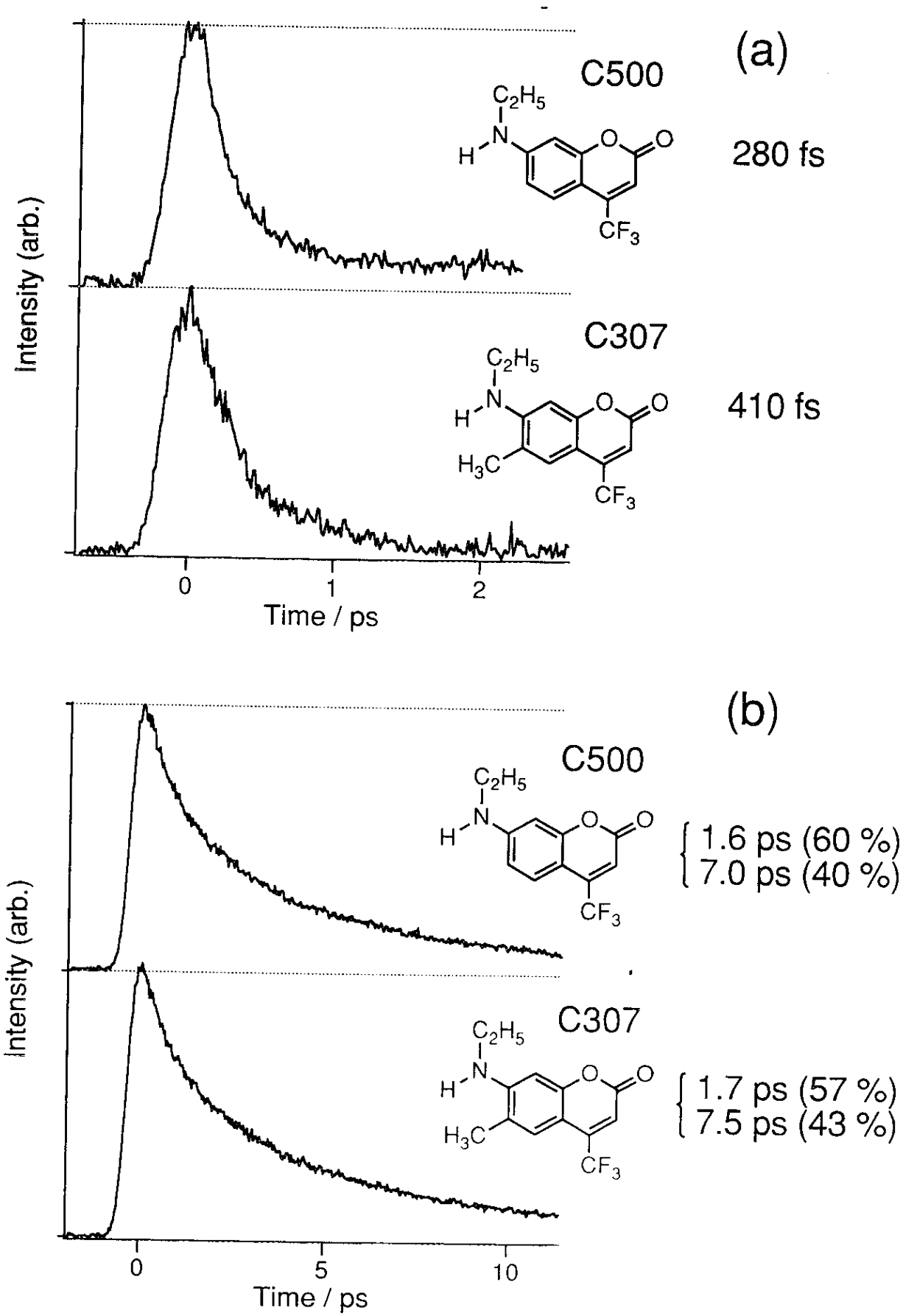

Figure V-6. Fluorescence decays of C500 and C307 (a) in DMA observed at 430 nm and (b) in AN observed at 470 nm.

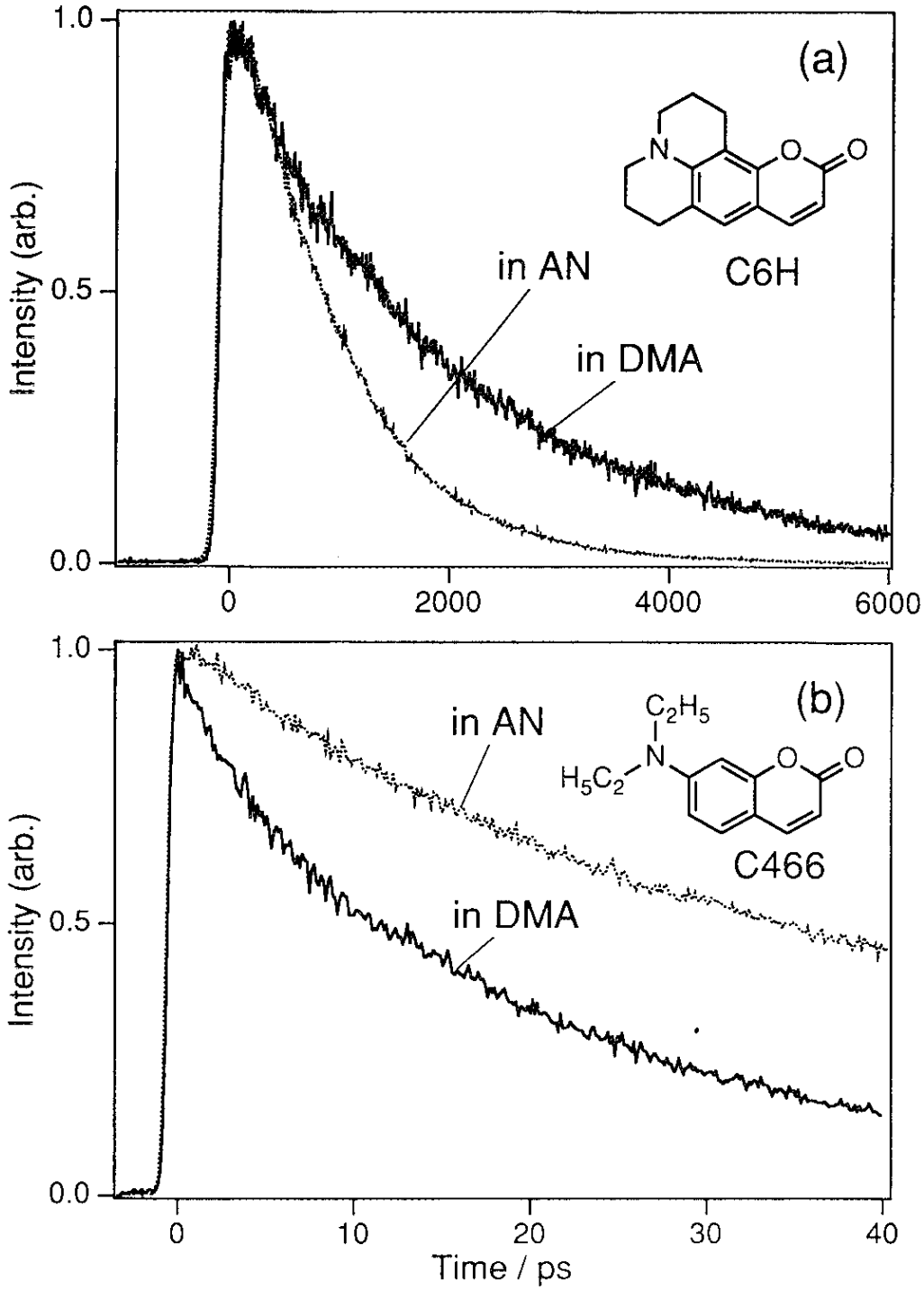

Figure V-7. Fluorescence decays of (a) C6H observed at 430 nm in DMA and 450 nm in AN, (b) C466 observed at 440 nm in DMA and 470 nm in AN.

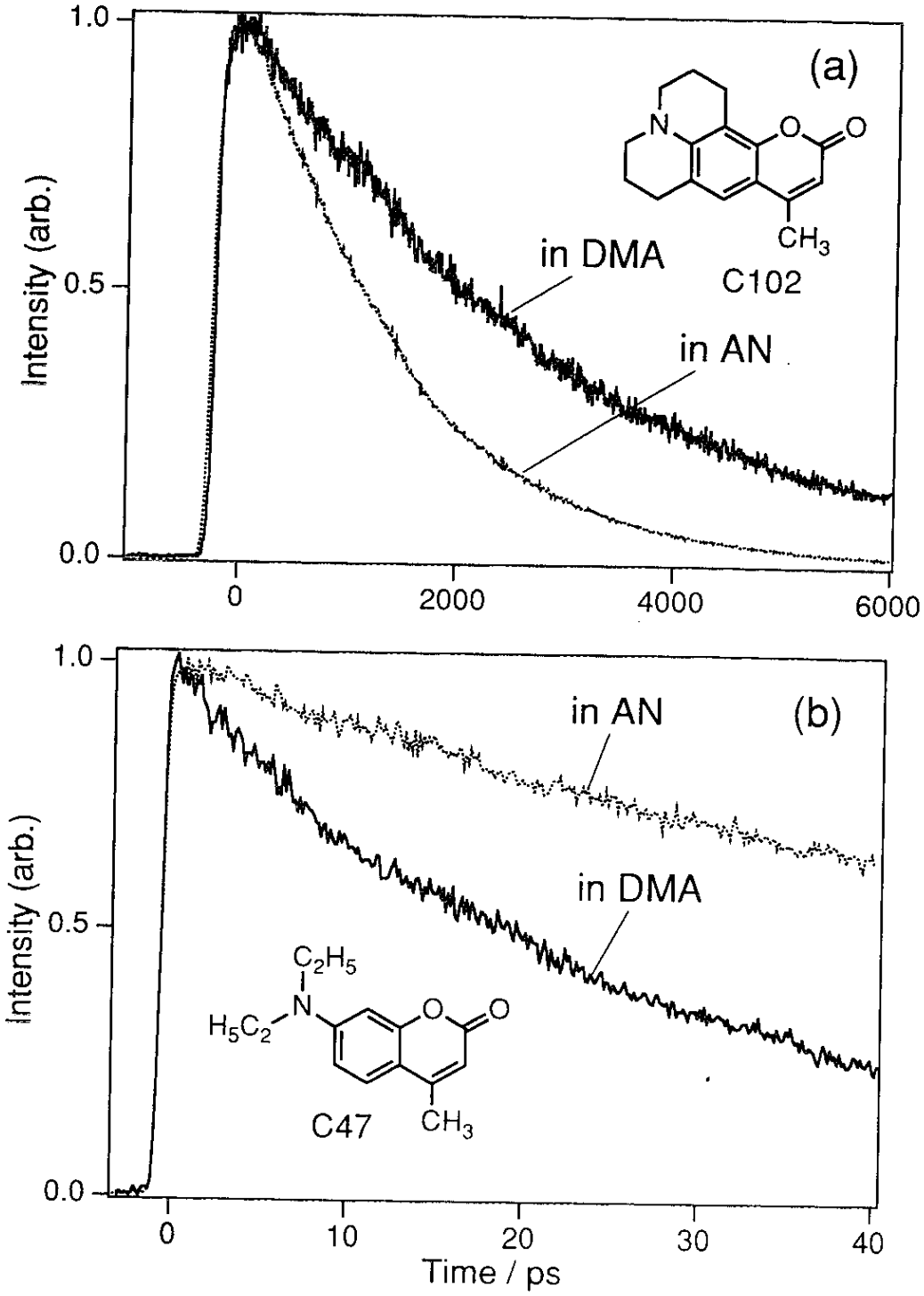

Figure V-8. Fluorescence decays of (a) C102 observed at 460 nm and (b) C47 observed at 445 nm.

Table V-2. Absorption λ_{abs} and fluorescence λ_{flu} maximum, Stokes shift $\Delta\nu$, and fluorescence lifetimes τ_{ET} of coumarins with no substitution on 4- position and 4-methyl coumarins.

	in DMA				in AN			
	λ_{abs} nm	λ_{fl} nm	$\Delta\nu$ cm^{-1}	τ_{ET}[c] ps	λ_{abs} nm	λ_{fl} nm	$\Delta\nu$ cm^{-1}	τ_{ET}[c] ps
C6H	390	443	3070	1.9×10^3 (100 %)	403	469	3490	880 (100 %)
C466	370	430	3770	4.7 (22 %) 25 (78 %) [21]	388	451	3600	33 (68 %) 150 (32 %) [71]
C102	381	436	3310	2.8×10^3 (100%)	391	462	3930	1.4×10^3 (100 %)
C47	363	427	4130	19 (44 %) 44 (56 %) [33]	378	445	3980	89 (100 %)

For the fast reactions, the lifetimes in DMA are always shorter than the ones of the same coumarins in AN. However, for a few dyes showing nanosecond lifetimes, the lifetime becomes longer in DMA than AN. (4) The reaction rate depends on the substituent groups of the coumarin. The rate changes systematically with the substituent group on 7-position and 4-position.

The results similar to observation (1) and (2) are already discussed in the previous chapter with oxazines. It was concluded that solvent relaxation dynamics does not necessarily limit the rate of ET in weakly polar solvents.[4~7] In polar solvents, solvation process often dominates ET.[11~14] This is because the energy relaxation by the solvation process becomes a driving force for the reaction. However, in weakly polar solvents this kind of driving force becomes weaker and the reaction will not be dominated by the solvation process. In such a case, intramolecular vibrational mode becomes responsible for the reaction and ET may occur much faster than the solvation process. Detailed discussions and simulations based on the two dimensional model of Sumi, Nadler and Marcus[15,16] was carried out in Chapter IV. This model divides the reaction coordinate into two coordinates, which are the solvent coordinate and vibrational nuclear coordinate.

Figure V-1 shows that the substituent groups in 4-position and 7-position are systematically changed. For the 4-position, reaction rate increases in the order of $CH_3 < H < CF_3$. Electrophilic substitution in 4-position enhances ET. In the 7-position, amino group is substituted. When alkyl chain on the 7-amino group is extended, the reaction becomes slower, and when it forms a hexagonal alkyl ring with the benzene moiety, the reaction becomes the slowest. For the 7-amino group, the reaction rates increase in the order of;

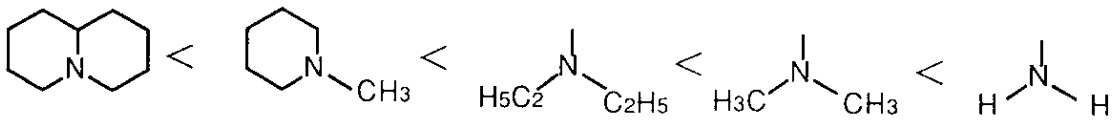

These effect of substitution can be discussed from two aspects, it can change (1) the vibrational mode of coumarin and (2) free energy difference of the reactant and product.

ET usually removes an electron from the HOMO of the donor to the LUMO of the acceptor, which may cause a rearrangement in molecular structure (bond lengths and bond angles) during the reaction. In the present system, extending the alkyl chain on the 7-amino group and forming a hexagonal alkyl ring may restrict the flexibility of the 7-amino group. Some vibrational modes of the 7-amino group may be involved in the reaction. The rotation of amino group is often discussed in the studies of twisted intramolecular charge transfer (TICT), as typically represented by N,N-dimethylaminobenzonitrile (DMABN).[17~19] DMABN is a molecule which has an amino group on one side of the benzene ring and a cyano group on the other side. When DMABN is photo-excited in polar solvents, charge transfer occurs from the amino group to the cyano group. In the initial locally excited (LE) state, it has an almost planar configuration between the amino group and the benzene moiety. However, it is said to become perpendicular in the charge transferred state. In the case of DMABN, a blue fluorescence from the LE state and a red fluorescence from the TICT state are observed. A planarly fixed derivative, 5-cyanoindoline, only emits from the LE state, while, orthogonally fixed derivative, 6-cyanobenzo-quinuclidine, emits only from the TICT state.[17]

However, in the case of intermolecular ET of coumarin, there are a few observations which differ from the TICT of DMABN. (1) Fixing of the amino group does not stop ET. (2) Some of the reactions of the coumarins are much faster than the reaction of DMABN. The average lifetime of C152, which has a dimethylamino group, is 0.71 ps in DMA, while that of the LE state of DMABN is 20 ps in methanol. (3) Changing the structure of the

amino group not only changes its flexibility but also changes the electronic state of the molecule. Usually the structural change caused by ET is not restricted to some particular part of the molecule. Therefore, vibrational mode involved in ET cannot be limited to a single particular mode. The reorganization of the nuclear should be promoted by the sum of several modes. Therefore, in the case of coumarins, it is better to say that the twisting mode of the amino group may be one of the modes introducing ET but not the only one.

Changing the structure of the amino group not only changes its flexibility but also changes the electronic state of the molecule. Amino group is an electron donating substituent, and extending the alkyl chain on the amino group increases its electron donating ability. Therefore, DMA is a better electron donor than AN, on the other hand, it decreases the electron affinity of coumarins. The same explanation can be applied to the effect of the substitution in 4-position, *i.e.* electron donating methyl group reduces ET, while electrophilic CF_3 group enhances it. These effects can be discussed in terms of the energy gap law.

V-3. Free energy gap dependence of electron transfer

The effect of substituent can also be discussed in terms of the free energy gap dependence of the reaction. From the steady-state spectroscopic and cyclic voltammetric measurements, we estimate a free energy gap between the reactant and the product by using the following equation,[20]

$$\Delta G_0 = - E_{00} + E_{ox}(solv.^{0/+}) - E_{red}(dye^{0/-}) - E_{IPS}. \qquad (V.\ 1)$$

Here E_{00} is the transition energy from the S_0 to the S_1 state of coumarin, $E_{ox}(solv.^{0/+})$ is the oxidation potential of the solvent, $E_{red}(dye^{0/-})$ is the

reduction potential of the coumarin, and E_{IPS} is the ion pair stabilization energy. Not all of these variables can be measured experimentally, therefore, relative values of energy gap ΔG_{rel} are used in the present calculation. The first terms are estimated from the absorption maxima, and the second terms are estimated from cyclic voltammetries. However, coumarins did not show reduction-return waves due to the irreversible reduction of the dye on the electrode,[21] as is shown in Figure V-9 and V-10. Therefore, the peak potentials are used. For $E_{OX(solv.}{}^{0/+)}$, the ionization potentials in gas phase I_{VAP} are known, namely, 7.12eV for DMA and 7.69eV for AN.[22] However, the oxidation potential of neat solvent cannot be measured experimentally by cyclic voltammetry. Therefore, difference in the oxidation potential between DMA and AN was estimated to be 0.17 eV using the equation (IV-4).

The free energy gap dependence of the ET rate is shown in Figure V-11 and Table V-1 for 4-CF_3, 7-amino coumarins. The square, triangle, and circle markers in Figure V-11 correspond to the lifetimes of first τ_1, second components τ_2, and their average $<\tau> = A_1\tau_1 + A_2\tau_2$, where A is the percentage of the component. Solid lines correspond to the reactions in DMA, and broken lines correspond to the ones in AN. Systematic changes of ΔG_{rel} are observed, which show good correlation with the change of the reaction rate; as the value of $-\Delta G_{rel}$ increases, the reaction becomes faster. This tendency is reasonable if we consider the reactions to be in the so-called Marcus "normal" region and not in the "inverted" region.[23] For 3-methyl substituted coumarins and coumarins with no substitution on 3-position, the values of ΔG_{rel} are not obtained. This is because $E_{red(dye}{}^{0/-)}$ of these dyes were not measurable, due to their high values, hidden in the edge of the solvent reduction peak. However, it can be concluded that they are still in the normal region, and the long

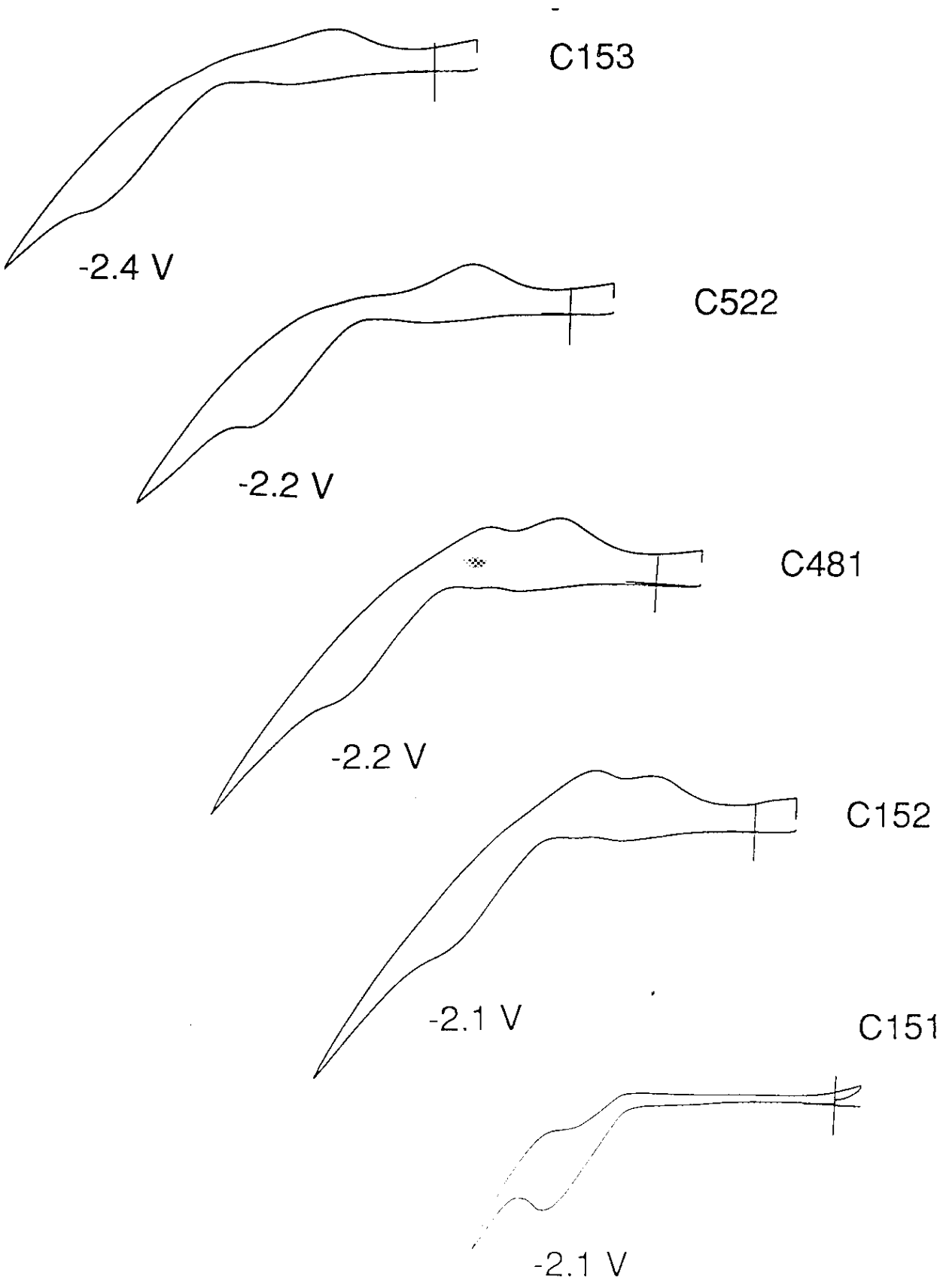

Figure V-9. Cyclic Voltammograms of coumarins in DMA. Concentration is 2x10-3 M.

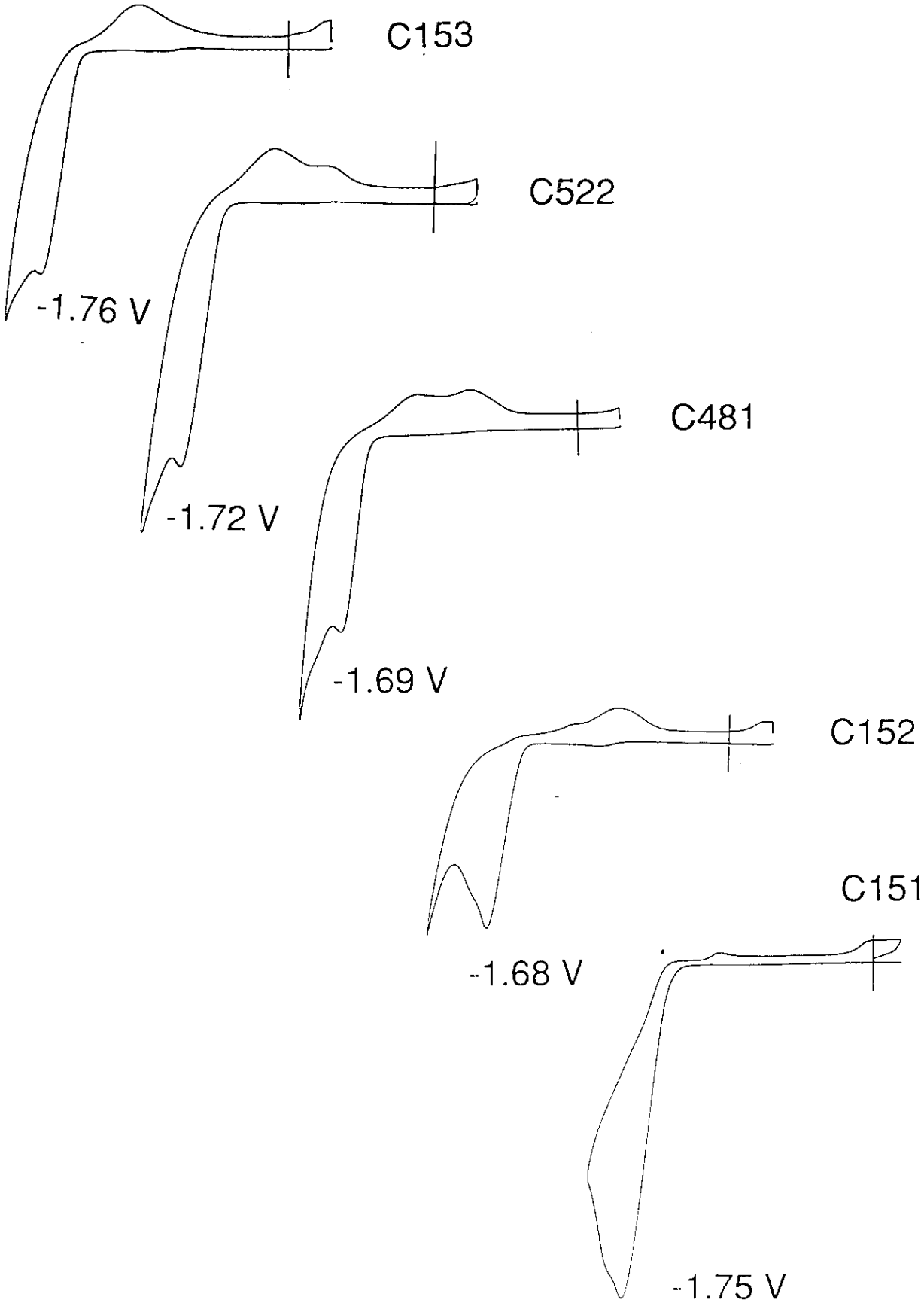

Figure V-10. Cyclic Voltammograms of coumarins in AN. Concentration is 2x10-3 M.

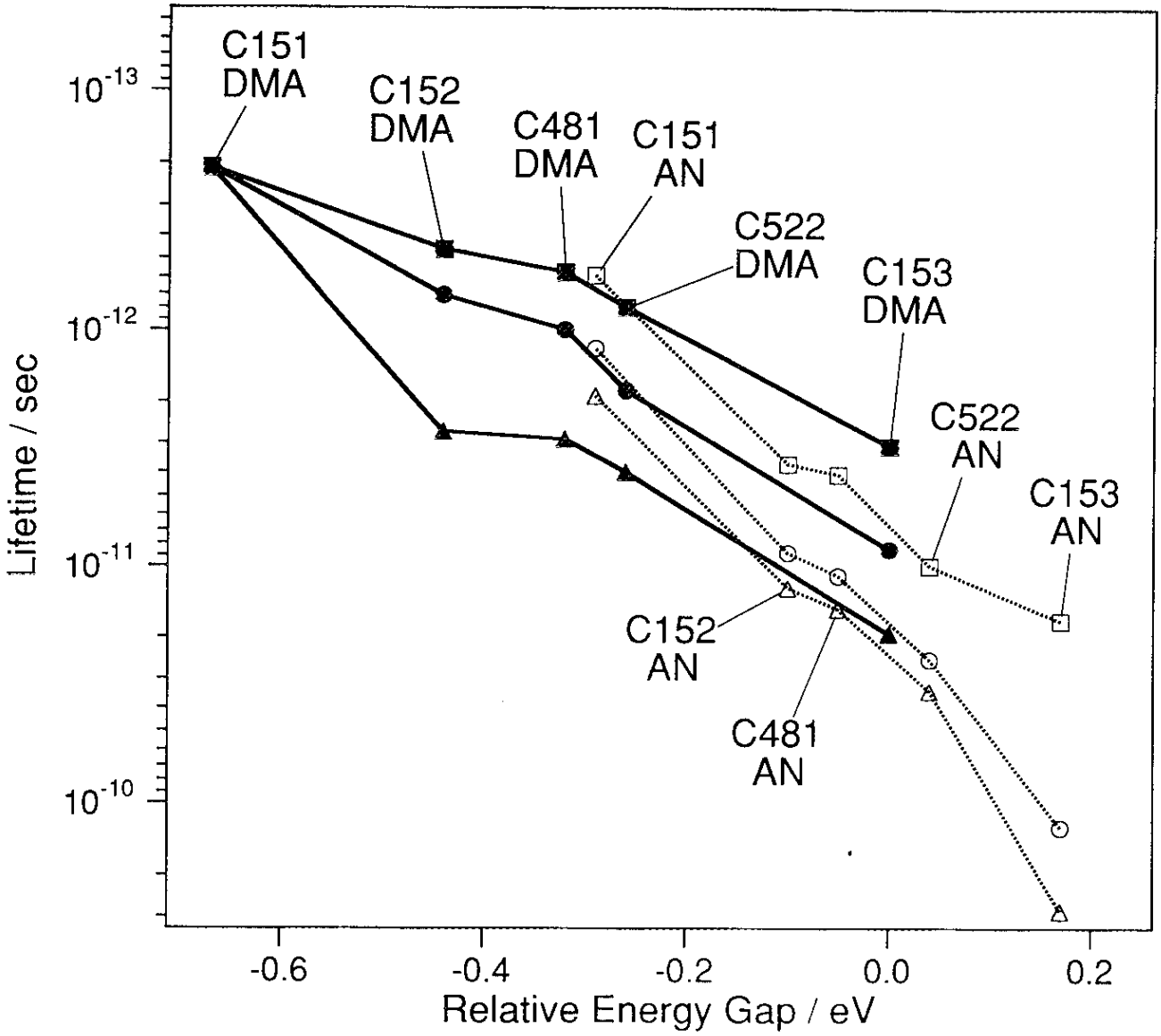

Figure V-11. Energy gap dependence of 4-CF_3 coumarins. Square, triangle, and circle markers corresponds to the first, second, and the average lifetimes, respectively. Solid line corresponds to the reactions in DMA, and broken line corresponds to the ones in AN.

fluorescence lifetimes observed for C102 and C6H are due to their small value of $-\Delta G_{rel}$.

The fluorescence decays of C102 and C6H are slower in DMA than in AN, as is can be seen in Figure V-7 (a) and V-8 (a). These observations seems to be against the energy gap law in the normal region. However, in nanosecond time domain, the fluorescence decay is affected not only by ET but also by their own excited state lifetime. The excited state lifetimes of these dyes may be shorter in DMA than in AN.

Simulations on energy gap dependence will be carried out in section V-6, however, the theories concerning the reactant distribution to be in thermal equilibrium cannot be used. It is because most of the reactions of 4-CF_3 coumarins occur faster than the solvation dynamics.

V-4. Excitation wavelength dependence of electron transfer

For C151, the excitation wavelength dependence of fluorescence decay was measured. The results are shown in Figure V-12. The fluorescence decay was observed at three different excitation wavelengths, *i.e.*, 405, 395, and 385 nm. All of these lights excite the red side of the absorption maximum of C151. The energy difference between 405 and 385 nm light is 0.16 eV, which is somewhat smaller than the value 0.21 eV between 675 and 605 nm, used for the experiments of oxazines. All the decays match within the experimental error, there is no deviation even for the slower part in AN like the one observed for OX1 (see Chapter IV). There seems to be no effect of IVR or exciting a dye with different solvent organization.

V-5. Fluorescence from non-equilibrium state

Coumarins are known to increase their dipole moments upon photo-excitation. For C153, it is calculated to be 9.51 D for S_1 and 5.63 D for

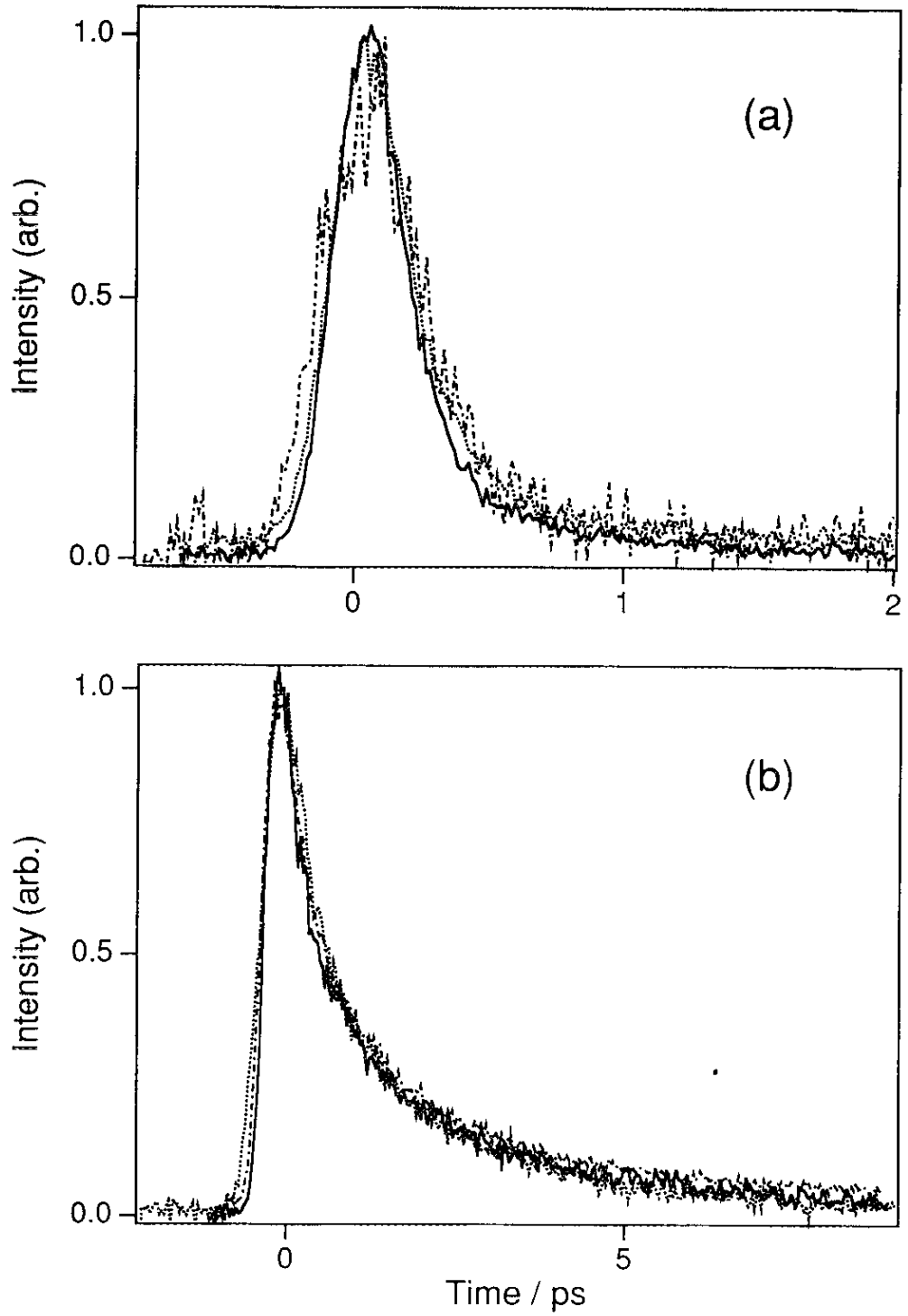

Figure V-12. Excitation wavelength dependence of the fluorescence decays of C151 (a) in DMA and (b) in AN. Solid line corresponds to the excitation at 405 nm, broken line to the 395 nm, dashed and dotted line to the 385 nm excitation.

S_0 state.[24] Therefore, coumarins show a large fluorescence Stokes shift. When the dipole moment instantaneously increases by photo-excitation, the initial solvent organization is the one suitable for the ground state dipole and not for the excited state. Therefore, the energy relaxation process caused by the solvent reorganization follows the photo-excitation. This process can be observed as a dynamic fluorescence Stokes shift. The solvent relaxation times were measured in Chapter III, they were 7.9 ps (19 %) and 18.7 ps (81 %) for DMA and 6.7 ps (81 %) and 13.3 ps (19 %) for AN. This means that the most of the ET of 4-CF_3 coumarins are occurring faster than the solvation process. For the ET dynamics simulation of OX1, the initial distribution on the excited state solvent coordinate, produced by the photo-excitation, is estimated to be close to thermal equilibrium. This is because the dipole moment of the dye does not change drastically on photo-excitation. However, this is not the case for coumarin dyes.

For the extremely fast reacting coumarins, it can be said that ET is finished before the solvation process is over. If we look at Table V-1 and V-2, an interesting trend can be found for coumarins which show ET much faster than solvation process. The Stokes shift obtained from the peak of the absorption and fluorescence spectra is larger than 4000 cm^{-1} for the most of the dyes, however, for the fast reacting dyes, it becomes smaller than 3000 cm^{-1}. C153 in DMA, which has a lifetime close to solvation time, still have a Stokes shift of 4200 cm^{-1}, for C522, it becomes 2910 cm^{-1}, and for C481, C152, and C151, it becomes smaller than 2800 cm^{-1}. The smallest Stoke shift is observed for C151 in DMA which is only 2630 cm^{-1}. When the reaction is occurring much faster than solvation process, photo-excited coumarins only have a chance to fluoresce from the non-equilibrium state before the solvent relaxation. If this is the case, fluorescence spectra shown in Figure V-13 and V-14 are

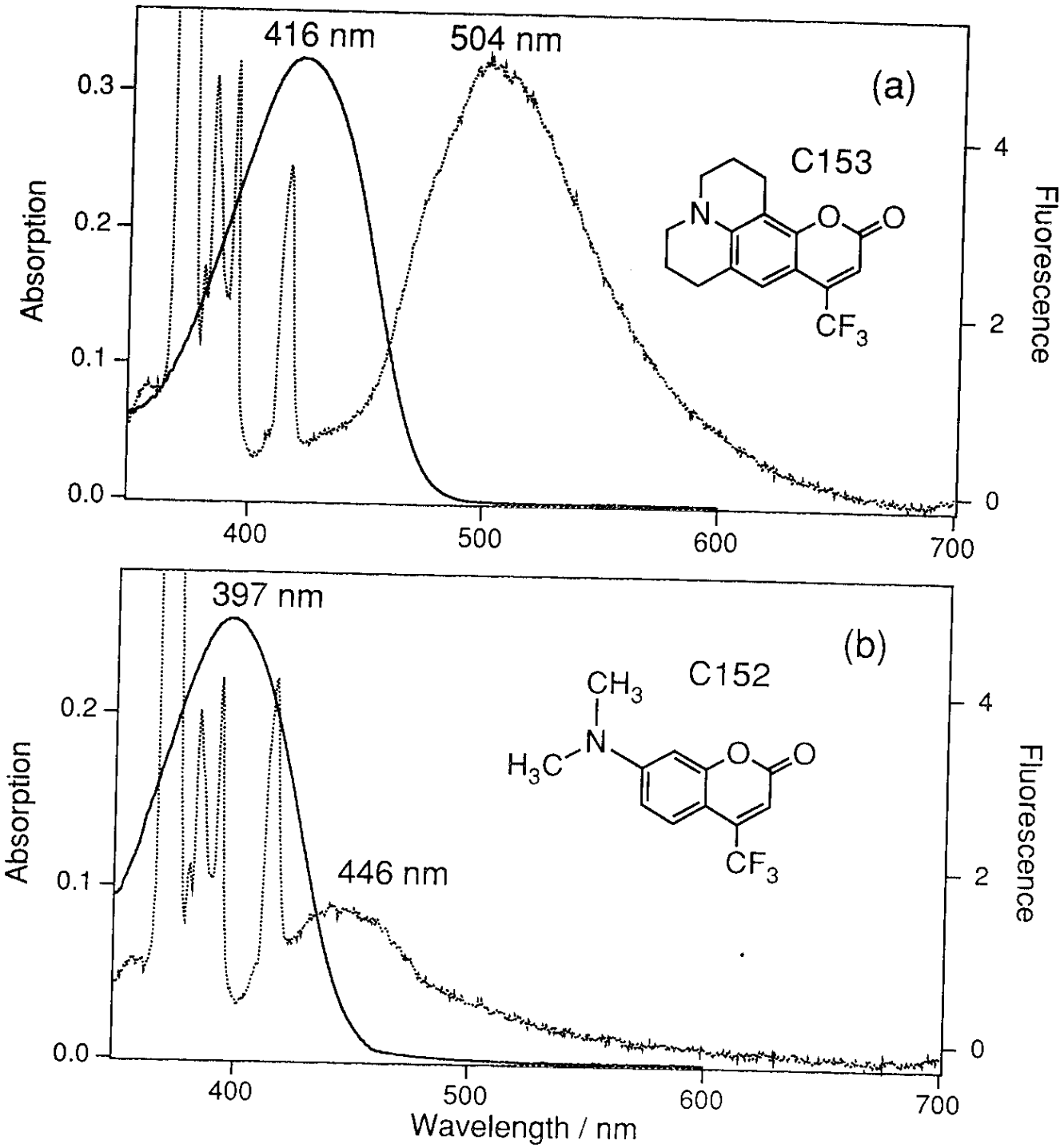

Figure V-13. Absorption and fluorescence spectra of (a) C153 and (b) C152 in DMA. Concentrations are 2×10^{-5} mol / l. Excitation wavelength is 370 nm.

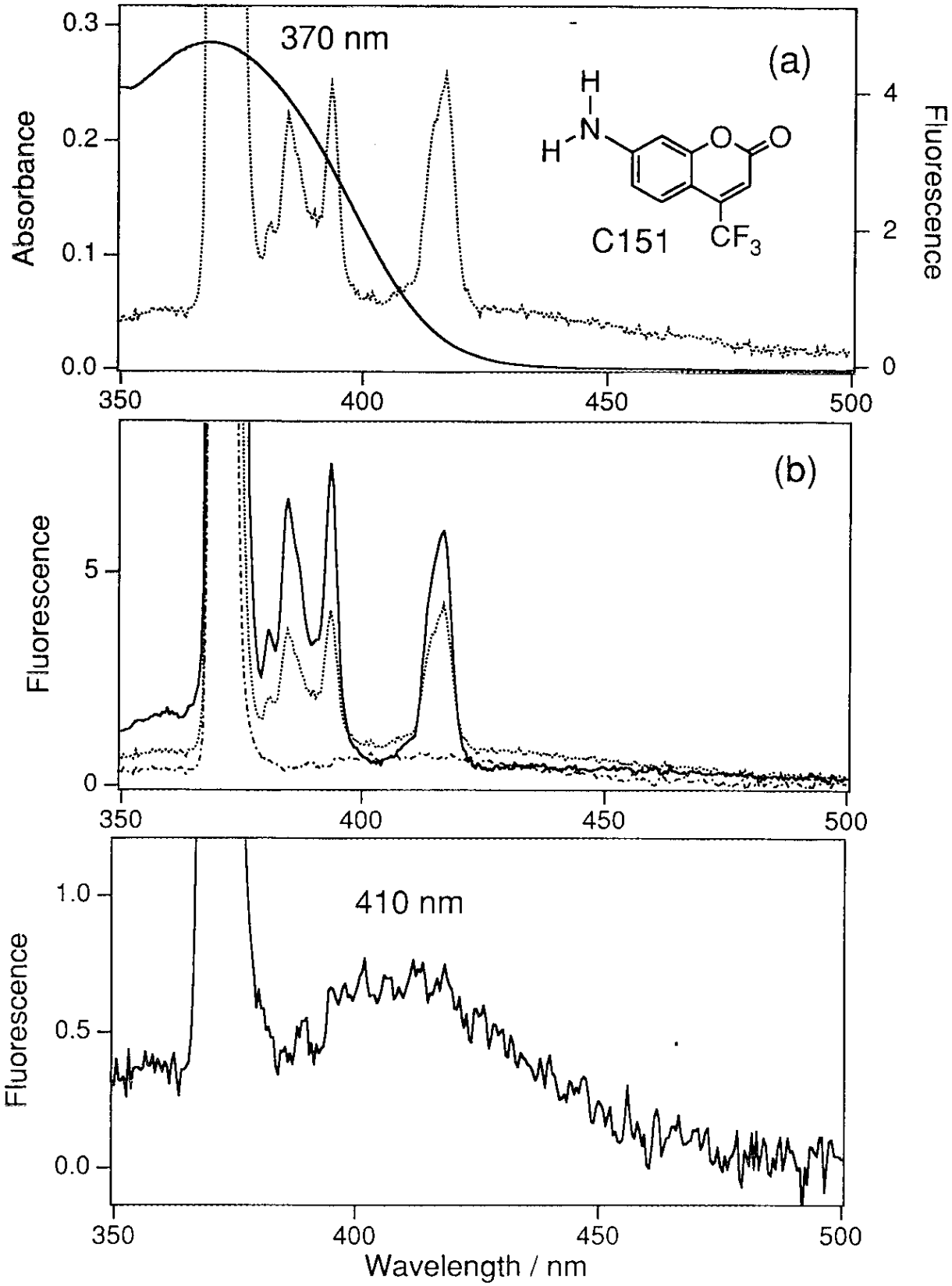

Figure V-14. (a) Absorption and emission spectra of C151 in DMA. $2x10^{-5}$ mol / l. The sharp peaks are solvent Raman bands. (b) Solid line corresponds to the fluorescence spectrum of C151 in DMA. Broken line is the Raman spectrum of DMA. Dashed and dotted line is the spectrum obtained by subtracting the Raman bands from the fluorescence. (c) Expansion of the Raman subtracted fluorescence spectrum of C151 in DMA.

the fluorescence from the non-equilibrium state. It can be seen in Figure V-13, that the absorption and fluorescence peaks are closer for C152 than those of C153. The relation between Stokes shifts and average lifetimes of 4-CF_3 coumarins are shown in Figure V-15. It can be seen that the Stokes shift becomes smaller as the lifetime becomes shorter. These effects can be called as a "chemical timing" effect of ET on solvation process.

Chemical timing using oxygen as a quencher is well known in the gas phase. Coveleshie *et al.* used chemical timing to decrease the effect of intramolecular vibrational redistribution (IVR) in the fluorescence spectrum of *p*-difluorobenzene.[25] IVR is a vibrational relaxation process from the selectively excited S_1 vibrational state to many other S_1 vibrational states. Therefore, IVR adds a broad fluorescence from many states to the sharp fluorescence from the initially excited state. When oxygen is added, the excited molecule is quenched by collision with oxygen molecules. This shortens the fluorescence lifetime, however, the rate constant of IVR is independent of collision. Therefore, when the pressure of oxygen is increased, the broad fluorescence decreases compared to the sharp fluorescence from the initially excited state.

In the present case, when ET becomes faster, it quenches the fluorescence from the solvent relaxed state, which means that the lifetime of the excited molecule becomes shorter than the solvent relaxation time. In such a case, the excited molecule can only emit from non-equilibrium state. Therefore, as the rate of ET increases, the amount of fluorescence Stokes shift decreases. This effect can be regarded as a chemical timing effect of ET on solvent relaxation process.

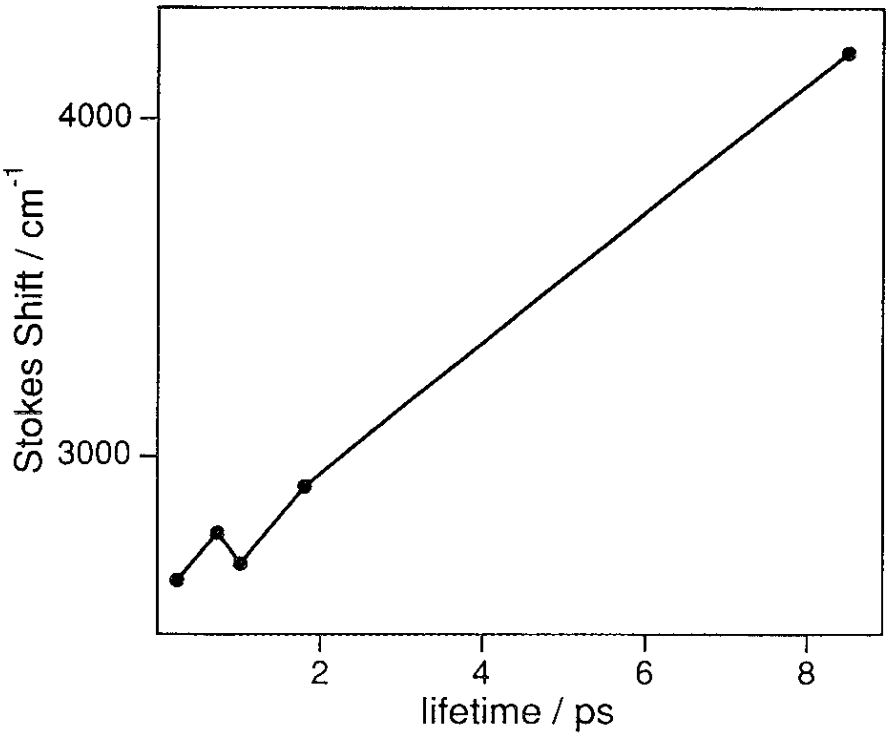

Figure V-15. The relation between Stokes shifts and average lifetimes of 4-CF_3 coumarins in DMA. As the lifetime becomes shorter, the Stokes shift becomes smaller.

V-6. Simulations based on Sumi-Marcus Jortner-Bixon hybrid model

Now a model is going to be developed based on the observations and the discussions mentioned above. When coumarins are excited to the S_1 state, the dipole moment increases drastically, therefore, solvent organization which was appropriate for the ground state dipole starts to reorganize. However, ET occurs simultaneously in donor solvents. In some cases, ET finishes before the solvent reorganization is finished. A conceptual drawing of these processes is illustrated in Figure V-16. The solvation process occurs on solvent coordinate, at the same time, the reaction occurs on the classical low frequency vibrational coordinate to the reactant surface. If the initially populated non-equilibrium state is distributed above the activation energy, the reaction also occurs to the higher vibrational levels of the quantum mechanical modes (see Chapter IV-6). The motion along the classical vibrational coordinate is treated to be infinitely fast compared to the motion along the solvent coordinate. This kind of model is called Sumi-Marcus Jortner-Bixon hybrid model[26] which was discussed in Chapter IV.

A simulation based on this two-dimensional model is carried out. Most of the parameters are based on the previous calculations for OX1, however, some are changed to fit the experimental data of coumarins. A normalized two-dimensional coordinate (X, q) is used, which are solvent coordinate X and classical vibrational coordinate q. The bottom of the S_1 free energy surface is located at (0, 0), that of the S_0 state at (0.5, 0), and the product state at (1, 1). The solvent reorganization energy λ_{sol} is 0.167 eV and that of the classical vibrational mode λ_v is 0.502 eV. This means that the reaction has a quite "large window", $\lambda_v / \lambda_{sol} = 3$. The frequency of the quantum mechanical vibrational mode ν_h is 1400 cm^{-1} and the reorganization energy λ_h is 0.124 eV. The electronic matrix element is 0.0161 eV, temperature is 293 K, the solvent relaxation times are 7 ps (50

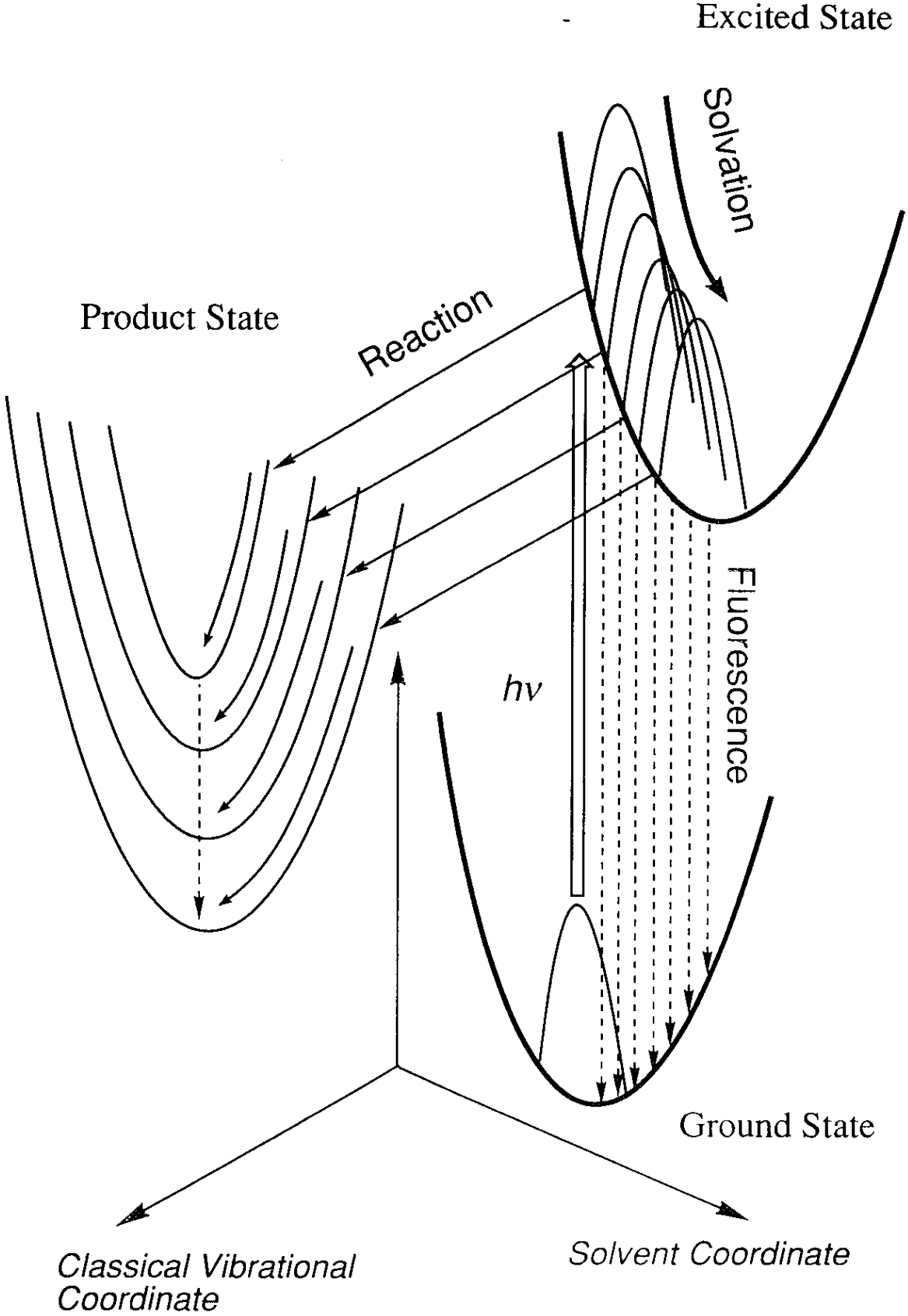

Figure V-16. The conceptual drawing of the ET of coumarins. The solvation process occurs on the solvent coordinate, while the reaction occurs through the classical low frequency vibrational coordinate to the reactant surface with quantum mechanical high frequency vibrational levels.

%) and 15 ps (50%) which is close to the measured relaxation time of AN and DMA. The reaction of C151 in DMA was considered to be close to the top of the bell-shape energy gap dependence (no energy barrier).

The calculated energy gap dependence of the ET rate is shown in Figure V-17. The broken line is the fitted lifetimes of the first component τ_1, the dashed and dotted line is the second components τ_2, and the solid line corresponds to the average lifetime $<\tau>$. These curves are obtained by fitting the population decays calculated at several different values of energy gap. Some of the ET kinetics used to obtain these lines are shown in Figure V-18. When the relative energy gap ΔG_{rel} is 0 eV (Figure V-18 (a)), the most part of the kinetics shows an exponential decay which is slower than the solvation process. However, there is a very rapid decay at the beginning of the kinetics, which is somewhat faster than the solvation process. It seems that this fast component is caused by the reaction occurring from the non-equilibrium state before the solvent relaxation. As the ΔG_{rel} becomes negative (Figure V-18 (b)), the decay becomes much faster and the whole kinetics become non-exponential. Near the top of the bell shape (Figure V-18 (c)), the kinetics shows a very rapid exponential decay, behavior already reported with the simulation of OX1 in Chapter IV. In the inverted region (Figure V-18 (d)), the reaction becomes somewhat slower again, however, the exponential feature of the decay is still hold.

The markers in Figure V-17 are the measured lifetimes in Figure V-11. When we compare them with the calculated average lifetime, a good agreement is obtained for $\Delta G_{rel} < 0.2$ eV. However, the agreement becomes poor at $\Delta G_{rel} > 0.2$ eV. Two reasons can be considered for this discrepancy, (1) the donor solvent is changed from DMA to AN, and (2) the structure of the acceptor dye is changed.

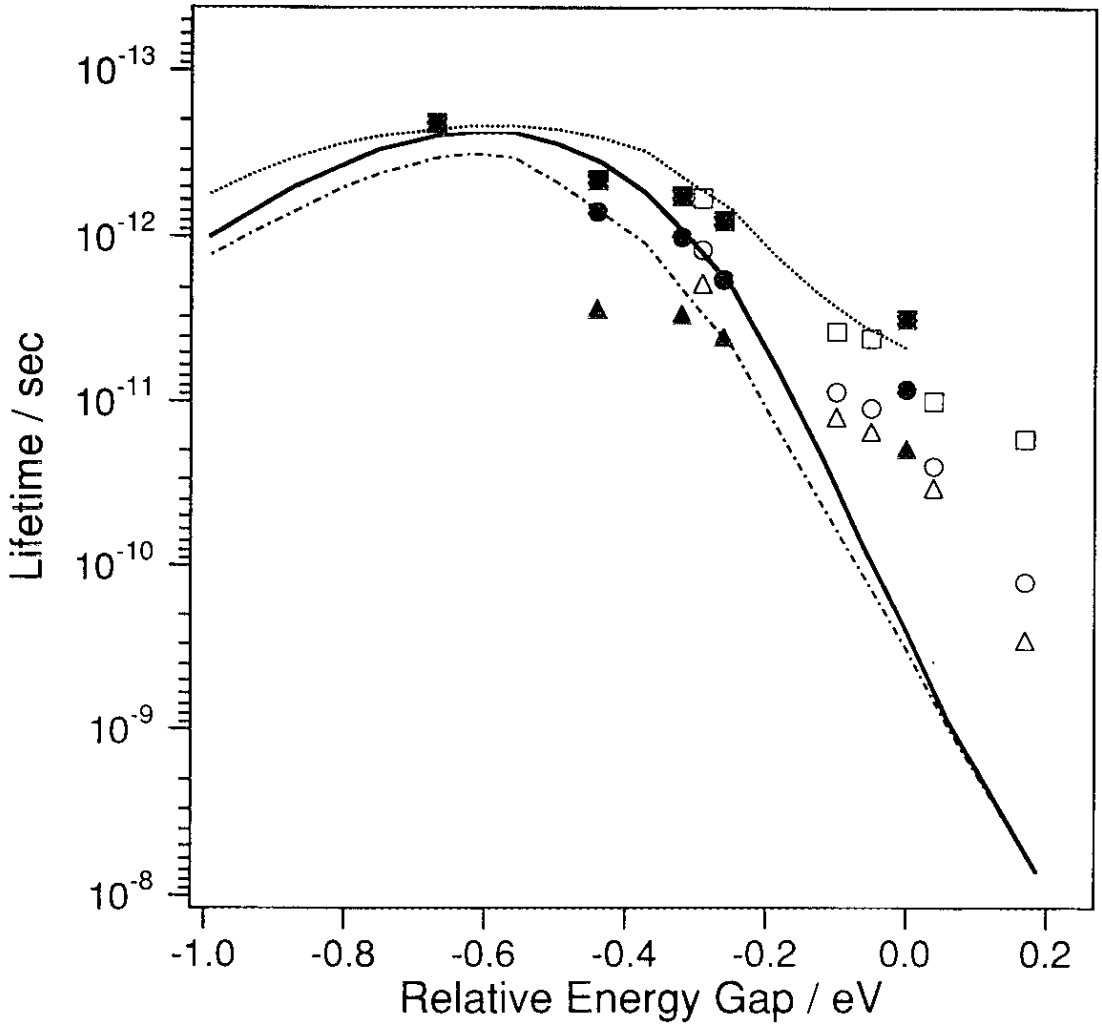

Figure V-17. The energy gap dependence of ET rate calculated by Sumi-Marcus Jortner-Bixon hybrid model. The broken line corresponds to the calculated lifetime of the first component, dashed and dotted line to the second component, and the solid line to their average. The markers are the experimental results shown in Figure V-11.

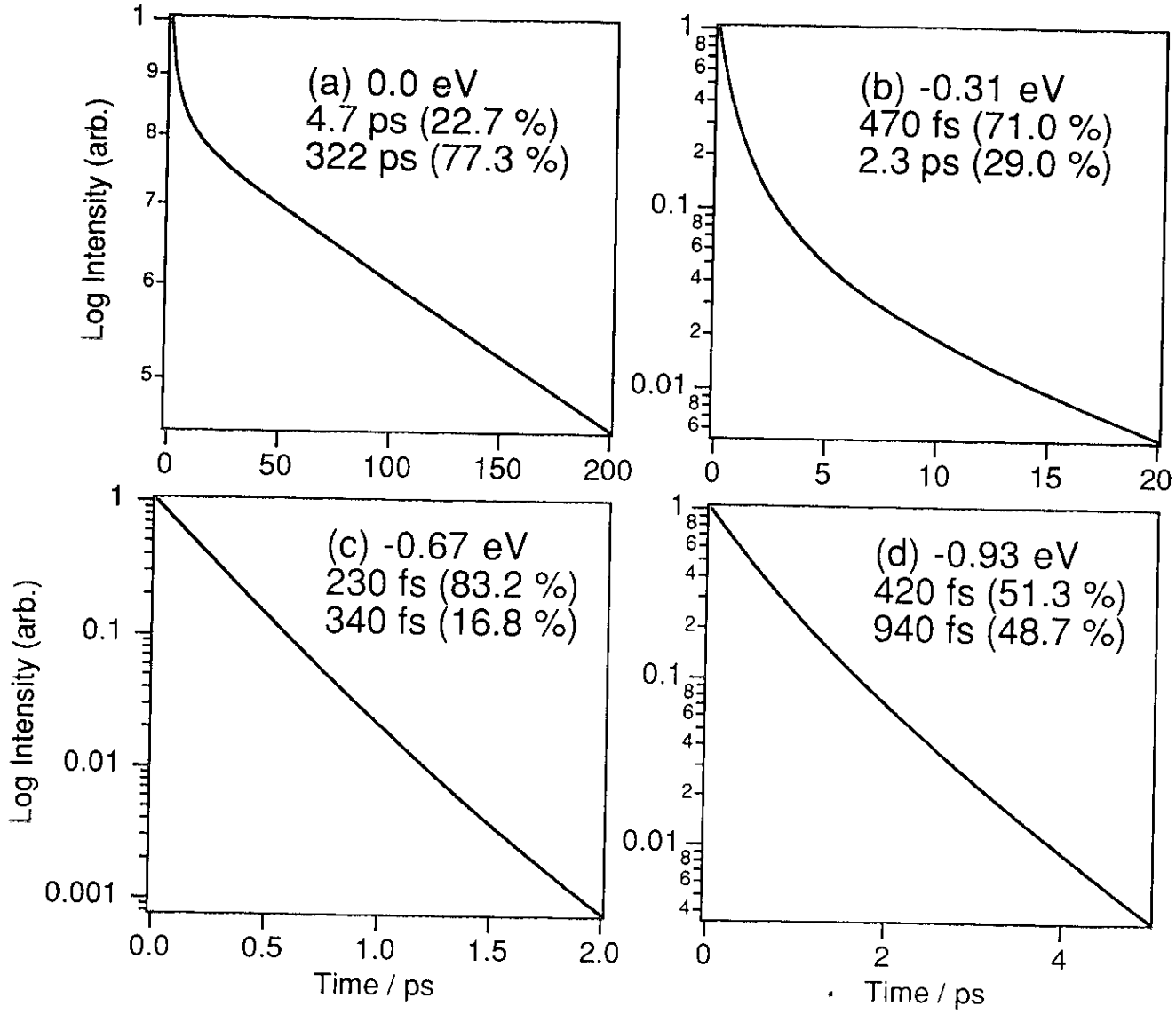

Figure V-18. The ET kinetics calculated by Sumi-Marcus Jortner-Bixon hybrid model. The values of energy gap and the results of double exponential fitting are shown in the figure. Parameters used are the same as the ones used for Figure V-16.

Physical properties of DMA and AN, which can affect the energy gap dependence are, (1) the solvent reorientation energy λ_{sol} and (2) oxidation potential. In the present simulation, λ_{sol} is treated to be the same in both solvents, however, if λ_{sol} changes, the bell-shape shifts. For oxidation energy, the difference between two solvents is estimated to be 0.17 eV. If this difference is estimated to be twice smaller (0.08 eV), the discrepancy will be much smaller. However, even when the comparison is made only in one solvent (only in DMA), there still is a discrepancy. The simulated reaction rate is still too slow compared to the experimental rate of C153 in DMA.

C153 has a 7-amino group fixed with double hexagonal alkyl ring. If the ET urges structural reorganization of the 7-amino group, the fixing may restrict this reorganization. This reorganization can be the change of C-N bond length or C-N-C angle. In such a case the intermolecular reorganization energy of the coumarins with fixed amino group may become smaller than the ones with free amino group. Decrease in reorganization energy will shift the maximum of the bell-shape towards a positive value of energy gap. Therefore, it can cause a kind of discrepancy observed in Figure V-17. If there is a difference in the intramolecular reorganization energy between coumarins with free and fixed amino group, the difference should also show up in the activation energy.

V-7. Temperature dependence of electron transfer of coumarins

To obtain information about activation energy, temperature dependence of the fluorescence decay was measured. The results of C153 are shown in Figure V-19. For C153 in AN (Figure V-19 (b)), a clear temperature dependence can be seen. The Arrhenius plot of the average lifetime $<\tau>$ gives an activation energy of 1.6 kcal / mol. On the other hand,

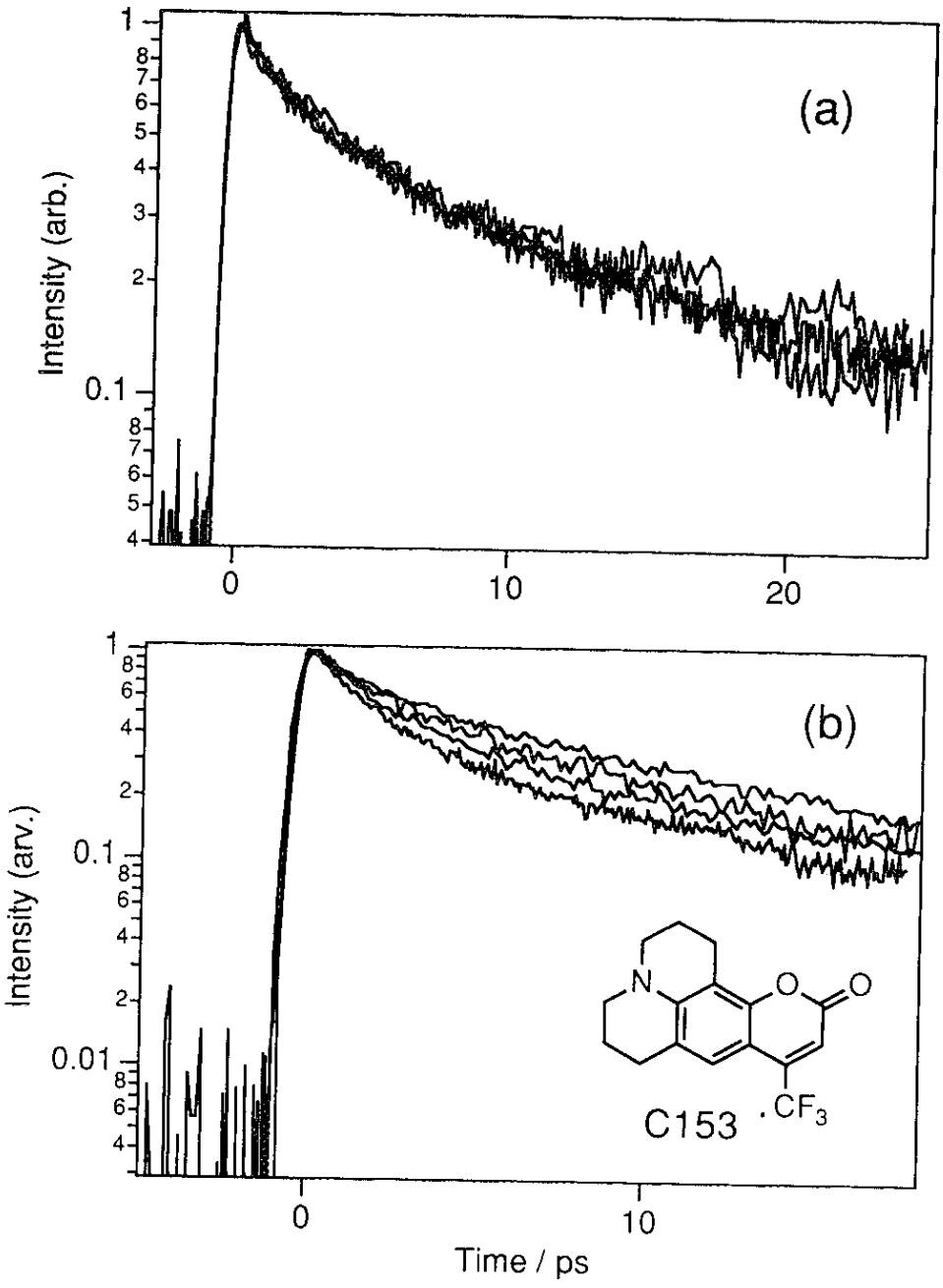

Figure V-19. Temperature dependence of C153 (a) in DMA, T= 297, 323, and 353 K, and (b) in AN, T = 278, 293, 323, and 353 K. The average lifetime of C153 in AN shows a temperature dependence which corresponds to an activation barrier of 1.6 kcal / mol.

no temperature dependence can be seen for C153 in DMA within the experimental error (Figure V-19 (a)). This is somewhat strange, because an activation process is expected for the ET of C153, which is on the slope of the normal region (Figure V-17). This observation indicates that the reorganization energy and other parameters may have been altered by changing the molecular structure of dye. If the intramolecular reorganization energy is smaller for coumarins with fixed amino group than the ones with free amino group, as is mentioned in the previous section, a different energy gap dependence should be expected. A conceptual model is drawn in Figure V-20. The energy gap dependence of fixed amino coumarins is shifted toward positive values of energy gap with smaller maximum rate constant. The reactions of C151 in DMA and C153 in DMA are positioned close to the maximum on each curve.

V-8. Fluorescence Stokes shift caused by electron transfer

In the simulations carried out in section V-6, even for the slow reacting systems, a very rapid ET was expected at the beginning of the kinetics caused by the non-equilibrium state. Therefore, to study this effect, the reconstruction of the time-resolved fluorescence spectra is carried out in this section. The sample is C153, which shows the slowest ET in AN for 4-CF_3 coumarins. The lifetimes are 17 ps (59 %) and 285 ps (41 %) as shown in Table V-1. However, these lifetimes were obtained from the fluorescence decay measured at 510 nm, which is close to the maximum of the steady-state fluorescence. This means that the fluorescence is dominated by the ones from the equilibrium state. If the fluorescence decay is measured at a shorter wavelength, the amount of fluorescence from the non-equilibrium state will increase. Therefore, it may show a rapid decay caused by ET from the non-equilibrium state. However, fluorescence decay at a shorter wavelength will also contain

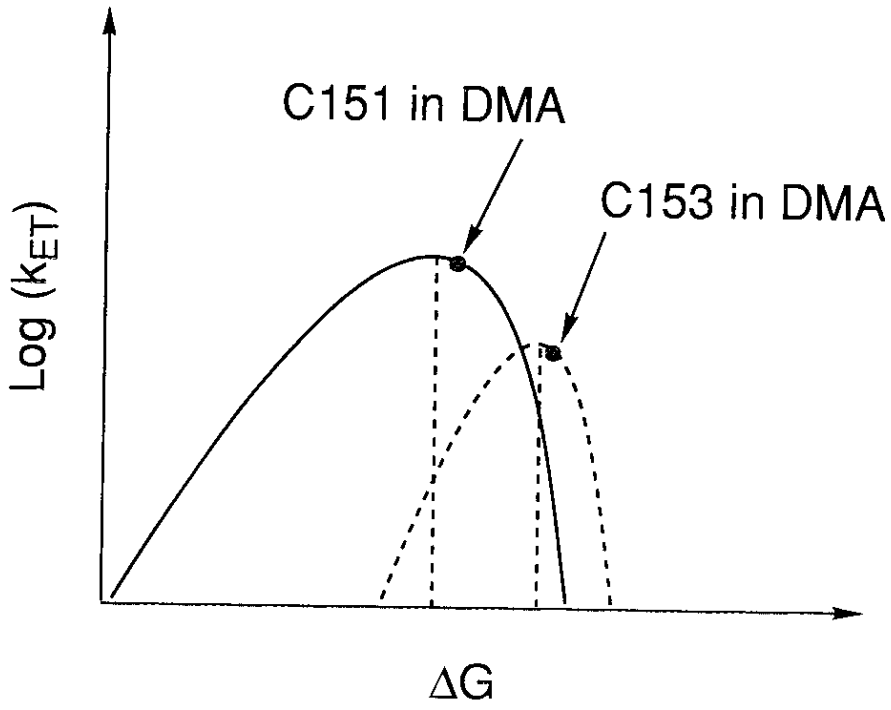

Figure V-20. Conceptual drawing of different energy gap dependence for free amino coumarins (solid line) and fixed amino coumarins (broken line).

solvent relaxation process. Therefore, to obtain detailed information about the reaction from the non-equilibrium state, reconstruction of the time-resolved fluorescence spectra has to be applied.

Fluorescence decays of C153 in AN at various wavelengths are shown in Figure V-21. The kinetics at shorter wavelengths show fast decays, while the ones at longer wavelengths show some rise. This means that the peak of the fluorescence is shifting to longer wavelengths with time. In the usual non-reactive solvents this kind of dynamic Stokes shift is caused mainly by solvent relaxation process. However, in electron donating solvents, the fast decays at the shorter wavelengths may also contain an effect of ET from non-equilibrium state. The lifetimes and risetimes of the decays at each wavelength are shown in Table V-3. To obtain these values, the global analysis program was used for the fitting. The longest lifetimes were linked together to give a same value at each wavelength. The reconstructed time-resolved fluorescence spectra obtained from these fittings is shown in Figure V-22 (a). The detail of this method is already mentioned in Chapter III. The markers are the reconstructed fluorescence intensities at the given wavelength and time. The lines are the results of the log-normal fitting to these intensities. In the time region shorter than 30 ps, the fluorescence peak shifts simultaneously with the decay. On the other hand, in the time region longer than 30 ps, the spectrum shows a decay only.

The normalized spectral shift correlation function $C(t)$, defined by equation (III. 1), for C153 in AN is shown in Figure V-22 (b). This function represents the fluorescence Stokes shift shown in Figure V-22 (a). The results of a double exponential fitting to this function are 2.9 ps (69 %) and 13.9 ps (31 %). The solvent relaxation time obtained by $C(t)$ of C102, were 6.7 ps (81 %) and 13.3 ps (19 %), for AN (see Chapter III). The value of the fast component for C153 is twice faster than that of C102, while the slow

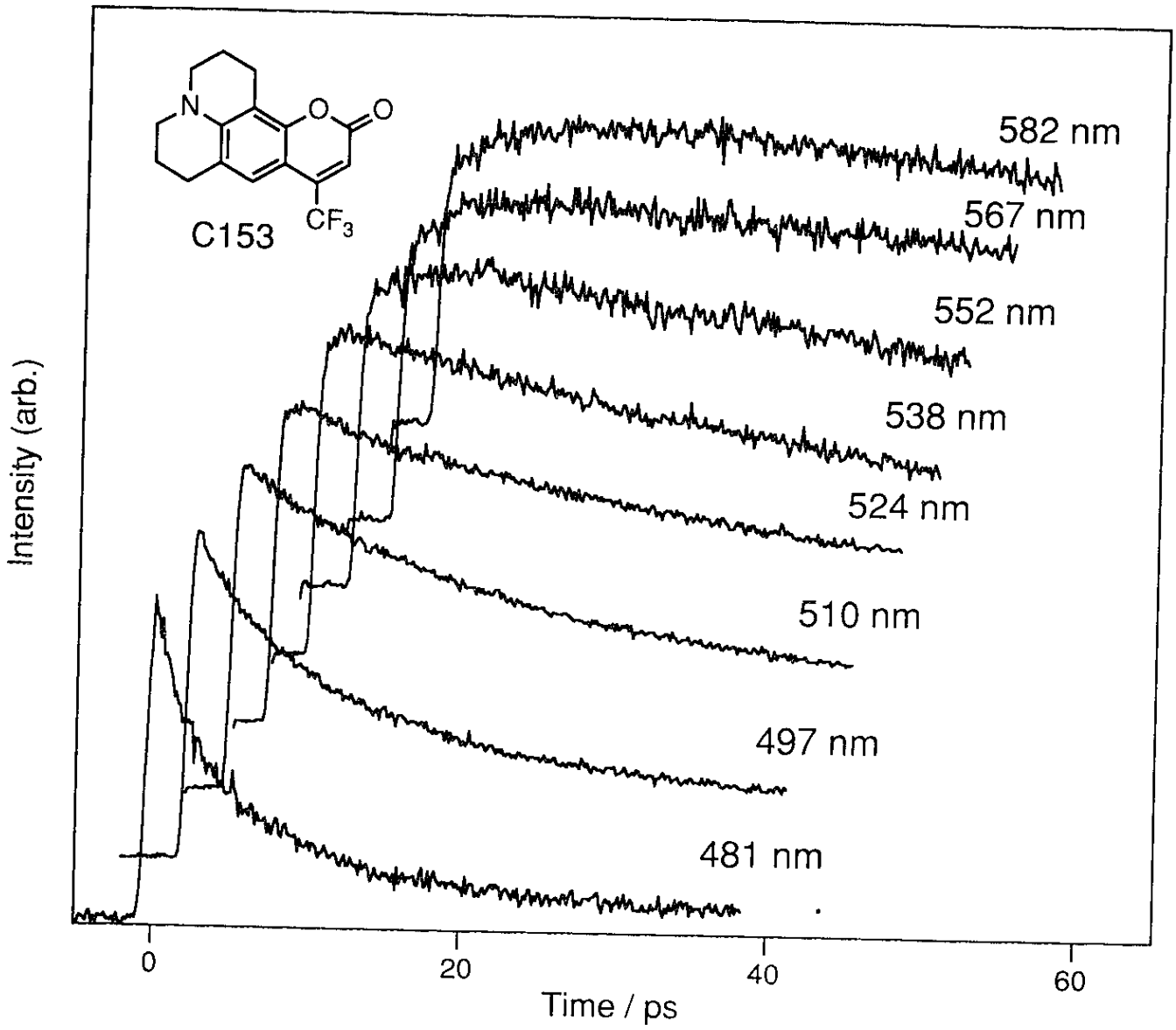

Figure V-21. Fluorescence decays of C153 in AN observed at various wavelengths.

Table V-3. Results of triple exponential fittings of fluorescence decays of C153 in AN at various wavelengths.

Wavelength (nm)	τ_1 (ps)	τ_2 (ps)	τ_3 (ps)
481	3.0 (49.8 %)	10.1 (41.4 %)	83.8 (8.8 %)
497	5.4 (32.6 %)	11.9 (32.0 %)	83.8 (35.4 %)
510		11.7 (36.8 %)	83.8 (63.2 %)
524		11.6 (8.2 %)	83.8 (91.8 %)
538			83.8 (100 %)
552		7.2 (-23.6 %)	83.8 (100 %)
567		15.7 (-38.4 %)	83.8 (100 %)
582		11.7 (-39.1 %)	83.8 (100 %)

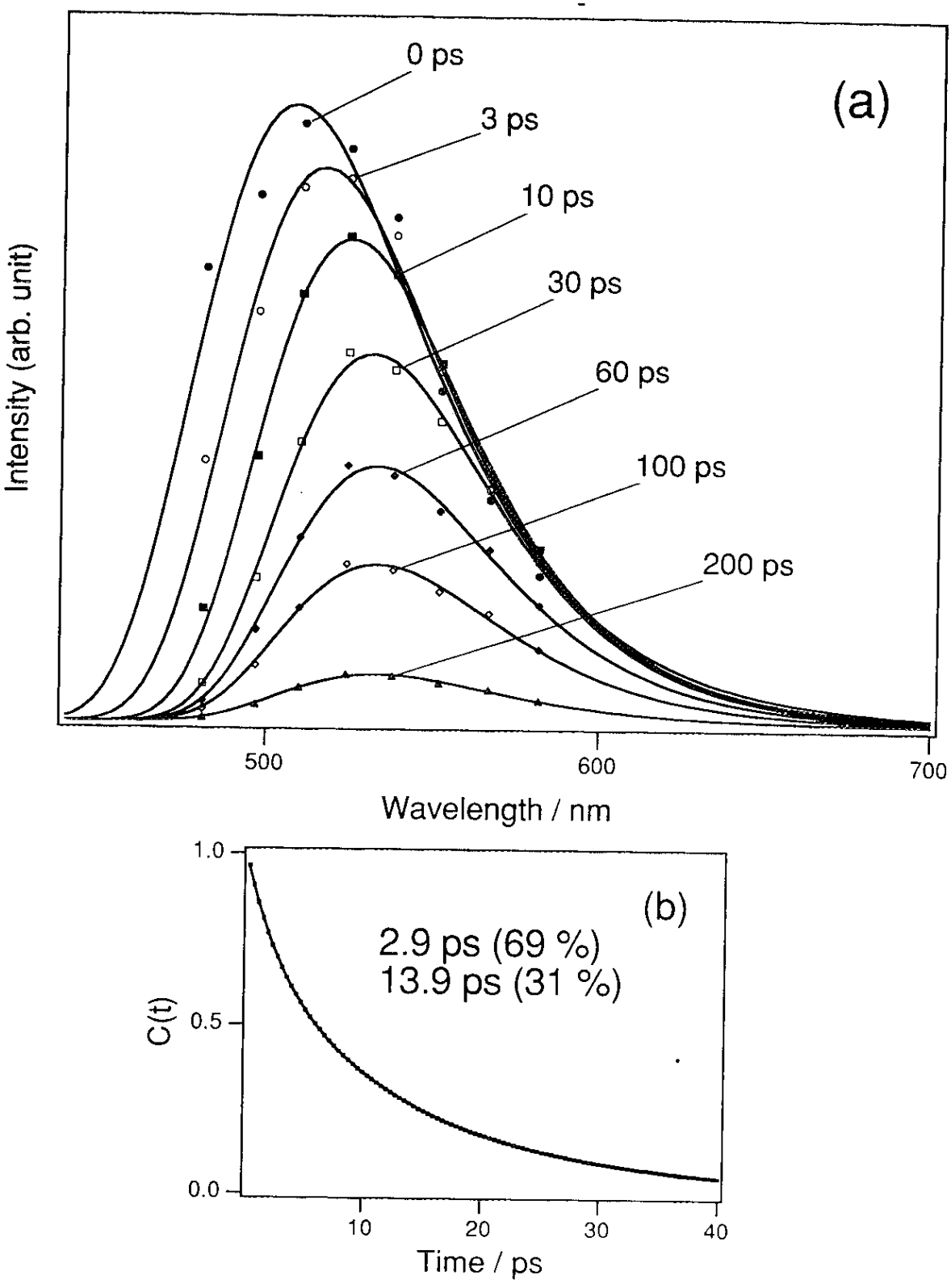

Figure V-22. (a) Reconstructed time-resolved fluorescence spectra of C153 in AN. The markers are the fluorescence intensities at the given wavelength and time. The lines are the results of fitting to these markers using log-normal function. (b) Normalized spectral shift correlation function *C(t)* of C153 in AN and the results of double exponential fitting.

component has a similar value. This difference indicates that the fluorescence Stokes shift of C153 is not only caused by solvation process but also by ET from non-equilibrium state. When the system is not relaxed, the reactant has an excess energy to cross the activation barrier for the reaction. Therefore, ET will occur faster at the non-equilibrium state, and cause a faster fluorescence Stokes shift than the one caused only by the solvation process.

For more detailed discussion, the decay of the full area of the fluorescence spectrum is analyzed. The exact decay of the full population of the reactant should be represented by the decay of the full area of the fluorescence spectrum and not by a decay at a single wavelength. The decay of the full spectrum area is shown in Figure V-23. The fluorescence area $M_{flu}(t)$ at each time t was obtained by integrating the intensity $I(\nu, t)$ over all frequency ν;

$$M_{flu}(t) = \int I(\nu, t)\nu^{-3} d\nu \qquad \text{(V. 1)}$$

The decay can be fitted by a double exponential function with lifetimes of 2.6 ps (13.7 %) and 86.3 ps (86.3 %). The longer lifetime (86.3 ps) matches with the longest lifetime obtained by the global analysis fitting of the fluorescence decays (see Table V-3). The shorter lifetime is the one caused by the fast ET from the non-equilibrium state, and the reason for the twice faster Stokes shift of C153 than C102.

V-9. Conclusions of Chapter V

Ultrafast fluorescence quenching of coumarin dyes in electron donating solvents regarded as an intermolecular electron transfer from the solvent to the dyes were observed. The most of the reactions of 4-CF_3

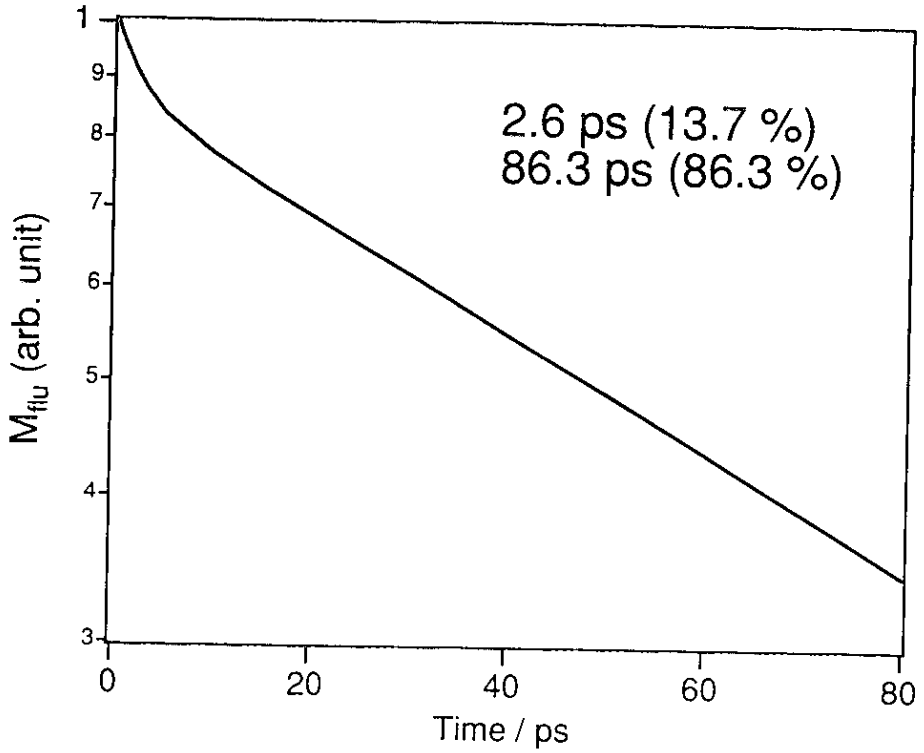

Figure V-23. Decay of the fluorescence spectrum area of C153 in AN obtained from the results shown in Figure V-21.

coumarins in DMA occurred much faster than the solvation process. For the coumarins which show reactions much faster than the solvation process, fluorescence spectra from non-equilibrium state was observed by a steady-state measurement. The Stokes shift of the fast reacting coumarins were much smaller than the ones of slower reacting coumarins. We regard this effect as a "chemical timing" of ET to the solvation process. This kind of phenomena was observed for the first time in condensed phases.

The reaction rate constant depends on the structure of the substituents at 4- and 7-positions. This dependence can be explained mainly by the difference in energy gap. The energy gap dependence indicates that all the reactions are in the normal region. However, there is a discrepancy between simulations based on Sumi-Marcus Jortner-Bixon hybrid model and the experimental results. Most noteworthy discrepancy was that the reaction of C153 was much faster than the calculated rate. This discrepancy may be due to the smaller value of intramolecular reorganization energy λ_i for the coumarins with fixed 7-amino group than the ones with free amino group. C153 has a tightly fixed 7-amino group with double hexagonal ring. If the reaction urges a structural reorganization of the 7-amino group, the value of λ_i will become smaller for the coumarins with fixed amino groups. This reorganization can be the change in C-N bond length or C-N-C angle. The unexpected small value of activation energy for C153 in AN, obtained from the temperature dependent experiments, may support this hypothesis. The coumarins with fixed amino group and the ones with free amino group have a different energy gap dependence according to their difference in the intramolecular reorganization energy.

The dynamic fluorescence Stokes shift of C153 in AN indicates that the ET from non-equilibrium state occurs faster than the one from solvent relaxed state. The dynamic fluorescence Stokes shift of the reactive coumarin (C153) was faster than the non-reactive coumarin (C102).

References for Chapter V

1. G. Jones II, W. R. Jackson, and A. M. Halpern, *Chem. Phys. Lett.*, **72**, 391 (1980).

2. G. Jones II, W. R. Jackson, C. Choi, and W. R. Bergmark, *J. Phys. Chem.*, **89**, 294, (1985).

3. *In Molecular Interactions, Vol.3 Ratajczak H. and Orville-Thomas W. J., Eds., John Wiley & Sons, Ltd.*, 249~265, (1993).

4. T. Kobayashi, Y. Takagi, H. Kandori, K. Kemnitz, and K. Yoshihara, *Chem. Phys. Lett.*, **180**, 416, (1991).

5. H. Kandori, K. Kemnitz, and K. Yoshihara, *J. Phys. Chem.*, **96**, 8042, (1992).

6. K. Yoshihara, A. P. Yartsev, Y. Nagasawa, H. Kandori, A. Douhal, and K. Kemnitz, *In Ultrafast Phenomena VIII, Martin, J.-L., Migus, A., Mourou, G. A., Zewail, A. H., Eds., Springer, Berlin*, 571, (1993).

7. A. P. Yartsev, Y. Nagasawa, A. Douhal, and K. Yoshihara, *Chem. Phys. Lett.*, **207**, 546 (1993).

8. J. Shah, *IEEE J. Quan, Electr.*, **24**, 276, (1988).

9. M. A. Kahlow, W. Jarzeba, T. P. DuBuruil, and P. F. Barbara, *Rev. Sci. Instrum.*, **59**, 1098, (1988).

10. K. Kemnitz, N. Nakashima, and K. Yoshihara, *J. Phys. Chem.*, **92**, 3915, (1988).

11. E. M. Kosower and D. Huppert, *Chem. Phys. Lett.*, **96**, 433, (1983)

12. T. J. Kang, W. Jarzeba, P. F. Barbara, and T. Fonseca, *Chem. Phys.*, **149**, 81, (1990).

13. K. Tominaga, G. C. Walker, W. Jarzeba, and P. F. Barbara, *J. Phys. Chem.*, **95**, 10475, (1991).

14. K. Tominaga, G. C. Walker, T. J. Kang, P. F. Barbara, and T. Fonseca, *J. Phys. Chem.*, **95**, 10485, (1991).

15. H. Sumi and R. A. Marcus, *J. Chem. Phys.*, **84**, 4894, (1986).

16. W. Nadler and R. A. Marcus, *J. Chem. Phys.*, **86**, 3906, (1987).

17. Z. R. Grabowski, K. Rotkiewicz, A. Siemiarczuk, D. J. Cowly, W. Baumann, *Nouv. J. Chem.*, **3**, 443, (1979).

18. E. Lippert, W. Rettig, V. Bonacic-Koutecky, F. Heisel, and J. A. Miehe, *Adv. Chem. Phys.*, **68**, 1, (1987).

19. S. Kato and Y. Amatatsu, *J. Chem. Phys.*, **92**, 15, 7241, (1990).

20. D. Rehm and A. Weller, *Z. Phys. Chem. N. F.*, **69**, 183, (1970).

21. G. Jones II, S. F. Griffin, C. Choi, and W. R. Bergmark, *J. Org. Chem.*, **49**, 2705, (1984).

22. M. Castella, P. Millie, F. Piuzzi, J. Caillet, J. Langlet, P. Claverie, and A. Tramer, *J. Phys. Chem.*, **93**, 3949, (1989).

23. R. A. Marcus, *Discuss. Faraday Soc.*, **29**, 21, (1960).

24. M. Maroncelli and G. R. Fleming, *J. Chem. Phys.*, **86**, 6221, (1987).

25. R. A. Coveleskie, D. A. Dolson, and C. S. Parmenter, *J. Chem. Phys.*, **72**, 5774, (1980).

26. G. C. Walker, E. Akesson, A. E. Johnson, N. E. Levinger, and P. F. Barbara, *J. Phys. Chem.*, **96**, 3728, (1992).

CHAPTER VI
DEUTERIUM ISOTOPE EFFECTS OF ELECTRON TRANSFER

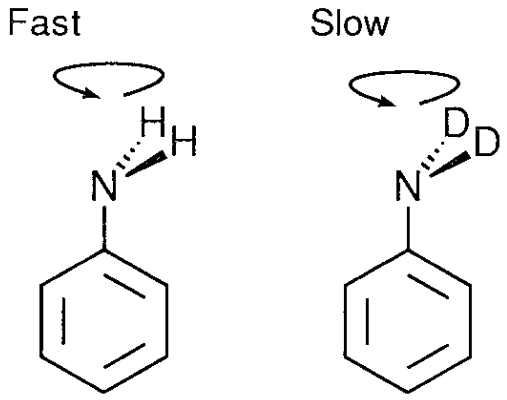

VI-1. Deuterium isotope effects of the electron donating solvent

Experiments on isotope effects were carried out to examine the role of vibrations on ET. The samples used are shown in Figure VI-1. The deuterium labeled solvents used are AN-d7, aniline with all the seven hydrogens changed to deuterium, and AN-d2, with only the two hydrogens on the amino group are deuterated.

In Figure VI-2 (a), the fluorescence decay of C153 in AN-d7 (solid line) is compared with the one in normal AN (broken line), which show no difference. The lifetimes of C153 in normal AN are 17 ps (59 %) and 285 ps (41 %), which are somewhat longer than the solvation time of AN. The solvent relaxation times of AN are 6.7 ps (81 %) and 13.3 ps (19 %) (see Chapter III). In Figure VI-2 (b), the fluorescence decay of C152 in AN-d7 (solid line) and in normal AN (broken line) are shown. The lifetimes of C152 in normal AN are 3.7 ps (41 %) and 12.4 ps (59 %), while in AN-d7, it becomes slightly longer. The ratio between the reaction rate constants for normal AN k_n and AN-d7 k_{d7} is $k_n / k_{d7} = 1.1$. The effect of the deuteration is more effective for the reactions faster than solvation process. Therefore, if the isotope effect is related to dynamical aspects of ET, it should be related to a process faster than the solvent diffusive motions.

The isotope effect of AN-d2 is shown in Figure VI-3. In Figure VI-3 (a), the fluorescence decay of C152 in AN-d2 (solid line) is compared with the one in normal AN (broken line). The ratio of the reaction rate constant is $k_n / k_{d2} = 1.2$. As is shown in Figure VI-3 (b), the decay in AN-d2 seems to be identical to the one in AN-d7 within the experimental error. Therefore, the deuteration of amino hydrogen seems to be much more important than that of the phenyl hydrogen.

The present experimental results show that some vibrational mode of the amino group may be related to ET faster than the solvation process. There are three candidates for such a mode, (i) librational mode of AN as a

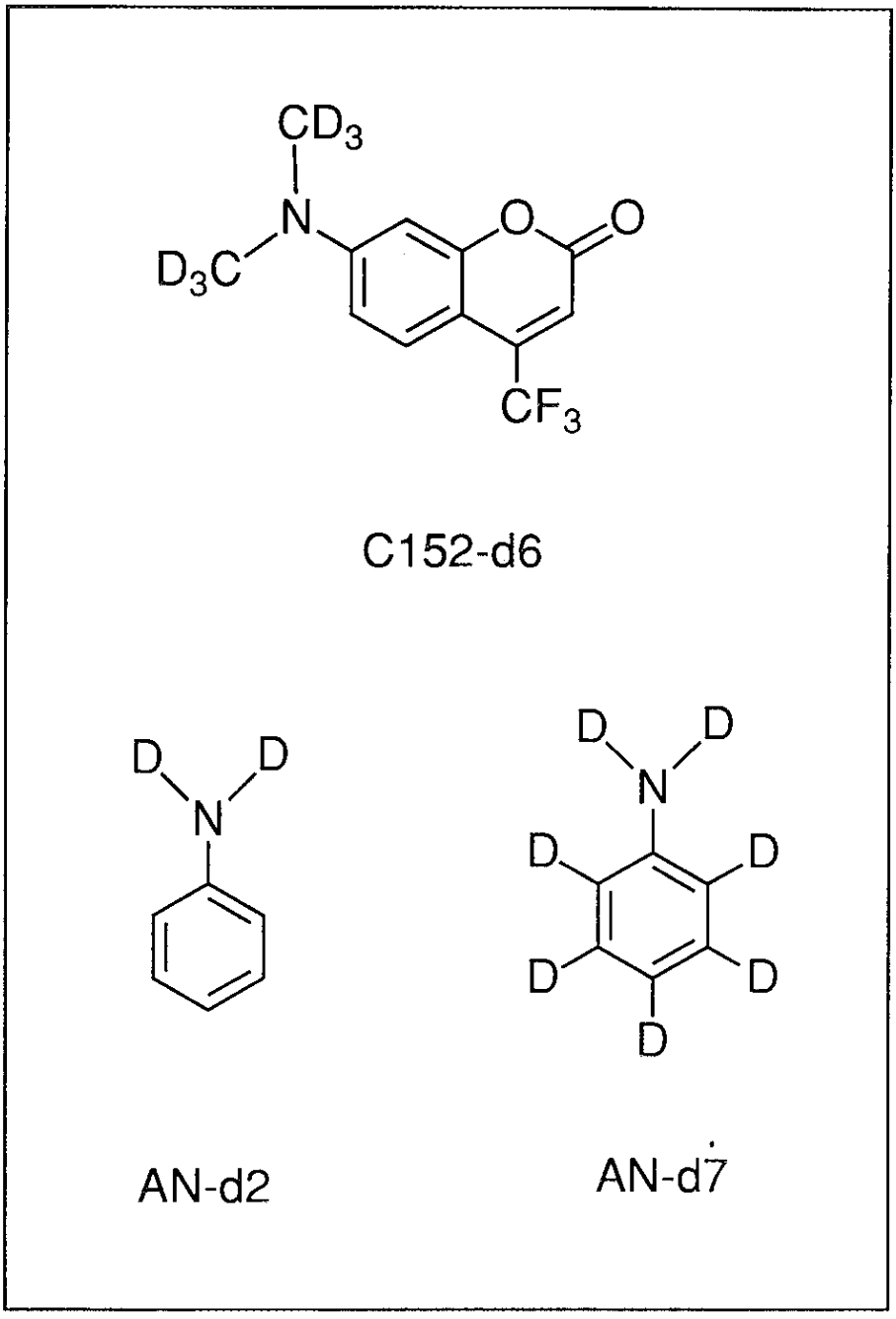

Figure VI-1. Dueterium labelled compounds used in this chapter.

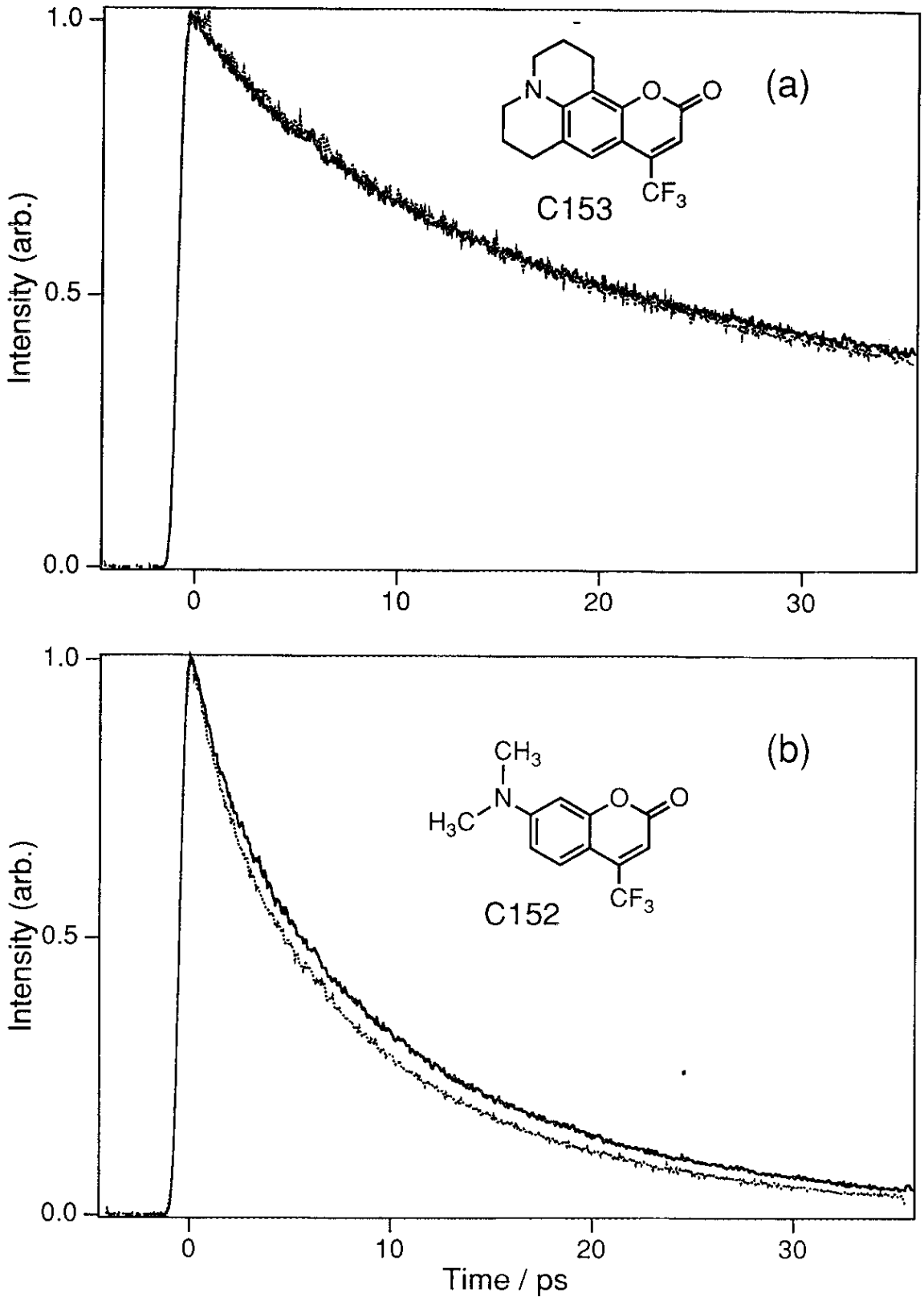

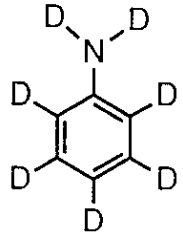

AN-d7

Figure VI-2. Fluorescence decays of (a) C153 in AN-d7 (solid line) and AN (broken line), and (b) C152 in AN-d7 (solid line) and AN (broken line), measured at 510 nm.

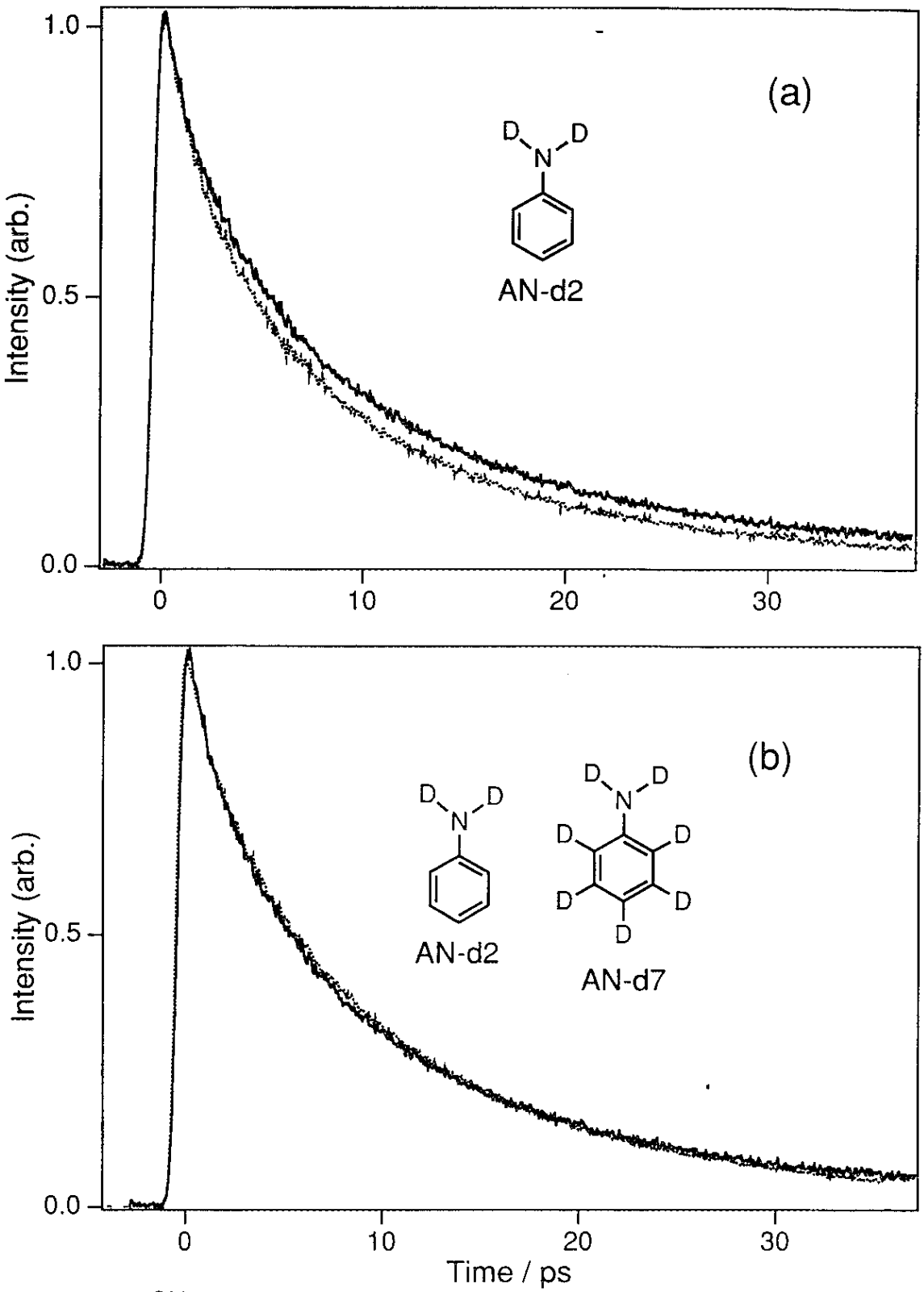

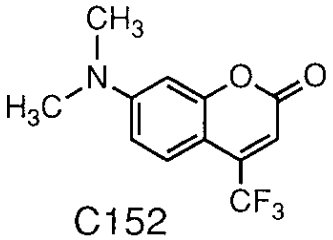

Figure VI-3. Fluorescence decays of (a) C152 in AN-d2 (solid line) and AN (broken line), and (b) C152 in AN-d2 (solid line) and AN-d7 (broken line), measured at 510 nm.

solvent, (ii) intermolecular mode between coumarin and AN, and (iii) intramolecular mode of AN as a donor.

(i) The deuterium effect may be ascribed to librational modes of solvent. Libration is a term usually used to describe a intramolecular vibration or a motion which is not diffusive. The solvent librational modes have previously been implicated in ET reaction mechanisms. Most of them are about deuteration of hydroxyl group of protic solvents. AN is also a protic solvent which can form hydrogen bonding by themselves with the amino group.

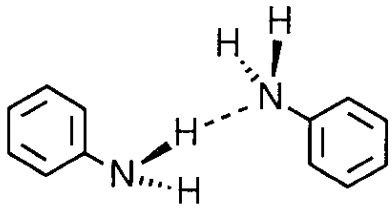

H-bonding between AN themselves.

Bader *et al.* made simulations on ferrous-ferric (Fe^{3+}/Fe^{2+}) exchange in water.[1~4] They calculated that the reaction in D_2O becomes twice slower than that in H_2O ($k_{H_2O} / k_{D_2O} = 2$). Experimentally, Hudis and Dodson found the ratio to be 2.5 Guarr *et al.* reported an isotope effect of 1.3 for cross reactions involving $Fe^{3+}_{(aq)}/Fe^{2+}_{(aq)}$, yielding a factor of 1.7 as an estimate of the isotope effect for the self-exchange reaction.[6] Tominaga *et al.* also observed an isotope effect for the ET of metal-metal charge transfer (MMCT) complex ($(NH_3)_5Ru^{III}NCRu^{II}(CN)_5^-$).[7] Photo-excitation of MMCT band leads to an optical ET between the metal centers followed by a radiationless back ET. In glycerol, the value of $k_{glycerol} / k_{glycerol\text{-}d3}$ was 1.2 at 20 °C and 1.5 at -100 °C. Since the isotope effect was observed even at cryogenic temperatures, where diffusive solvent motions should be too slow to be significant, they concluded that this effect should most likely be ascribed to solvent librational modes. Here, libration

is mainly related to the rotation of the hydroxyl group and also to the hydrogen bond. The hydrogen bond has to break for the hydroxyl group to rotate. For DMA, the rotation of the dimethyl amino group may be also related to solvent libration. In this case, the rotation is free from hydrogen bonding, however, it is somewhat heavier and bulky.

(ii) The second candidate is a hydrogen bonding effect of carbonyl group of coumarins with the amino group of AN.

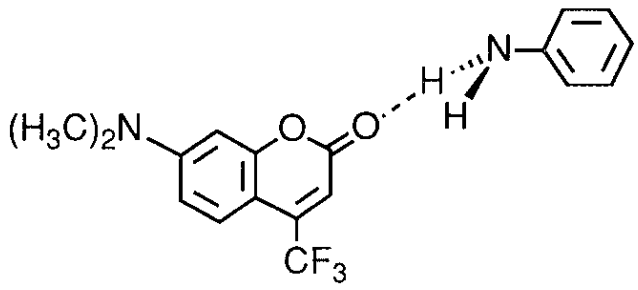

H-bonding between C152 and AN.

The isotope effect may be due to an intermolecular mode of hydrogen bond between the donor and acceptor. However, this kind of intermolecular mode seems to be not important, since in aprotic solvent DMA, ET occurs much faster.

(iii) The third candidate is the intermolecular vibrational modes of AN itself as an electron donor. In Chapter V, the effect of the vibrational mode of 7-amino group of coumarin was discussed. A possibility of these modes to promote ET was suggested. A similar discussion can be applied to a deuterium effect of AN. In this case, the discussion can be separated into three aspects, (1) a change in zero-point energy, (2) the effect of high frequency mode, and (3) low frequency mode.

(1) Changing the hydrogen of the amino group to deuterium will decrease the frequency of N-H stretching mode around ~3400 cm^{-1} down to ~2300 cm^{-1}. This decrease will also decrease the value of zero-point

energy of the mode. If such a decrease of zero-point energy is larger for the reactant than the product, it will increase the activation energy and, thus the reaction will become slower. Therefore, the isotope effect may be ascribed to a slight difference in energy gap. If this is the case, the deuteration should affect not only the fast reaction but also the slow reaction. If there is a slight change in the energy gap for the reaction of C152, same amount of change should also occur for that of C153. From the energy gap dependence shown in Figure V-17, a larger change in rate constant is expected for C153 than in C152, when same amount of energy gap is slightly changed. This is because the slope of the energy gap dependence should be steeper for C153 than C152. However, ET of C153 in AN was not affected by deuteration (Figure VI-2 (a)). The deuteration only affects reaction faster than diffusive solvation process. Moreover, deuteration of the benzene moiety of AN should also decrease the zero-point energy. However, the fluorescence decay of C152 in AN-d7 and AN-d2 matched within the experimental error. Therefore, this explanation seems to be not appropriate for the present deuterium effect.

(2) The deuteration of aromatic compounds are known to reduce the rate of radiationless transition.[8,9] The phosphorescence lifetime of normal naphthalene is 2.1 sec in durene at 77 K, while that of naphthalene-d8 is 16.9 sec. This deuterium effect is ascribed to a change in the rate of triplet-singlet internal conversion. The internal conversion is thought to occur through the high vibrational levels of C-H mode of the S_0 ground state (Figure VI-4). The energy difference between the vibrational levels of C-H mode is large because of high frequency, however it becomes smaller for C-D mode. Therefore, the T_1 state of the deuterated compound has to cross the vibrational levels with larger quantum numbers than that of the normal compound. Therefore, deuteration reduces the Franck-Condon factor, and thus the internal conversion rate constant. It can also increase

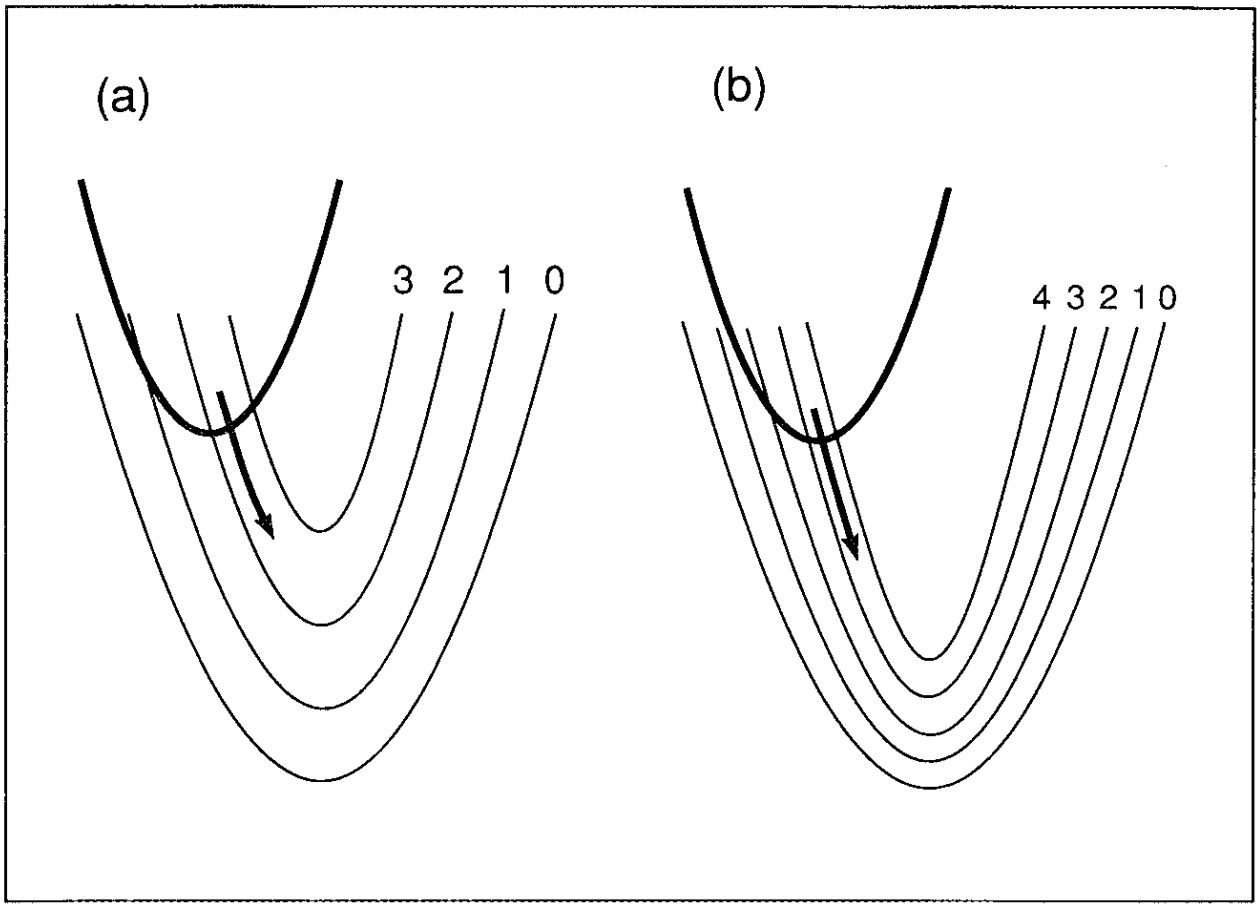

Figure VI-4. A dueterium effect for high frequency mode. (a) Normal compound. Vibrational level of the product state with quantum number of n = 2, crosses the bottom of the reactant state surface. (b) Dueterated compound. A vibrational level with n = 3, crosses the bottom of the reactant state surface.

the density of states, however, it is not discussed. The deuterium effect of high frequency mode is expected to be significant in the inverted region and not in the normal region. The reaction of C152 in AN is expected to be in the normal region, thus this explanation seems not appropriate for the present experiments.

(3) As is shown in Figure VI-2, the isopote effect is much significant for the reaction faster than diffusive solvation process. Therefore, if the isotope effect is related to dynamical aspects of ET, it should be related to a process faster than the solvent diffusive motions. One of the candidate is the low frequency classical vibrational modes, which were introduced in Sumi-Marcus two-dimensional model. Intramolecular low frequency mode of amino group may be responsible for the ultrafast ET.

As a summery, isotope effect was observed for ET of coumarins in AN-d7 and d2. The effect was significant for the ET faster than diffusive solvation process. Thus it cannot be ascribed to the diffusive motion of the solvent. Also it cannot be due to a change in zero-point energy nor high frequency mode of AN. Therefore, the final candidate for the isotope effect is the low frequency mode of the amino group of AN, which can be treated as a solvent librational mode or an intramolecular mode of the donor.

VI-2. Deuterium isotope effects of coumarin

If the intramolecular low frequency mode of the amino group is promoting ET, similar deuterium effect may be observed for the 7-amino group of coumarin. Therefore, C152-d6, a coumarin with deuterated dimethyl amino group, was synthesized. Figure VI-5 shows the fluorescence decays of C152-d6 in DMA and AN (solid lines) with decays of normal C152 (broken lines) for comparison. Both decays matches completely, no deuterium isotope effect was observed. The ratio of the

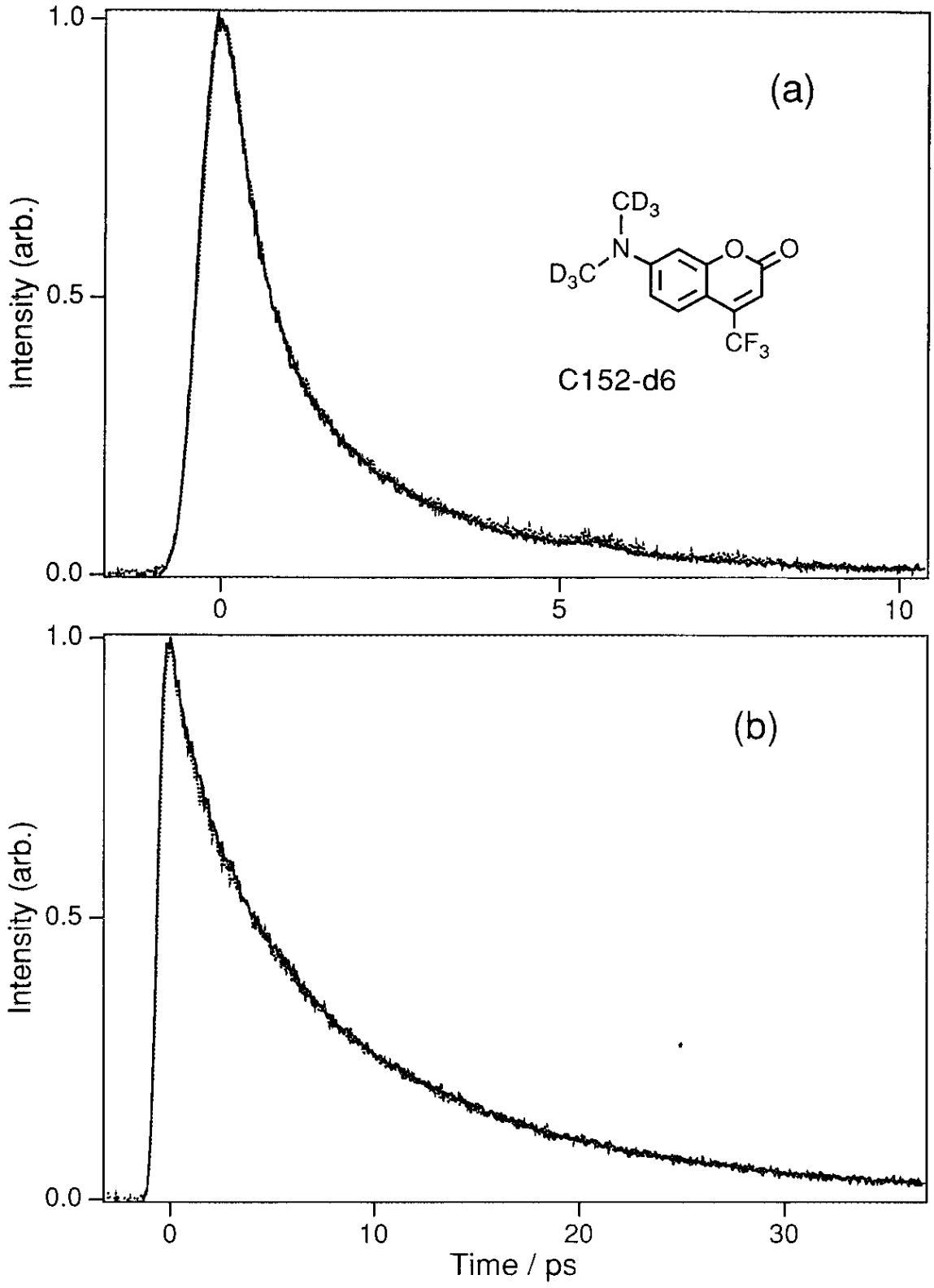

Figure VI-5. Fluorescence decays of C153-d6 (solid line) and C153 (broken line) (a) in DMA and (b) in AN, measured at 510 nm.

mass between methyl group is CD_3 / CH_3 = 1.2, while that of hydrogen is D / H = 2. This difference may be not enough to observe the isotope effects. Experiments using C151-d2, a coumarin with deuterated amino group may be adequate. Such experiment s are under progress.

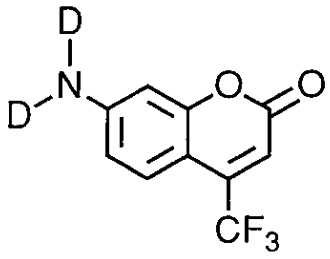

C152-d2

References for Chapter VI

1. R. A. Kuharski, J. S. Bader, D. Chandler, M. Sprik, M. L. Klein, and R. W. Impey, *J. Chem. Phys.*, **89**, 3248, (1988).

2. J. S. Bader and D. Chandler, *Chem. Phys. Lett.*, **157**, 501, (1989).

3. J. S. Bader, R. A. Kuharski, and D. Chandler, *J. Chem. Phys.*, **93**, 203, (1990).

4. M. Marchi, and D. Chandler, *J. Chem. Phys.*, **95**, 889, (1991).

5. J. Hudis and R. W. Dodson, *J. Chem. Phys.*, **78**, 911, (1956).

6. T. Guarr, E. Buhks, and G. Mclendon, *J. Am. Chem. Soc.*, **105**, 3763, (1983).

7. K. Tominaga, D. A. V. Kliner, A. E. Johnson, N. E. Levinger, and P. F. Barbara, *J. Chem. Phys.*, **98**, 1228, (1993).

8. C. A. Hutchison Jr. and B. W. Mangum, *J. Chem. Phys.*, **32**, 1261, (1960).

9. M. R. Wright R. P. Frosch, and G. W. Robinson, *J. Chem. Phys.*, **33**, 934, (1960).

謝辞

本論文は、総合研究大学院大学数物科学研究科構造分子科学専攻に在籍し、平成３年４月から５年１０月までの２年半にわたる研究成果をまとめたものです。

本研究を遂行するにあたり、指導教官の吉原經太郎教授より適切かつ丁寧な御教授と快適な研究環境を賜わりました。感謝の意を表するとともに御礼申し上げます。

Arkadiy P. Yartsev 博士にはフェムト秒レーザーの立ち上げを御指導頂きました。本研究は同博士の御指導なしでは遂行できなかったでしょう。またこの研究の先駆者である小林徹博士と Klaus Kemnitz 博士に感謝の意を表します。

富永圭介助手には電子移動の理論面およびシミュレーションに関して多大の御指導を賜わりました。私の電子移動に関する理解は同博士の御助言に負うところが大きいです。

熊崎茂一氏、伊名波良二博士、神取秀樹助手等、その他の吉原グループの皆様にも研究および生活面ともにたいへんお世話になりました。短い期間ではありましたが、Alan E. Johnson 博士と Prem B. Bisht 博士には測定の一部を手伝って頂きました。Julie M. Rehm 氏には論文の英語のチェックをして頂きました。また秘書の山下智春様、伊藤泰代様にもお世話になりました。ありがとうございました。

分子研在籍の大学院生の皆様にもたいへんお世話になりました。特に、夏の学校の手伝いをして頂いた津田健一郎氏、六車千鶴氏、サイクリックボルタンメトリーや溶媒蒸留等の実験を手伝って頂いた小嵜正敏氏、米田修敏氏に感謝の意を表したいと思います。

また、早稲田大学時代に御教授賜わりました高橋博彰教授および、あの狭い研究室でともに研究していた皆様にもこの場をお借りして感謝の意を表したいと思います。特に私をこの世界に引きずり込んだ阿部二郎博士、私に分子研行きを決意させた日浦英文博士、ナノ秒ラマンシステムとそのプログラムを立ち上げた湯沢哲朗博士、いつも夢のあるお話をして頂いた河野正規博士、色々な面で社会勉強させて頂いた根本修克博士に感謝の意を表します。

1993年11月30日　長澤裕